# Mechanism of Interaction between *Solanum tuberosum* Plant Specific Insert with Phospholipid Membranes Using NMR Spectroscopy

by

Jingxin Tian

BSc. McGill University, 2014

A THESIS SUBMITTED IN PARTIAL FULFILLMENT OF

THE REQUIREMENTS FOR THE DEGREE OF

MASTER OF SCIENCE

in

THE FACULTY OF GRADUATE AND POSTDOCTORAL STUDIES

(FOOD SCIENCE)

THE UNIVERSITY OF BRITISH COLUMBIA

(Vancouver)

June 2017

## Abstract

Plants rely on their innate immunity as a first line of host defense against external pathogens. In potatoes, *Solanum tuberosum*, upon the infestation of the late blight disease causing pathogen, *Phytophthora infestans*, there is an increased expression of aspartic proteases. Most plant aspartic proteases are characterized by a hydrophobic signal peptide, a prosegment, and an N-terminal and C-terminal domain separated by a plant specific insert. Like saposins and various other members in this family, PSI of *Solanum tuberosum* was discovered to have antimicrobial and antifungal activities. PSI is active under acidic pH conditions by self-assembling into a dimer and it interacts with phospholipid membranes from pathogens to cause leakage activities.

The objectives of this thesis were to elucidate the pH dependent protein monomer-dimer equilibrium and the backbone chemical shift assignments of PSI by solution NMR ,the dynamic properties of PSI by the NMR relaxation, PSI-membrane interaction by solid-state NMR, and the topology of PSI-membrane complex.

A combination of solution state and solid-state NMR were used to study the characteristics of PSI in solution and PSI-membrane interactions at different pH conditions. Protein backbone assignments and dynamics characterization were performed on the PSI in solution. Protein-membrane interaction was examined through NMR titration, NMR based H/D exchange, and protein-lipid interactions by solid-state NMR.

PSI monomer-dimer equilibrium occurred between pH 2.0 and 7.0. From dynamics studies, the average $^{15}N$ longitudinal relaxation ($T_1$) times were $0.99 \pm 0.18$ s and $0.53 \pm 0.03$ s for pH 2.0 and 7.0, respectively, this demonstrated that PSI was a dimer at pH 2.0 and a monomer at pH 7.0. Comparison of the transverse relaxation ($T_2$) times of PSI at different pH

values yielded the same conclusion. $^{1}H$-$^{15}N$ heteronuclear NOE determined that PSI had rigid helical segments connected with flexible long loops. Solid-state NMR data suggested that protein-membrane interaction occurred on the phosphate head group and protein is embedded in the lipid environment after PSI-membrane interaction.

These results contributed to protein dynamics and mechanisms of PSI and its interactions with phospholipid membrane, and therefore, a better mechanistic understanding of the innate natural plant host defense response against pathogen invasions.

## Lay Summary

The plant specific insert (PSI) from potatoes, *Solanum tuberosum,* is a saposin-like-protein which has the potential to impact on both food safety and agricultural practices. Plants rely on their innate immunity as a first line of host defense against external pathogens. Like saposins and various other members in the saposin like protein family, PSI was discovered to have antimicrobial, antifungal, protein folding, vacuolar targeting/sorting, membrane disruption and vesicle leakage activities. These self-defense mechanisms are essential for the natural health of the plant. The study elucidated the interaction between the recombinantly expressed $^{15}N$ and $^{13}C$ labeled PSI with phospholipids through nuclear magnetic resonance (NMR) spectroscopy. The results obtained suggested that PSI interacted with phospholipid membranes in the helical segments and that these regions were rigid. By answering a fundamental and hypothesis-driven question, these studies will undoubtedly play a critical role towards future innovative food safety and food supply solutions.

## Preface

A part of the work in Chapter 4, results and discussion for NMR experiments were conducted in at the NMR Center at Peking University under the guidance of Dr. Shenlin Wang and facility managers.

The rest of the work in this thesis project and all analysis was completed by the author, Jingxin (Jenny) Tian under the guidance of supervisor Dr. Rickey Yada and Dr. Shenlin Wang. The committee member, Dr. Christine Scaman provided additional advice and support for the research.

The work in this thesis has not been previously published.

# Table of Contents

## List of Tables

## List of Figures

## List of Abbreviations

| | |
|---|---|
| AFM | Atomic Force Microscopy |
| AP | Aspartic Protease |
| CD | Circular Dichroism Spectropolarimetry |
| CSI | Chemical Shift Index |
| DNA | Deoxyribonucleic Acid |
| DTT | Dithiothreitol |
| FID | Free Induction Decay |
| HSQC | Heteronuclear Single Quantum Coherence |
| IPTG | Isopropyl β-D-1-thiogalactopyranoside |
| LUV | Large Unilamellar Vesicle |
| NMR | Nuclear Magnetic Resonance |
| NOE | Nuclear Overhauser Effect |
| PC | Phosphatidyl-choline |
| PDB | Protein Data Base |
| PE | Phosphatidylethanolamine |
| PL | Phospholipid |
| POPC | 1-palmitoyl-2-oleoyl-sn-glycero-3-phosphocholine |
| POPE | 1-palmitoyl-2-oleoyl-sn-glycero-3-phosphoethanolamine |
| POPS | 1-palmitoyl-2-oleoyl-sn-glycero-3-phosphoserine |
| PS | Phosphatidylserine |
| PSI | Plant Specific Insert |
| SAPLIP | Saposin-Like Protein |
| StAP | *Solanum tuberosum* Aspartic Protease |
| Trp | Tryptophan |
| TRX | Thioredoxin |
| UV | Ultraviolet |

## Acknowledgements

I would like to express my enduring gratitude to my supervisor, Dr. Rickey Yada for his continuous mentorship, patient guidance, invaluable advice and allowing me to grow as a research scientist throughout the past nine years, from my high school days to the end of my Masters. His immense passion for the field of Food Science is my greatest inspiration to strive for my goals and follow my dreams.

I would also like to give my deepest thanks to my collaboration supervisor at Peking University, Dr. Shenlin Wang for his continuous guidance, profound thoughts and the immense amount of time in teaching me the background of Nuclear Magnetic Resonance. He provided enormous support during my research in China. Another thank you goes to the Peking University NMR center for providing me with the facility to conduct my research and the personnel in operating the equipments.

Additionally, many thanks to my committee members, Dr. Rickey Yada, Dr. Shenlin Wang and Dr. Christine Scaman, for providing valuable advice and support throughout my master's thesis research project and mentorship for my seminars.

I am also grateful for my lab mate from the University of British Columbia, John Dupuis for keeping me sane and taking care of all my administrative errands during my exchange; my lab mates from the University of Guelph, Brian Bryksa, Douglas Grahame, and Reena Pinhero for making the Guelph lab a second home, special thanks to Brian Bryksa for teaching me all the wet lab skills and is always there to answer my questions; and my lab mates in Peking University, thanks for having me during my six months of exchange in China. I would also like to thank the FNH Grad Office 120 for the ever lasting friendships that was developed during my time at UBC. Special mention to my "buddy", Gracia Windiasti, for being my partner in crime

during graduate school and all the profound memories that we created; thanks for being my life saver and sending me the starting materials to China, without that shipment, none of this would have been possible.

A special thanks to my beloved parents for trusting me and supporting my decisions in life and during my studies. Their endless support allowed me to reach my goals, continuously learn more and constantly moving forward.

Lastly, I would like to acknowledge my friend Andrea Hill, for believing in me, reminding me that it's okay if I don't succeed the first time, always being there for me, putting up with my craziness, and bringing out the best within me. I also thank her for teaching me the skills in conducting research during my undergraduate research project which prepared me for my graduate degree. Her passion, wisdom and moral support were extremely meaningful to me throughout this MSc journey.

## Dedication

This thesis is dedicated to my beloved grandparents for their endless support and encouragement throughout my education. They have taught me how to overcome my fears, pursue my passion and reach for my dreams. They are my backbone and the greatest blessings in my life.

# Chapter 1: Literature Review

## 1.1 Introduction

Every year, approximately 1.95 million to 3.9 million tons of the total food produced worldwide are lost from food-related fungi infections (Pitt and Hocking, 2009). This equals approximately 5-10% of the total food supplies worldwide. Food can be rich in nutrients and under compatible physio-chemical conditions; they provide ideal habitats for microorganisms (Pitt and Hocking, 2009). Infections in potato tubers commonly occur through wounds and one of the common diseases caused by pathogen is the disease, late blight. However, prior to harvest the potato has an extremely powerful natural defense mechanisms against microbial and fungi invasions. The plant is constantly battling microbial and fungal related infections (Agrawal et al, 2002). Thus, it is critical to investigate fungal food spoilage and prevention strategies such as natural plant defense responses.

Natural defense mechanism of plants can be induced directly or indirectly (Agrawal et al., 2002). For potatoes, upon invasion of the late blight disease causing *Phytophthora infestans*, the expression of an aspartic protease (AP) was shown at faster and higher levels (Guevara et al., 2002). The aspartic protease expressed belongs to the pepsin A1 family (Rao et al., 1998) which are characterized by two catalytic aspartic residues, 3D structural similarities, optimal activity in acidic pH, high sequence homology, inhibition by pepstatin and the expression as zymogens (Davies, 1990). Unlike the aspartic proteases from mammals, microbes and viruses, most plant aspartic proteases contain a unique sequence of approximately 100 residues within their C-terminus; this unique domain is termed the plant specific insert (Kervinen et al., 1999; Bryksa et al., 2011; De Moura et al., 2014; Munoz et al., 2014). The plant specific insert, unlike other aspartic protease components, belongs to the saposin-like proteins (SAPLIP) family (Munoz et

al., 2011). It has similar functions to the animal innate immune system proteins NK-lysin and granulysin that are active against dangerous food pathogens (Bryksa et al., 2011). In addition, the plant specific insert has sequence homology and functional similarities with the mature saposin C, derived from prosaposins (Tormakangas et al., 2001). The potato plant specific insert (PSI) can be recombinantly expressed and purified to examine its innate immunity in host defense against external pathogens. It was found that this domain can interact with phospholipid membrane (Bryksa et al., 2011) and cause disruption which contributes to the natural defense mechanism of plants. However, the exact mechanism of interaction, protein characteristics and topology are still unknown.

The overall objective of this study was to investigate the interaction between the recombinantly expressed *Solanum tuberosum* plant specific insert with phospholipids through nuclear magnetic resonance spectroscopy (NMR).

## 1.2 Background and Rationale of Research

Hunger is a continuing epidemic which affected many developing countries in the world (FAO, 2015). Globally every year, from agricultural production to consumption at home, approximately 1.3 billion tons of food are lost or wasted (FAO, 2015). Within this number, it is estimated that, food-related fungi infections causes a total of 5-10% loss from all food produced, equaling 1.95 million to 3.9 million of the 1.3 billion tons of total food lost. Food loss from fungi infections is an enormous problem throughout the world which can be extremely toxic to humans and livestock (Pitt and Hocking, 2009). Thus, it is critical to investigate fungal related food spoilage and study its prevention through natural plant defense responses. The development of environmentally friendly crop protection strategies are of utmost important to maintain agricultural food business, increase food security, and to ensure a constant food supply chain.

Under suitable physio-chemical conditions, food provides an ideal habitat for microorganisms as it is rich in nutrients. However, prior to harvest, plants possess extremely powerful natural defense mechanisms against microbial invasions (Pitt and Hocking, 2009). Potatoes are often at risk due to fungal diseases including silver scurf, skin spot, and the late blight disease (Pitt and Hocking, 2009). As most of the infections in potatoes occur through wounds, the natural plant defense mechanism is constantly battling fungal invasions.

## 1.3 Potatoes

### 1.3.1 Common Invasive Disease and Cause

The affordable unit price of potatoes makes them a stable food security crop, especially in developing countries. Infectious diseases in potatoes can hinder their continuous production, causing a shortage of supply. Diseases affecting the cultivation of potatoes come from fungi, bacteria, virus, nematodes and insect injuries (O'Brien and Rich, 1976). Fungal diseases are one of the most common infectious diseases. A few common disease causing pathogens include: *Fusarium solani, Polyscytalum pustulans,* and *Phytophthora infestans* (Pitt and Hocking, 2009).

The catastrophic potato famine that occurred in the 1840's was caused by the late blight disease as a result of the oomycete pathogen, *Phytophthora infestans*; this was known as one of the most significant crop failures in history (Schumann and D'Arcy, 2005) resulting in 1.5 million people dying due to starvation with a similar number of citizens emigrating to various parts of North America (Schumann and D'Arcy, 2005).

The late blight disease is apparent on the plant leaves, stems and the potato tubers. On the plant leaves and stems, infections often occur through wounds and they can be identified by black/brown lesions (O'Brien and Rich, 1976; Schumann and D'Arcy, 2005; Pitt and Hocking, 2009). The sizes of these lesions are relatively small at first, but soon expand rapidly becoming

necrotic. Under warm and moist conditions, the center of these lesions will die and turn dark brown or black. Sporangia and sporangiospores are produced by *Phytophthora infestans*, forming white growth on the infected surface around the dead areas on lower side of the leaves. The entire crop field can be destroyed within a few days after the first appearance of infectious wounds (Schumann and D'Arcy, 2005; Pitt and Hocking, 2009). As the sporangia on leaves and stems of the potato plant leak into the soil, tubers also become infected (Schumann and D'Arcy, 2005). Thus, it is imperative to implement control measures in order to provide a sustainable supply of the crop. The International Potato Center and research partners cultivated late blight resistant potato cultivars (Hijmans et al., 2000) which were found to have natural defense properties against invasive pathogens.

### 1.3.2 Natural Defense Response of Plants

Healthy plants can be cultivated by introducing resistant cultivars or by applying chemical control agents (Dever et al., 2006). In resistant plant species, natural plant defense mechanisms are often expressed in the presence of infections, either directly or indirectly (Agrawal et al., 2002). The classes of terpenoid, cucurbitacins are some of the bitterest compounds known, and they are produced in cucumber plants to defend against herbivores (Agrawal et al., 2002). Agrawal found that in cucumbers which produce the bitter cucurbitacins, they attracted 37% less predatory mites (Agrawal et al, 2002). The mode of action for the natural defense response was unclear.

Another natural plant defense mechanism includes the expression of aspartic proteases, which has been shown to occur in tomato plants (Schaller and Ryan, 1996), *Arabidopsis* (Xia et al., 2004), potato tubers (Guevara et al., 2002), potato leaves (Guevara et al., 2004), tomato leaves and tobacco leaves (Rodrigo et al., 1991). Most plant aspartic proteases contain a unique

sequence of approximately 100 amino acid residues, referred to as the plant specific insert, in the C-terminus. This sequence is found to interact with membrane bilayer and cause bilayer disruption (Egas et al., 2000; Munoz et al., 2010; Munoz et al., 2014). The plant specific insert may function independently or as part of the parent enzyme, the aspartic protease.

## 1.4 Aspartic Proteases

### 1.4.1 Sources and Classification

Aspartic proteases are found ubiquitously in nature such as in viruses, bacteria, yeast, plants, fungi and animals (Davies, 1990; Dunn, 2002) and have been divided into families based on their similarity in amino acid sequence, then further assigned as a clan based on their evolutionary relationships and tertiary structures using the MEROPS data base (http://www.merops.ac.uk) created by Rawlings and Barrett (Simoe and Faro, 2004). Aspartic proteases are divided into the pepsin A1 family, retropepsin A2 family and pararetrovirus A3 family. However, most of the aspartic proteases examined to date are in the pepsin A1 family (Rao et al., 1998). Characteristics of aspartic proteases in general include the 3D structural similarities, optimal activity in the acidic pH range, two catalytic aspartic acid residues, high sequence homology, inhibition by pepstatin, and the expression as zymogens (Davies, 1990). The following review will focus mainly on aspartic proteases, and structures (saposin and plant specific insert) within the pepsin A1 family.

### 1.4.2 Structure

Most known aspartic proteases are from a single chain preproenzyme which are then converted into either a homomeric or heterodimeric mature enzyme (Laloi et al., 2002; Simoes and Faro, 2004). Aspartic proteases from plants contribute to a large proportion of all aspartic proteases. Within the plant aspartic protease, the biggest subgroup is represented by the vacuolar

aspartic protease (Kadek, 2014) as the cDNA derived amino acid sequences have shown a high degree of similarity in their precursors (Runeberg-Roos et al., 1991; Asakura et al., 1995; Laloi et al., 2002). These aspartic proteases are characterized by a hydrophobic signal peptide, a prosegment of approximately 40 amino acid residues, and the mature protein region composed of an N-terminal domain and a C-terminal domain, separated by the plant specific insert of approximately 100 amino acids (Koelsch et al., 1994; Asakura et al., 1995). The plant specific insert, highly similar to saposin and saposin-like proteins, is not seen in mammalian and yeast aspartic proteases (Runeberg-Roos et al., 1991; Asakura et al., 1995; Laloi et al., 2002); thus, the presence of plant specific insert is an unique characteristic for plant aspartic proteases. In addition, the position of introns and exons differ in various aspartic proteases (Runeberg-Roos et al., 1991; Asakura et al., 1995), which suggests that dissimilar post translational activities take place during processing. Figure 1 shows a schematic comparison between the mammalian aspartic protease and the typical plant aspartic protease.

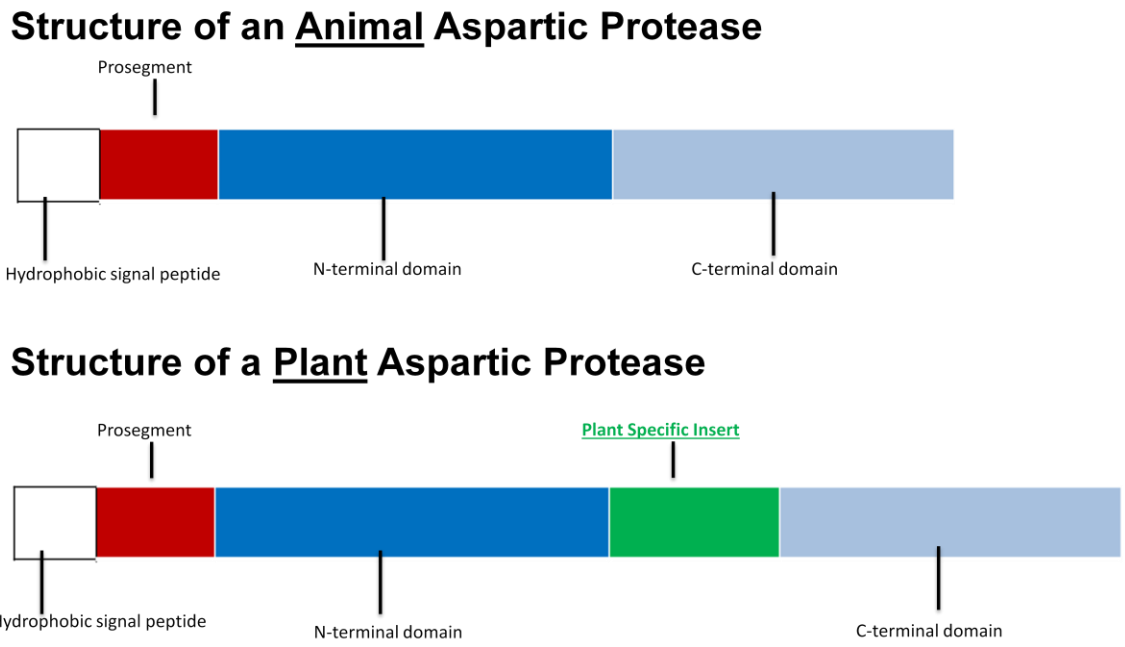


**Figure 1.1 Schematic comparison between mammalian aspartic protease and plant aspartic protease.**

Kadek et al. (2014) reported that the plant aspartic proteases from the nepenthesins subgroup are different in their biochemical and enzymatic properties from the vacuolar plant aspartic proteases subgroup. Nepenthesin-1 is expressed from *Nepenthes gracilis*, it has dissimilar amino acid sequence and lacks the plant specific insert segment. Instead, Nepenthesin-1 contains a nepenthesin-type AP- specific insert, which has more cysteines in its primary structure. In addition, nepenthesin-1 is sensitive to denaturing and reducing agents and has different cleavage properties than other aspartic proteases (Kadek et al., 2014). Further, it was found that the plant specific insert sequence was lacking in both nucellin from barley aspartic protease (Chen and Foolad, 1997) and the aspartic protease from *Arabidopsis* (Xia et al., 2004).

Through comparison of sequences of various plant aspartic proteases, it was found that each aspartic protease contains two active sites. The catalytic amino acid residues surrounding the active site are generally conserved for most plant aspartic proteases, sharing a consecutive three-residue sequence: Asp-Thr-Gly and Asp-Ser-Gly (Runeberg-Roos et al., 1991; Asakura et al., 1995; Laloi et al., 2002). This differs from animal aspartic proteases with two Asp-Thr-Gly amino acid sequences. All plant aspartic proteases except for chlapsin belong to the A1 family; the active site being similar to those in animal aspartic proteases (Simoes and Faro, 2004). In general, most plant aspartic proteases share a high sequence similarity in their N- and C- terminal domains.

### 1.4.3 Catalytic Mechanism

Aspartic proteases are highly specific and various catalytic mechanisms have been proposed, the exact mechanism remains controversial. Attempts to demonstrate that covalent intermediates exist in the active site have been successful (Davies, 1990; Szecsi, 1992). Nonetheless, the most generally accepted mechanism of action is the acid - base catalysis model

in which a water molecule is activated in the aspartic active site (Davies, 1990; Andreeva and Rumsh, 2001). A tetrahedral intermediate is generated through the polarization of the carbonyl oxygen of the peptide bond; it is unclear, however, whether the proton is shared between the two aspartic residues, serving as an electrophile or if a nucleophilic attack occurs on the carbonyl of the scissile peptide bond (Davies, 1990; Szeci, 1992; Andreeva and Rumsh, 2001).

### 1.4.4 Functions of Plant Aspartic Proteases

Plant aspartic proteases have implications in protein processing, plant organ degradation, plant senescence, stress response, programmed cell death and cell reproduction (Simoes and Faro, 2004). A few studies have explored the role of plant aspartic protease in stress response. Rodrigo et al. (1991) suggested that the aspartic proteases contained in tobacco and tomato leaves degrades pathogenesis-related proteins into discrete fragments, this suggests that the proteases may be involved in conserving pathogenesis-related proteins. In addition, a cDNA encoding an aspartic protease has been induced in tomato leaves by wounding and was found to be similar to the defense response system proteins in tomato plants against herbivore attacks (Schaller and Ryan, 1996). Xia et al. (2004) suggested an apoplastic aspartic protease induction in *Arabidopsis* from virus attack through mediating a peptide signal system involved in the activation of inducible plant resistance mechanism.

Guevera et al. (2002) studied the change in the levels of aspartic protease response from intercellular washing fluid of tuber disks in two potato cultivars differing in their susceptibility towards the infection by *Phytophthora infestans.* It was observed that the level of accumulation of aspartic protease in the intercellular washing fluid after infection in the resistant cultivar was much higher and faster compared to the susceptible cultivar. In addition, from antifungal activity studies through proteolysis, the cyst germination for *P. infestans* was inhibited at 0.33 μg/ml of

aspartic protease, a lower concentration than the natural presence found in fresh potatoes (Guevara et al., 2002). Thus, aspartic protease has direct inhibitory effects and plays a role in the natural defense response of potatoes. In a subsequent study, Guevara et al. (2004) reported the stress response of aspartic protease in *Solanum tuberosum* leaves upon the infection with *Phytophthora infestans.* Similar results were obtained in their 2002 study; the aspartic protease content and activity in potato leaves of the resistant cultivar were higher and more active than in the susceptible cultivar. Antimicrobial activities were performed based on substrate specificity for both aspartic proteases from leaves and the tuber; similar results were obtained comparing to the previous study using proteolysis (Guevara et al., 2004). In 2005, a further study by Guevara et al. (2005) encoded the cDNA of aspartic protease from *Solanum tuberosum* to further support the involvement of aspartic protease in plant defense response. From northern blot analysis, the accumulation of aspartic protease transcripts of *Solanum tuberosum* was found higher in the resistance cultivar than in the susceptible cultivar; this supports the results obtained from the previous studies, i.e., resistance is cultivar specific and that aspartic proteases are involved in the natural plant defense response.

In a similar study, Pagano et al. (2007) investigated the importance of glycosylation, to *Solanum tuberosum* aspartic protease. It was observed that aspartic protease accumulation into the apoplast tubers and leaves after wounding required assistance from its carbohydrate portions (Pagano et al., 2007). This suggests that glycosylation may be necessary for *Solanum tuberosum* aspartic protease membrane and/or protein interactions. Another unique feature interesting to the natural plant defense response by aspartic proteases is the plant specific insert within the C-terminus of the enzyme; this domain may function alone or in conjunction with aspartic protease

against pathogens (Egas et al., 2000; Munoz et al., 2010; Munoz et al., 2014). Roles and characteristics of plant specific insert will be discussed later.

## 1.5 Saposin-like Proteins (SAPLIP)

### 1.5.1 Prosaposin

Prosaposins exist in three different forms - as a precursor for mature saposins, in a secreted form and as an integral membrane component (Hiraiwa et al., 1993). Prosaposin as a precursor for mature saposins will be mainly discussed here; the latter two forms are not as well elucidated. Prosaposin as a precursor for mature saposins exists in a major intracellular form of 68 kDa and a major extracellular form of 73 kDa. Both forms are converted to a 50 kDa form after deglycosylation with N-glycosidase. In addition, prosaposin exists as a multimer in neutral pH and as a dimer in acidic pH (Hiraiwa et al., 1993). Prosaposin is biosynthesized, glycosylated, secreted extracellularly and it is proteolytically processed in the intracellular space of the lysosome to generate mature saposin A, B, C and D (Kishimoto et al., 1992).

Prosaposins are found in various human and rat tissues including the brain, testes, kidney, spleen, liver, skeletal muscles, heart, and platelets (O'Brien and Kishimoto, 1991; Kishimoto et al., 1992; Hiraiwa et al., 1993). In both rat and human milk, a 16-residue signal peptide is first cleaved off to generate the prosaposin. This is indicated by the N-terminal amino acid, glycine, at the $17^{th}$ position from the N-terminal end of the preprosaposin. The prosaposin isolated from human seminal plasma has the identical N-terminal amino acid sequence as the milk prosaposin. Higher molecular weights of the milk prosaposins correlate to larger carbohydrate chains; deglycosylation precedes its proteolysis to mature saposins (Kishimoto et al., 1992). A survey conducted by Sano et al. (1989) found that in different rat tissues, the distribution and proteolytic processing of saposins, prosaposins and intermediate forms are diverse. Prosaposins were

predominant in the plasma and the concentration in the brain increased during development. Saposins were present in the spleen, lung, liver and kidney. Large amounts of nonglycosylated saposins were present in the nuclear fraction for nucleic acid metabolism (Sano et al., 1989).

Prosaposins can also be recombinantly expressed and purified. The relatively low stimulatory activities from the human milk and seminal plasma prosaposins may be due to oligosaccharide side chains masking the stimulatory regions (Kishimoto et al., 1992; Hiraiwa et al., 1993). Similar to mature saposins, both recombinant and native prosaposins can stimulate lysosomal beta-glucosidase and beta-galactosidase activities bound to gangliosides. However, both of the prosaposins cannot stimulate hydrolysis of sulfatides (Hiraiwa et al., 1993). Thus, the recombinant prosaposin is structurally and functionally identical to native prosaposins and they can be used as a source for characterization of prosaposins.

Kishimoto et al. (1992) demonstrated that a thiol protease was responsible for the proteolysis of the recombinant prosaposin to subsequent mature saposin domains (A, B, C and D) by cleavage at the peptide linkages. Two proteins of 39 kDa and 26 kDa were found in the partially purified preparations of recombinant prosaposin that cross-reacted with the anti-saposin C antibody. Through N-terminal sequencing, the 39 kDa protein was formed by cleavage between leucine$^{179}$ and phenylalanine$^{180}$, situated between the domains for saposin A and B, leaving a tri-saposin composed of B, C and D. The 26 kDa protein was formed by the cleavage between glutamic acid$^{297}$ and leucine$^{298}$, this occurred between saposins B and C, leaving a di-saposin of C and D (Hiraiwa et al., 1993; Kishimoto et al., 1992). Two interesting observations were also identified: the apparent cleavage site was different for human seminal plasma prosaposin and insect prosaposin and that the cleavage of saposin A generates a derivative with 20 extra residues from the N-terminus. This suggests that post proteolysis activities are required

to generate mature saposin A (Kishimoto et al., 1992). These findings suggest that the acid protease cleaved off a protein sequence between saposin A and B, B and C, and C and D, giving rise to mature saposins. The functions of prosaposin resides in its mature saposins (A, B, C and D) such as glycosphingolipid catabolism and neurotrophic activities (O'Brien and Kishimoto, 1991), which will be discussed in the following sections.

### 1.5.2 Structure and Functions of Mature Saposins (ABCD)

Mature saposins belong to the saposins-like protein family; they are structurally similar and are composed of six cysteines forming three intramolecular disulfide bonds, a glycosylation site and having conserved prolines in identical positions (Kishimoto et al., 1992). It was proposed that saposin A, B and C have a triple helix structure stabilized by disulfide linkages; saposins B in particular, has an amphipathic helical lipid binding center (O'Brien and Kishimoto, 1991). Under neutral conditions, saposin A, C and D are monomeric, whereas saposins B is dimeric (Popovic and Prive, 2008). However, under acidic conditions at pH 4.8, saposins A assembles into dimers, saposin C forms trimers, saposin B remains dimeric and no evidence was suggested for saposins D (Ahn et al., 2006). Saposin B, C and D do not contain any tryptophan, whereas saposin A contains one tryptophan (Qi and Grabowski, 2001). The four saposins differ in their hinge regions and in the alpha-3 sites which may result in changes during association with lipids or lipid bilayer. The first 24 amino acids of saposins B from the N-terminus suggests β-sheet configurations, differing in other saposins (A, C and D), where helical structures are predominant (Chou and Fasman, 1978). O'Brien and Kishimoto (2001)later confirmed the high β-sheet content in saposins B using CD analysis. In addition, saposins are rich in carbohydrates, approximately 40% are found in saposin A and about 20% were present in saposins B, C and D. However, the carbohydrate moiety is not essential for the activation of glucoylceramidase (Sano

and Radin, 1988). Saposin A is also found to have two N-linked chains, whereas in saposins B, C and D, only one N-linked chain is present (Yamashita et al., 1990). Each saposin is composed of approximately 80 amino acid residues. Saposin A is between amino acids 60 and 143 which activate β-glucosylceramidase, β-glucosidase and β-galactosylceramidase (Fabbro and Grabowski, 1991). Saposin B is between amino acids 195 and 275, responsible for the activation of arylsulfatase A, α-galactosidase A, GM1-β-galactosidase and various other enzymes. Saposin C is between amino acids 311 and 390, activating β-glucosylceramidase, β-glucosidase and β-galactosylceramidase. Lastly, saposin D is between amino acids 405 and 487, and it is responsible for the activation of sphingomylinase (O'Brien and Kishimoto, 1991). Although both saposin A and saposin C have stimulatory effects for β-glucosidase, the activity of saposin A is only one third of saposin C (Kishimoto et al., 1992). However, Morimoto et al. (year) found that saposin A is as active as saposin C. In general, the proteolytic cleavage is critical for the formation of these mature saposins.

Through $^{15}N$ labeled NMR spectroscopy for all four human saposins at both neutral and acidic pH, it was found that they were highly unstable at pH 4.0 (John et al., 2006), but exhibited maximal α-helical content at pH 4.5, the optimal pH for most lysosomal hydrolases. This finding suggested that their α-helical structures were important for their physiological functions. Saposins were considered to be extremely dense and firmly disulfide-linked molecules due to their high heat stability, extensive disulfide linkages and resistance to many proteases (O'Brien and Kishimoto, 1991). The physiological importance of mature saposins is their accumulation in tissues of lysosomal storage disease and the occurrence of sphingolipidosis (Kishimoto et al., 1992). Saposin A and saposin C are involved the *in vitro* hydrolysis of cerebrosides by glucosylceramide β-glucosidase and galactosylceramide β-galactosidase. Saposin B, on the other

hand stimulates sphingolipid hydrolases. In addition, saposins D is required for the hydrolysis of sphingomyelin (O'Brien and Kishimoto, 1991). All four mature saposins are important for lysosomal activities and play vital roles in biological systems.

#### 1.5.2.1 Saposin A

Locatelli-Hoops et al. (2006) examined the binding and lipid mobilization capacity of saposin A expressed and purified from *Pichia pastoris*, by interacting with liposomes and examining the protein-liposome complex through surface plasmon resonance spectroscopy and discovered that at or below pH 4.7, saposin A can mobilize lipids from liposomes. In addition, to increasing lipid extraction, low levels of cholesterol with increasing concentrations of bis(monoacylglycero)phosphate are desired. Another interesting finding was that saposin A does not require galactosylceramide during lipid mobilization (Locatelli-Hoops et al., 2006). For the first time, Locatelli-Hoops et al. (2006) demonstrated that glycosylation of saposin A is vital for lipid extraction activities In addition, it was found that in the galactosylceramide hydrolysis, saposin A/lipid disc is potentially the effective substrate. They are able to solubilize phospholipids, sphingolipids and cholesterol into individual particles (Popovic et al., 2012). Thus, saposin A has an important role in the activation of galactosylceramide hydrolysis. In contrast, Kondoh et al. (1991) suggested that saposins A has no effect on glucosylceramide beta-glucosidase (Kondoh et al., 1991).

The presence and regulation of saposin A is relevant to sphingolipidosis such as Krabbe disease. Matsuda et al. (2001) introduced an amino acid substitution in the saposin A domain to eliminate a disulfide bond in the mice saposin A. These mice progressively developed leg paralysis after 2.5 months and survived up to 5 months. During the terminal stage, tremors and shaking were apparent. These symptoms were observed in Krabbe disease in humans and other

mammals caused by globoid cell leukodystrophy (Matsuda et al., 2001). Thus, the regulation of saposins A is critical in the physiological well-being of humans and animals.

#### 1.5.2.2 Saposin B

Similar to the work of Locatelli-Hoops et al. (2006) on saposin A, Remmel et al. (2007) demonstrated that the glycosylation of saposin B was essential for the lipid extraction activities through surface plasmon resonance spectroscopy and a method based on the release of radioactively labeled lipids from liposomal membranes. The interaction between recombinantly expressed unglycosylated saposin B and immobilized liposomes was monitored. Upon initial binding, saposin B mobilizes lipids by disrupting the membrane structure. This occurs in the acid pH range with the presence of anionic lipids. In addition, removal of carbohydrate from saposin B hinders its activity in membrane-destabilizing qualities (Remmel et al., 2007). Ahn et al. (2003) established that during target lipic extraction, a conformational change occurred to facilitate access to the inner saposin B cavity. Saposin B was presented by a shell-like dimer consisting of a monolayer of alpha-helices enclosing in a large hydrophobic cavity. These helices were repacked to form a homodimers. Thus, glycosylation and specific environmental conditions were essential for saposin B to carry out its activities.

In addition, Yuan et al. (2007) suggested that saposin B plays an important role in lipid binding to CD1d molecules by natural killer T cells through the endocytic pathway. Adding exogenous saposins to the expressed prosaposin negative and CD1d positive cells, saposins B appeared to be the most effective in restoring CD1d recognition. In addition, it was also the most efficient in mediating β-galactosylceramide binding, activating natural killer cells, and mediate lipid binding to soluble CD1d molecules. Although no individual saposin was necessary in the lipid binding of CD1d molecules, low recognition of β-galactosylceramide by natural killer cells

is apparent in the absence of saposin B (Yuan et al., 2007). Unlike other studies, it was also determined that saposin B mediated lipid binding to CD1d occurs at an optimal pH of 6.0, which is higher than the lysosome condition (around pH 5.0). This suggested that saposin B could be required for lipid binding to CD1d molecules from the endocytic pathway.

Recently, another study performed by Sun et al. (2013) examined the unique phenotypes of mice by mutating both saposin A and saposin B causing insufficient degradation of myelin-related glycosphingolipids including galactosylceramid, galactosylsphingosine and sulfatide. A mutation was created in both saposin A and saposin B of the mice, keeping saposin C and saposin D unmodified. It was observed that after 61 days, these mice begun to develop neuromotor deteriorations. In addition, storage materials were present in Schwann cells and neuronal processes, an accumulation of p62 and sulfatide, increased levels of LC3-II in the brainstem and lactosylceramide in the liver. These analyses continue to elucidate the importance of saposins in glycosphingolipid metabolism.

#### 1.5.2.3 Saposin C

Saposin C plays a role in the detection and visualization for potential cancer treatment and therapy. Kaimal et al. (2010) suggested that nanovesicles composed of the phospholipid dioleylphosphatidylserine (DOPS) and saposin C can detect cancer cells in human and animal *in vivo* starting in early stages of diagnosis. Using the optical and magnetic resonance (MR) system for tumor detection, nanovesicles were labeled with either a far-red fluorescent probe or conjugated with a dextran coated MR contrast agent; the ultra-small superparamagnetic iron oxide were placed into the xenografts. The nanovesicles demonstrated cancer-selective properties from both techniques. Thus, saposin C can be used as part of a theranostic agent in selective cancer detection and visualization.

Along with prosaposin, saposin C was found to be active as a neurotrophic factor for the stimulation of neurite outgrowth in murine neuroblastoma and choline acetyltransferases activity in human neuroblastoma cells (O'Brien et al., 1994). In a dose-dependent manner, both prosaposin and saposin C stimulated neurite outgrowth and increased choline acetyltranserase activity through a mechanism independent of the nervous growth factor, brain-derived neurotrophic factor and neurotrophin. Binding assays demonstrated that using saposin C as a ligand gave a high-affinity and a low affinity constant; and phosphorylation stimulation experiments showed enhanced phosphorylation of a variety of proteins in the presence of saposin C. A latter study by O'Brien et al. (1995) suggested that this neurotrophic activity of prosaposin is situated in the saposin C domain. A 22 amino acid peptide containing the saposin C active region (LIDNNKTEKEIL) was radiolabeled and identified high affinity binding sites for receptor-ligand interaction. It was also found that this sequence stimulates neurite outgrowth and choline acetyltransferases activity and preventing cell apoptosis in neuro-blastoma cells (O'Brien et al., 1995). These findings indicate that saposin C is a neurotrophic factor which stimulates signal transduction by binding to receptors and assists in protein phosphorylation.

You et al.(2003) suggested that saposin C induced patch-like domain membrane restructuring and destabilized phospholipid membranes by investigating saposin C's interaction with acid phospholipid membrane in an aqueous solution using atomic force microscopy. For the first time, saposin C provided evidence that the patch-like structural domains caused thickness increase and was independent of the acidic phospholipids; whereas membrane destabilization was dependent on acidic phospholipids. In addition, the membrane restructuring effects of saposin C on a structural basis was examined further using two synthetic peptides (H1 and H2), these peptides correspond to the alpha-helical domains 1 and 2 on saposin C. The authors

indicated that H1 did not induce any membrane restructuring, but H2 contributed to the formation of patch-like domains, only. Interestingly, it was also found that H1 can mimic saposin C's destabilization effects in conjunction with H2, but this was true only when H1 was present first and H2 was added afterwards. The composition of H1 and H2 were different, this suggested that their mode of action would be dissimilar. Thus, these researchers provided more insights on the structure-function studies of the interaction of phospholipids with saposin C (You et al., 2003). Another study by Alattia et al. (2007) supported You et al. (2003) findings by investigating the interactions of acid-glucosidase and saposin C with lipid bilayers. The saposin C's mechanism of action was suggested a three step process including the adsorption of the unfolded peptides at the membrane surface; through either hydrophobic or electrostatic forces, peptides can interact with the membrane; and once the peptide is inserted into the membrane, an alpha-helical structure would be adopted (You et al., 2003).

It was widely known that saposin C has an important role in stimulating enzyme activities and their interactions with lipid bilayers; the insight of these functions revealed by nuclear magnetic resonance (NMR). Hawkins et al. (2005) determined the three-dimensional structure of saposin C using NMR in the presence of sodium dodecyl sulfate (SDS) to demonstrate the membrane bound saposin C at the atomic level. SDS was used to mimic the membrane environment for these proteins thereby making the elucidation simpler. In the absence of SDS, saposin C was a compact monomer with its α-helices packed against each other and a hydrophobic core. As SDS was added, saposin C formed an open conformation with exposed hydrophobic pockets; where helix I moved close to helix V and helix II were spatially close to helices III and IV. This was similar to a monomer in the saposin B homodimer structure (Hawkins et al., 2005). The hydrophobic regions on saposin C are responsible for its interaction

with membranes under acidic pH (Alba et al., 2003; Hawkins et al., 2005). The largest conformational change occurred on the loops between helices one and two and between helices four and five. This change in conformation was dependent upon the relative concentration of saposin C and SDS. Structural studies of the saposin C with SDS suggested that membrane interaction was dependent on the presence of lysine residues (Hawkins et al., 2005). Favourable electrostatic interaction with negatively charged lipids was observed with the positively charged $Lys^{23}$ at the bottom of the hydrophobic pocket and other lysine residues near the edge of the pocket. Saposin C has binding preference to membranes which are composed of anionic phospholipids (Hawkins et al., 2005).

Solution state NMR has confirmed the previously determined saposin C structure, six α-helices and three disulfide bridges (Alba et al., 2003). Alba et al. (2003) investigated the titration of saposin C with phospholipid vesicles at various pH through solution NMR signal intensity by observing the $^{1}H$ and $^{15}N$ chemical shift changes through the $^{1}H$-$^{15}N$-HSQC spectra. The signals observed were from free proteins without binding to vesicles in the solution. Large vesicles of greater than 100 kDa introduced slow molecular tumbling and this broadened the NMR signals to an unobservable level. With the decrease in pH from 6.8 to 5.4, 35% of the saposin C molecules were bound to vesicles. Thus, binding of saposin C was favourable in the acidic pH. It was also observed that as the pH was increased to 6.8; the signal recovered. This suggested that the binding process was reversible. In addition, in order for saposin C to trigger membrane binding, the negatively charged electrostatic surface of saposin C was partially neutralized. The mutant of saposin C (replacing two Glu to Gln molecules) with decreased negative charge on the electrostatic surface supported the results obtained from the native saposin C. When saposin C was in neutral pH, charged amino acid side chains were solvent exposed, whereas all of the

hydrophobic residues were partially or totally buried in the protein core (Alba et al., 2003). As the environmental pH was lowered, the hydrophobic core of saposin C were solvent exposed. This suggested that the hydrophobic regions on the saposin C were responsible for lipid binding (Alba et al., 2003).

Alba et al. (2003) suggested that the charge on phospholipid membranes did not have a dominant role in saposin C-phospholipid interaction; saposin C interacted with neutral detergent Triton X-100. The key factor that affects interaction was the neutralization of the electrostatic surface on saposin C (Alba et al., 2003). Binding of saposin C with an electrostatic surface revealed through NMR was surprisingly different than the saposin-fold, found in all saposin members (Alba et al., 2003). The pH gradient did not affect membrane binding for Nk-lysin as its surface was positively charged (Liepinsh et al., 1997). The membrane interaction of plant specific insert from phytepsin was predicted to be through another mechanism than that in saposin C due to the difference in the electrostatic surface (Alba et al., 2003). Thus, membrane interaction with saposin-like proteins and saposins depended on the electrostatic charges and the environmental conditions.

To further confirm these findings from a phospholipid perspective, Abu-Baker et al. (2005) determined that the binding between saposin C to phospholipids (mixture of dioleoylphosphatidylglycerol (DOPG) and dioleoylphosphatidylserine (DOPS)) were concentration dependent under acidic conditions using solid-state NMR. Concentrations of 0 mol%, 1 mol% and 3 mol% of saposin C with respect to phospholipids were examined. Slight lipid binding was observed at 1 mol%, whereas for 3 mol %, the saposin C and phospholipid interactions were predominant. Although most lysosomal enzymes are the most active in acidic conditions, some have neutral pH optimums. The lysosomal pH can fluctuate between acidic and

the neutral conditions to accommodate both types of enzymes. A later study by Abu-Baker et al. (2007) suggested that saposin C could disturb the negatively charged POPC but not the neutral POPS. Saposin C was inserted into multilamellar vesicles consisting of either POPS or POPC and examined using solid-state NMR at neutral pH. From acidic conditions to the neutral pH, saposin C formed a stable complex with the lipids which disturbed the POPS bilayer. Unlike the results obtained by Alba et al. (2007), interaction was not observed for the neutral (POPC) lipid bilayer (Abu-Baker et al., 2007). Additionally, protonated saposin C could perturb POPS in the neutral pH, but not in POPC; and unprotonated saposin C did not have perturbation effects (Abu-Baker et al., 2007). The proposed structural model demonstrated that only saposin C's helix I and V were partially inserted in the phospholipid bilayer while the other regions of saposin C were exposed to the aqueous phase. These results contributed to the understanding for the saposin C structure-function relationships, interaction with phospholipids and as well as its functionality relating to other saposins.

#### 1.5.2.4 Saposin D

Saposin D is the least understood of the saposins. Although the structure of saposin C and D are very similar, saposin D does not stimulate glucosylceramidases' activities; rather, it is found to activate sphingomyelinase (Fiirst et al., 1988; Morimoto et al., 1988; Kishimoto et al., 1992). Morimoto et al. (1998) isolated saposin D from the spleen of patient with Gaucher to test its stimulation. Saposin D was found to be antibody specific and with Triton X-100, a low concentration of this domain can stimulate sphingomylinase at 100%. Thus, saposin D performed different activities as compared to the other three saposins. In addition, Azuma et al. (1994) suggested that saposin D was a ceramide modulator as it facilitated acid ceramidase activity in the hydrolysis forming ceramide and sphingosine. In a kinetic study, saposin D activity was

triggered by decreasing the $K_m$ value for ceramide and from the binding study, saposin D was able to bind to ceramide at neutral pH but not in the acidic pH (Azuma et al., 1994). These findings suggested that saposin D stimulates acid ceramidase based on the interactions with the enzyme. Thus, saposin D has a pivotal role in sphingolipid regulation. Moreover, Ciaffoni et al. (2001) demonstrated saposin D's ability to solubilize intralysosomal/late endosomal anionic phospholipid-containing membranes by the transformation of large vesicles to smaller particles. Saposin D's effect on solubilization was highly dependent on pH, lipid to saposin ratio, and the presence of anionic phospholipid. During the solubilization process, anionic phospholipids attracted saposin D from the medium until a critical value is reached; then, the membrane broke down into recombinant small particles (Ciaffoni et al., 2001). Thus, saposin D's functions remains unclear.

### 1.6 Other Saposin-Like Proteins

Saposin-like proteins could be derived from a variety of sources such as animals, humans, plants, fungi and microbes. In general, the imbalance of saposins A, B, C and D could lead to lysosomal storage diseases (Morimoto et al., 1990). However, within their normal levels, they are known to be sphingolipid hydrolase activators and have other diverse roles and applications.

From a nutritional perspective, Byers et al. (2014) suggested that goat milk prosaposin and its mature saposin A, B, C and D have therapeutic attributes and they were important for the development, maintenance and restoration of the nervous system of mammals. Both prosaposin and saposin C are found present in all breeds of goat's milk; prosaposin and all of its mature saposins have been identified in caprine's milk. These results were verified through gel

electrophoresis (Byers et al., 2014). The abundance of these neurotrophic prosaposins and mature saposins in goat's milk are associated with potential health benefits.

Despite the conserved structure of other saposin-like proteins, they also have various biological functions in plants, animals and humans. Espino and Hillyer (2003) elucidated a saposin-like protein encoded from cDNA of *Fasciola hepatica* (FhSAP-2) with a conserved feature of six cysteine residues arranged within five amphipatic α-helical domains and seven hydrophobic residues. This saposin-like protein has significant homology to *F.hepatica* NK-lysin and other saposin-like proteins. FhSAP-2 is highly affective with rabbit and human sera infected with *F.hepatica*, and significant lytic activities on human erythrocytes and peripheral blood mononuclear cells (Espino and Hillyer, 2003). Additionally, it is found that the recombinant saposin-like protein from *Fasciola hepatica* has similar properties (Gram et al., 2006). Three different saposin-like proteins were isolated from various stages of *F.gigantica* with antiserum properties against the parasite's excretion/secretion antigens (Gram et al., 2006). *Fasciola* could give rise to various saposin-like proteins performing different functions.

NK-lysin is another member of the saposin-like protein family and an antimicrobial and antitumor polypeptide. It also has lytic activities against bacteria, fungi and protozoan parasites (Hong et al., 2008). Additionally, Don et al. (2008) suggested that the saposin-like protein expressed from the gastrodermis of *Schistosoma mansoni* (Sm-SLP-1) was hemolytic and it had immunogenic properties. The expressed saposin-like protein was tested for its recognition by sera from chronically infected humans and mice and the vaccine efficacy was tested in a mouse model. In both the human and the mouse model, specific antibody recognition to the saposin-like protein was observed. However, the mouse model tested for vaccine efficacy was not successful. Thus, further exploration for host-parasite interactions would be required.

A disulfide cross-linked construct of 34-residues termed mini-B was found in surfactant protein B (in lungs); it had α-helical N- and C-terminal domains closely mimicking important components of the saposin-folding patterns of surfactant protein B, exhibiting membrane-lipid interactions (Waring et al., 2005). Mini-B's activities were dependent on the three dimensional structure and its charge distributions. It interacts through its cationic residues with anionic lipids, similar to previously described in saposin C (Abu-Baker et al., 2007). It was also found that mini-B's active site configuration has been observed in the N- and C-terminal domains of other saposins. This gives rise to mini-B and surfactant protein B as a saposin-like protein. The calcium binding protein derived from *Histoplasma capsulatum* also adopts a saposin fold (Beck et al., 2009). This protein functions in lipid binding such as its interaction with glycolipids. However, it has no homology with other calcium binding proteins and it does not contain any identified calcium binding motifs (Beck et al., 2009). The virulence mechanism of this fungal calcium binding protein has not been elucidated.

Recently, Michalek and Leippe (2015) determined that invaposin, a saposin-like protein from *Entamoeba invadens* exhibited lipid solubilizing activities extracting phospholipids from whole membrane bilayers, similar to saposin B. Unlike most other saposin-like proteins produced from amoeboid protozoans, invaposin does not have cell lytic properties. Invaposin is similar to saposin A-D and the plant specific insert in potatoes and shows pH dependecy; it changes conformations from a closed to an open form in the presence of membranes, selectively binds to anionic lipids, aggregated lipid vesicles, dimerized upon acidification and becomes monomeric at pH above 4.5 (Michalek and Leippe, 2015). However, unlike saposins and the plant specific insert from potatoes, invaposins does not induce membrane permeabilization, vesicle leakage, it does not exhibit antimicrobial activities, therefore, it does not perturb

membranes (Michalek and Leippe, 2015). In addition to the saposin-like proteins, many others are present. For example, acyloxyacyl hydrolase is a phagocytic cell lipase, acid sphingomyelinase is a sphingolipid hydrolase, amoebapore A has pore-forming activities in *Entamoeba histolytica* granule protein, amoebapore B and amoebapore C both have pore-forming activities in *E. histolytica* granule protein, and NK-lysin plays a role in the lysis of procine T cell and NK cell granule proteins (Clayberger and Krensky, 2003). Thus, saposin-like proteins have diverse functions.

## 1.7 The Plant Specific Insert

### 1.7.1 Evolution

It had been predicted that the development of the plant specific insert took place very early in plant evolution. The exact reason was still unknown. However, possible ways that this occurred had been suggested: new exon insertion was made during a stage of evolution or it was introduced through introns-exon exchange (Cordeiro et al., 1994). In addition, as demonstrated through the positions of introns and exons, gene coding for aspartic proteases are likely to be highly conserved. It was shown that the plant specific insert region corresponds to intron 7 of the mammalian enzymes, giving rise to the possibility that the mammalian intron genes correspond to the exon of the plant genes encoding the plant specific insert (Cordeiro et al., 1994). Cordeiro and colleagues further examined the positions of introns and exons through isolating plant genes encoding an aspartic proteinase, cyprosin. To date, it is not apparent that other research groups have explored the evolution of plant specific insert in detail.

### 1.7.2 Structure

A major distinguishing feature between the plant aspartic proteases compared to mammalian and microbial aspartic proteases is the presence of the plant specific insert (PSI)

located at the C-terminal domain (Kervinen et al., 1999; Simoes and Faro, 2004; Bryksa et al., 2011; De Moura et al., 2014; Munoz et al., 2014). The plant specific insert is approximately 100 residues and its structure resembles those of saposin-like proteins. Hence, it belongs to the saposin-like protein family. Most plant aspartic proteases contained a plant specific insert except for barley nucellin, tobacco chloroplasts and the cdr-1 encoding gene from *Arabidopsis* (Simoes and Faro, 2004). The plant specific insert is conserved in structure and contains five amphipathic alpha-helices that fold into a compact conformation; six cysteine residues form the three stabilizing disulfide bridges and a glycosylation site (Frazao et al., 1999; Kervinen et al., 1999; White et al., 1999; Egas et al., 2000; Bryksa et al., 2011; Munoz et al., 2014). In the plant specific insert of *Solanum tuberosum* (potato) aspartic protease, barley aspartic protease, cyprosin aspartic protease and in various other sources, the N and C-terminal domains are swapped compared to the saposin-like proteins (Kervinen et al., 1999; White et al., 1999; Egas et al., 2010; Bryksa et al., 2011; Munoz et al., 2014). Thus, the plant specific insert is termed a swaposin.

To date, two plant specific insert have been elucidated in detail: the plant specific insert from barley phytepsin and from *Solanum tuberosum* aspartic protease (StAsp-PSI). Kervinen et al. (1999) reported that the plant specific insert from phytepsin had a closed saposin fold and it shared topology with NK-lysin, containing 59% of alpha-helices in its secondary structure. These alpha-helices organize in an up-down-up-down manner and interact through the hydrophobic side chains and disulfide bridges located at: $Cys^{6}$–$Cys^{100}$, $Cys^{31}$–$Cys^{72}$ and $Cys^{37}$–$Cys^{69}$ (Kervinen et al., 1999). The plant specific insert has a hydrophilic outer surface with a hydrophobic inner region. In the mature enzyme, side chains form the hydrophobic core through the interface between the plant-specific domain and the mature phytepsin. This is surrounded by

hydrogen bonds and ionic interactions (Kervinen et al., 1999). In addition, all lysine side chains of the PSI domain of the mature enzyme are important in the formation of a positively charged ring surrounding the hydrophobic region.

In contrast to the plant specific insert of phytepsin, the StAP-PSI has an open, V-shaped conformation (Bryksa et al., 2011). The helical structures represent approximately 54% followed by 40% of random structures and 6% of beta-sheet components of the secondary structures. In hydrophilic environments, StAsp-PSI is present in the monomeric form; whereas in hydrophobic conditions, dimers are apparent (Munoz et al., 2011). Bryksa et al. (2011) reported that in the acidic conditions, high helix content was present, and that the stability of the structure depends on the presence of disulfide bridges formed by cysteine residues. In agreement with Bryksa et al. (2011), Munoz et al. (2014) found helical and unordered structures with a high degree of conformational stability of the StAsp-PSI in solution. At 20 ℃, the secondary structure was composed of about 13% turns, 26% alpha-helices, 28% of random coils and 33% of beta-sheets. An increase in aggregated structure was apparent with an increase in temperature from 45 to 50 $^{\circ}$C. In addition, no secondary structure changes were observed when StAsp-PSI interacted with membranes. The interaction was similar to hemaglutinin fusion peptides, resulting in pH-dependent bilayer fusogenic activities which arose from helix-kink-helix motif at the StAsp-PSI's N-terminus (Bryksa et al., 2011). From the tertiary and quaternary structures, the StAsp-PSI resembles a boomerang shape and with four helices. The disulfide linkage between Cys6 and Cys99 connects helix 1 and helix 4, the disulfide linkage between Cys31 and Cys71 cross-links helix 3 to helix 2, and another disulfide links $Cys^{37}$ and $Cys^{68}$ (Bryksa et al., 2011). As a tight dimer is formed, polar residues are on the protein surface, while hydrophobic residues were buried within the protein (Bryksa et al., 2011). De Moura et al. examined the StAsp-PSI structure

and found that the closed conformation resembling the classic saposin fold also exists. However, unlike the PSI in barley phytepsin in which the saposin fold remains attached to the N-and C-termini of the parent enzyme, StAsp-PSI exists in a free form (De Moura et al., 2014). This form was mainly adopted by the monomeric PSI, corresponding to helices 1 and 4 collapsing onto helices 2 and 3 (De Moura et al., 2014). The structure of the plant specific insert from aspartic proteases can be compared with those in the saposin-like protein family.

### 1.7.3 Homology of Plant Specific Insert with the Saposin-like Protein Family

The plant specific insert does not have sequence homology with mammalian or microbial aspartic proteases (Simoes and Faro, 2004). However, similar mechanistic functions are observed between the plant specific insert and the saposin-like protein family due to their high sequence homology (Kervinen et al., 1999; Egas et al., 2000; Tormakangas et al., 2001). The plant specific insert of cyprosin has similar activities to saposin C such as lipid-binding. However, it does not exhibit neurite outgrowth (Brodelius et al., 2005). In terms of its structure, the plant specific insert has remarkable similarities to saposin B, granulysin, saposin C and NK-lysin: length and position of the helices, three disulfide bridges and a kink between helices three and four. In general, between the mature saposin and the plant specific insert, approximately 40% identity of over a 35 residue stretch is observed (Brodelius et al., 2005). The structure of the plant specific insert from phytepsin in barley has also been compared with NK-lysin (Kervinen et al., 1999) and saposin C (Tormakangas et al., 2001). As in cyprosin, structural data and sequence homology of phytepsin has comparable structural similarities to NK-lysin and saposin C. However, the plant specific insert's N- and C-terminal domains in phytepsin are swapped. The swapping does not influence the orientation or the direction of the helices of phytepsin (Kervinen et al., 1999). The major difference between the plant specific insert of phytepsin, NK-lysin and

saposin C is the loop connecting helices H3 and H4. It is unknown whether if the plant specific insert can effectively replace the functions of NK-lysin or saposin C, or vice versa.

Recently, the plant specific insert from potatoes, *Solanum tuberosum*, was elucidated. Similar to barley's phytepsin, the plant specific insert from potatoes also had its N-and C-terminals swapped, named a swaposin (Guevara et al., 2005; Bryksa et al., 2011). Its structure has high similarities with NK-lysin, granulysin and saposin C: cysteine residue boundaries, amphipathic alpha-helices folding into a globular domain and linked to each other by two disulfide bridges (Munoz et al., 2010). Munoz et al. (2010) explored the sequence identity of the plant specific insert from potatoes to other plant specific inserts. It was observed that the highest being 95% identity with LycoAP-PSI from *Lycopersicon esculentum*. The plant specific insert of potatoes has high sequence similarity with other plant specific inserts and the saposin-like proteins.

### 1.7.4 Plant Specific Insert during Proteolytic Processing

In the monomeric plant aspartic protease, the plant specific insert is retained within the enzyme; whereas in the heterodimeric plant aspartic protease, the plant specific insert is partially or completely cleaved off during processing and maturation (Simoes and Faro, 2004). Ramalho-Santos et al. (1998) suggested that the plant specific insert from cardosin A, which was isolated from the flowers of cardoon, is completely removed after proteolytic processing in the acidic condition. Sequence analysis demonstrated that the plant specific insert was comprised of amino acids from $Asn^{313}$-$Ser^{416}$ in the cardosin A. This sequence is located between the 31 kDa fragment and the 15 kDa fragment as the cleavage site borders between the 31 kDa fragment (including prosegment and N-terminus) and the plant specific insert and between the plant specific insert and the 15 kDa fragment in the C-terminus. In addition, immunoblot analysis

demonstrated that the plant specific insert removal occurred under acidic conditions. From the extract of immature pistils at pH 3, the reaction of the anti-PSI Ig with procardosin A did not occur; whereas at pH 7, a partial reaction was exhibited. The addition of pepstatin at pH 3 inhibited proteolytic processing of the plant specific insert and suggests that cleavage is carried out by an aspartic protease, possibly by cardosin A itself (Ramalho-Santos et al., 1998). Thus, the removal of the plant specific insert gives rise to mature aspartic protease similar to those observed in mammals and microorganisms.

### 1.7.5 Functions

Plants rely on their innate immunity as a first line of host defense against external pathogens. It was discovered that the PSI from plant aspartic proteases had an imperative role for the innate immunity in plants. Like saposins and various other members in the saposin-like protein family, plant specific insert was discovered to have antimicrobial (Guevara et al., 2005; Munoz et al., 2010), antifungal (Curto et al., 2014), vacuolar targeting/sorting (Faro et al., 1999; Kervinen et al., 1999; Tormakangas et al., 2001), membrane disruption (Munoz et al., 2011; Munoz et al., 2014) and vesicle leakage activities (Egas et al., 2010; Bryksa et al., 2011). These self-defense mechanisms are essential for the natural health of the plant.

Kervinen et al. (1999) suggested that the plant specific insert from barley's phytepsin or prophytepsin have important roles in vacuolar targeting and membrane binding activities. This was also observed from the plant specific insert of cardosin A (Faro et al., 1999). Possibly with membrane-bound receptor proteins in the Golgi apparatus, the plant specific insert brings phytepsin into contact with membranes. The resulting complex including the enzyme targets the vacuoles in the form of vesicles. The prophytepsin is then activated by proteolytic cleavage and the plant specific insert is subsequently removed which breaks the interaction of the membrane

receptor or the membrane itself (Kervinen et al., 1999). The mature phytepsin is formed as a result. Consistent with these findings, Tormakangas et al. (2001) further suggested that the plant specific insert also influences the route that phytepsin takes after leaving the endoplasmic reticulum, in addition to vacuolar sorting. It is currently unclear whether the plant specific insert has two sorting signals: one for the endoplasmic reticulum export or another one for vacuolar sorting or if the vacuolar sorting motif is recognized at the endoplasmic reticulum export site. Tormakangas et al. (2001) determined that removing the plant specific domain has no effect on phytepsin's activity; however, it does cause an accumulation of phytepsin in the extracellular space of the plant. These findings confirmed the plant specific insert's role in vacuolar target and sorting.

The plant specific insert is essential in the formation and proper folding of the active mature enzyme. White et al. (1999) reported that the plant specific insert from cyprosin has an important role in ensuring that the parent polypeptide is properly folded and the activation of the enzyme. Brodelius et al. (2005) had similar findings in terms of peptide folding and activation. In addition, these authors examined saposin C and the plant specific insert for their activation activity for glucosylceramidase. All these domains were found to have enzyme activation properties. However, it was shown that the peptide sequence responsible for activation in saposin C was partially different from the corresponding sequence in the plant specific insert (CKTLVSQYGKTMIEMLL). This suggests that the primary structure of the domain is not required for the activation of the enzyme but the secondary and tertiary structures of the peptide region are essential (Brodelius et al., 2005). In terms of lipid binding, the plant specific insert has a conserved hydrophobic patch mainly embedded in the insert's domain that is responsible for its function: $Phe^{280}$ and $Ala^{301}$ of the mature protein and $Met^{320}$, $Val^{323}$, $Trp^{324}$, $Leu^{345}$ and $Leu^{349}$ of

the PSI (Brodelius et al., 2005). This is different with respect to saposin C, where the hydrophobic patch is mostly in the protein. These results suggest that the mechanism of action for the plant specific insert might be different than those in saposin C. In fact, binding achieved through the plant specific insert involved hydrophobic interactions and ionic bonding between basic residues located around the hydrophobic surfaces and the negatively charged phospholipid head groups on the membrane surface. From these dissimilarities, unlike saposin C, the plant specific insert cannot bind to the receptors on the nerve cells (Brodelius et al., 2005). Thus, the plant specific insert does not exhibit any neurogenic activity.

Egas et al. (2000) reported that the plant specific insert in procardosin can induce vesicle leakage under acidic conditions. Fluorescent probe calcein was trapped inside vesicles to monitor vesicle leakage. It was observed that no release of calcein particles under physiological pH; however, decreasing pH increased the release of calcein. The optimal pH to induce vesicle leakage was observed at pH 4.5. The destabilization of phospholipid membranes causing vesicle leakage was also phospholipid composition dependent. It was found that the combination of acidic phospholipids in acidic conditions produced the best results (Egas et al., 2000). Supporting these findings, Bryksa et al. (2011) examined the StAsp-PSI in inducing vesicle leakage and also did not observe leakage in neutral vesicles. However, it was found that PSI caused a rearrangement of an acidic phospholipid bilayer and resulted in an increased thickness and membrane destabilization (Egas et al., 2000). This finding agrees to the previous optimal conditions determined (Bryksa et al., 2011).

The StAsp-PSI also has antimicrobial (Guevara et al., 2005; Munoz et al., 2010) and antifungal properties (Curto et al., 2014). In the defense against late blight disease, StAsp-PSI was found to reduce cell viability and cause membrane permeabilization of *P.infestans* (Munoz

et al., 2010). The plant specific insert can reduce the spore viability and spore germination in both *P.infestans* and *F.solani*. Stronger antimicrobial properties of the PSI were found against *P.infestans* and are mediated through plasma membrane permeabilization in spores of the microbial causing cell death. The cysteine bridges from tertiary structure of the StAsp-PSI are essential for cytotoxic activities and binding capacities (Munoz et al., 2010; Bryksa et al., 2011). The plant specific insert in the aspartic protease can either function alone or in conjunction with the enzyme as a defensive mechanism against pathogens.

The plant specific insert is found in the protective tissues of plants such as the epidermal, roots, stems and part of the flower (Brodelius et al., 2005). The plant specific domain is germane for plant defensive response and regulating lipid metabolism. They are responsible for protection against pathogenic microorganisms and are important for the growth and turnover of plant cells.

### 1.8 Nuclear Magnetic Resonance

Nuclear magnetic resonance (NMR) spectroscopy is known as one of the most important and powerful techniques for elucidating the conformation, structure, dynamics and interactions of biological molecules such as proteins (Berg et al., 2002; Pietzsch, 2003; Rangus, 2007; Marion, 2013). It has taken over 60 years to reach the modern interdisciplinary technology (Marion, 2013). Table 1 outlines the key advancements of the NMR technology through history.

| Protein NMR Through History | | |
|---|---|---|
| **Year** | **Personnel** | **Significance** |
| 1946 | Bloch, Purcell | First NMR |
| 1955 | Solomon | Nuclear Overhauser Effect (NOE) |
| 1966 | Ernst, Anderson | Fourier Transform NMR |
| 1975 | Jeener, Ernst | 2D NMR |
| 1985 | Wutherich | First solution structure of a small protein (BPTI) from NOE derived distance restraints |
| 1987 | Not Available | 3D NMR and isotopic labeling of recombinant proteins |
| 1990 | Not Available | Pulse field gradients |
| 1996/7 | Not Available | New long range structural parameters, TROSY |

**Table 1.1 Key advancements of Protein NMR through history are outlined. Information adapted from Sattler (2004) lecture slides.**

NMR is practical for a wide range of applications through either solution state NMR or solid-state NMR. Some of the predominant uses include: structural characterization for proteins, nucleic acids and sugars; conformational dynamics and mobility of biomolecules in solution; chemical exchange and conformational exchange; enzyme mechanism and chemical reactions; folding studies of proteins; and interactional studies (Sattler, 2004).

In bimolecular NMR, half spin nuclei, including $^{1}H$, $^{13}C$ and $^{15}N$ are the mostly used. In proteins, the most abundant half spin nucleus is hydrogen ($^{1}H$). In contrast, no NMR signals would be produced in the most abundant isotopes of carbon ($^{12}C$) and oxygen ($^{16}O$), while broad signals would be detected on nitrogen ($^{14}N$), which hinders the application of $^{14}N$ in biomolecules (Marion, 2013). Table 2 shows the most common half spin nuclei and their natural abundance. Due to the low abundance of $^{13}C$ and $^{15}N$ in proteins, these atoms need to be enriched through isotopic labeling, which enhance the sensitivities. Briefly, this is performed by using a nutrient controlled minimal media which only has the desired isotopes for the specific types of elements. Commonly, nitrogen is labeled with ammonium chloride ($^{15}NH_4Cl$) to obtain the desired $^{15}N$ uniformly isotope-labeled in proteins, and $^{13}C$ labeling of protein is achieved by using $^{13}C_6$-D-Glucose (Teng, 2013).

| Common ½ Spin Nucleus | Natural Abundance (%) |
|---|---|
| $^{1}H$ | 99.98 |
| $^{13}C$ | 1.11 |
| $^{15}N$ | 0.36 |
| $^{31}P$ | 100.00 |

**Table 1.2 Natural abundance of the common half spin nuclei (Teng, 2013).**

The atomic nuclei with odd mass numbers can rotate around a given axis. By applying an external magnetic field ($B_0$), the rotating nuclei will precess around the axis of the applied magnetic field (Sattler, 2004). This generates a signal known as the free induction decay (FID) and it is measured as a function of time in the x- and y- directions perpendicular to the magnetic field. The time domain FID signal is subsequently converted through Fourier Transform into frequency, labeled in hertz (Hz), and displayed as a chemical shift in parts-per-million (ppm) on the NMR spectrum (Marion, 2013). The chemical shift is converted through the following equation:

$$\delta(ppm) = 10^6 * \frac{\nu - \nu o}{\nu o} \qquad (1)$$

Where $\delta$ is the chemical shift in ppm, $\nu$ is the resonance frequency in Hz, and $\nu o$ is the reference frequency. Thus, the use of chemical shift in ppm can compare the resonance lines in the spectra obtained from different external magnetic fields (Marion, 2013).

Chemical shifts can provide information on the surrounding environment and act as a blue print to the compound of interest (Tekely and Malcolm, 2002; Higman, 2012). In proteins for example, the amide proton (HN) resonates at around 8 ppm, the Hα spins have resonance frequencies at around 4 ppm, and the methyl protons are around 1 ppm (Sattler, 2004; Hitchens, 2006). The difference in chemical shift is due to the electronegativity of the atoms and it provides a way of determining the chemical environment of the nucleus (Tekely and Malcolm, 2002). Chemical shifts are displayed from right to left on an axis, where the small and negative chemical shifts are the upfield and large chemical shifts are referred as the downfield (Higman, 2012).

Chemical shifts have high sensitivity to the electronic environment of a nucleus. A slight change in the covalent molecular structure or non-covalent interactions can cause chemical shift

perturbations (Higman, 2012). Generally, a $^{1}H$-$^{15}N$ Heteronuclear Single Quantum Coherence (HSQC) is used as the first experiment to identify and monitor the quality of the sample of interest as the cross peaks of each amino acid could be observed (Higman, 2012), except for proline which had no amide group. Altering the environment of the sample or adding an interaction partner such as a phospholipid may cause structural changes on the sample of interest (Higman, 2012). Thus, chemical shift perturbation will be observed.

NMR can be used to measure the movements of individual molecular groups in protein or whole domains of proteins, as it can measure dynamic motions on a time scale between a billionth of a second to a few seconds. The rapid and effective measurements make it ideal in determining protein structure and folding (Pietzsch, 2003). Figure 1.2 displays the time scale in high resolution NMR. Fast motions are identified closer to the 1 ps terminal and slow motions are referred to the 1 s terminal (Sattler, 2004). For example, the chemical exchange within part of the protein occurs between the microseconds to the milliseconds motions (Higman, 2012).

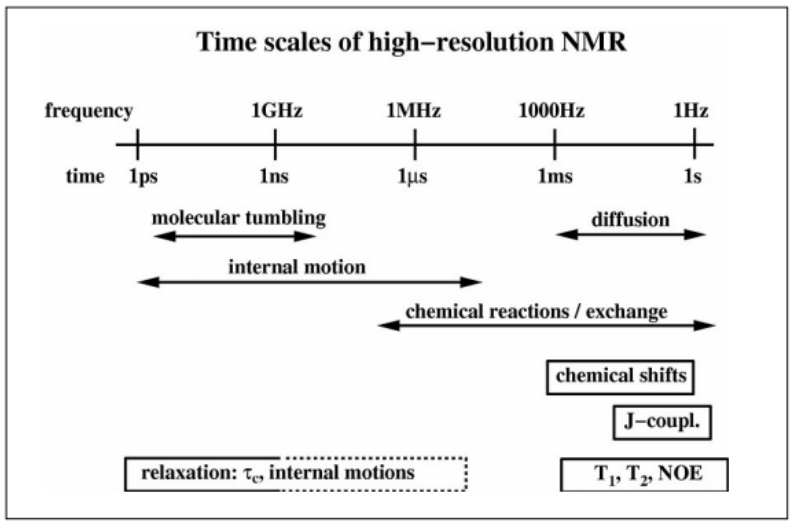


**Figure 1.2 Motion of atoms from a time scale perspective in NMR (Sattler, 2004) lecture series.**

### 1.8.1 NMR Sample Preparation

An NMR sample can be in the liquid form for solution state NMR or in the solid form for solid-state NMR. The protein used in NMR can be recombinantly expressed from a bacterial host and subsequently purified prior to sample preparation with isotopic labeling. The foundation of a high quality NMR spectrum requires good signal-to-noise ratio and high spectral resolution (Wider, 2000). To achieve this, protein molecules larger than 10 kDa requires to be isotopically labeled with $^{13}C$ and $^{15}N$ isotopes, larger molecules of 25 kDa or above require a $^{2}H$-labeling (Wider, 2000). In solution state NMR, upon obtaining the pure protein sample, selecting a suitable buffer is imperative. Samples in solution state NMR requires an addition of 5 % $D_2O$ for locking the frequency (Wider, 2000). In contrast, in solid-state NMR, sample homogeneity is crucial in order to produce sharp signals (Teng, 2013). For solid-state NMR, the typical sample amount is between 1 to 10 mg depending on the size of the rotor used. However, small sample size should be tested to obtain the ideal experimental condition (Teng, 2013).

### 1.8.2 Solution State NMR

Solution state NMR can provide spectra with good resolution and high sensitivity for molecules less than 40 kDa (Wider, 2000). Smaller protein molecules can rotate rapidly in solution, producing sharp resonances and narrow lines (Rangus, 2007; Marion, 2013). Larger molecules are difficult to characterize in solution state NMR as they tumble slower and result in fast relaxation. The NMR spectrum would consequently be composed of broader lines and it becomes extremely difficult to be interpreted (Wider, 2000). With high sample quality and small molecular size, solution state NMR can provide both structural and dynamical information at a residue-specific level. The information obtained is utmost important for the study of dynamic systems.

### 1.8.3 Solid-State NMR

In contrast to solution state NMR, solid-state NMR requires a sample that is in the solid or semi-solid form. Solid-state NMR is a good candidate to determine the molecular structure and dynamics of membrane proteins and to examine the protein-membrane interactions. However, the resulting spectrum often consists of broad resonances due to the absence of molecular tumbling, which introduce anisotropic chemical shift and strong dipolar couplings (Wider, 2000). To achieve high resolution NMR spectra, magic-angle-spinning (around an angle of 54.3 $^{o}$ between rotating axis and external field) are usually used to average the CSA and the DD (Schurko, 2003). Solid-state NMR can provide the same types of information as in solution state NMR when specific techniques are employed to improve the resolution.

### 1.8.4 Backbone Assignment

The sequence specific spectra resonance of a protein must be identified through protein backbone assignment prior to studying its structure and dynamics (Teng, 2013). Following the 2D $^{15}$N HSQC, backbone assignment is usually carried out through a series of 3D triple-resonance experiments including HNCA, HNCO, HNCACB, CBCA(CO)NH, HN(CO)CA, and HN(CA)CO (Higman, 2012; Teng, 2013). Methods for backbone resonance assignment of proteins with moderate size (MW less than 30 kDa) usually require $^{15}$N and $^{13}$C isotropic labeled proteins (Higman, 2012). In contrast, large proteins over 30 kDa tumble slowly in solution and will produce broad NMR spectra with many cross-peaks overlapped with each other. Consequently, protein deuteration is needed for the NMR assignments of larger proteins (Higman, 2012). In addition to protein deuteration, spectra collection on large proteins may require spectrometer with magnetic fields higher than 750 MHz. In this case, techniques such as TROSY can be employed to further improve the spectral resolution (Higman, 2012). This section

outlines the most commonly used experiments for the sequence specific backbone assignment in proteins.

$^{1}$H-$^{15}$N-HSQC

The $^{1}$H-$^{15}$N-HSQC experiment is a type of 2D experiment that was usually conducted on protein as the first heteronuclear experiment. It provides a 'fingerprint' for the protein molecule as it, in principle, shows all of the H-N correlations of every amino acid except for proline (Higman, 2012). On the HSQC spectrum, side chains from tryptophan, asparagine and glutamine may also be present as they have HN groups. HSQC provides a simple and efficient assessment in determining the sample condition and whether if additional labeling is necessary for producing higher quality spectra. Figure 1.3 presents the magnetization transfer for HSQC.

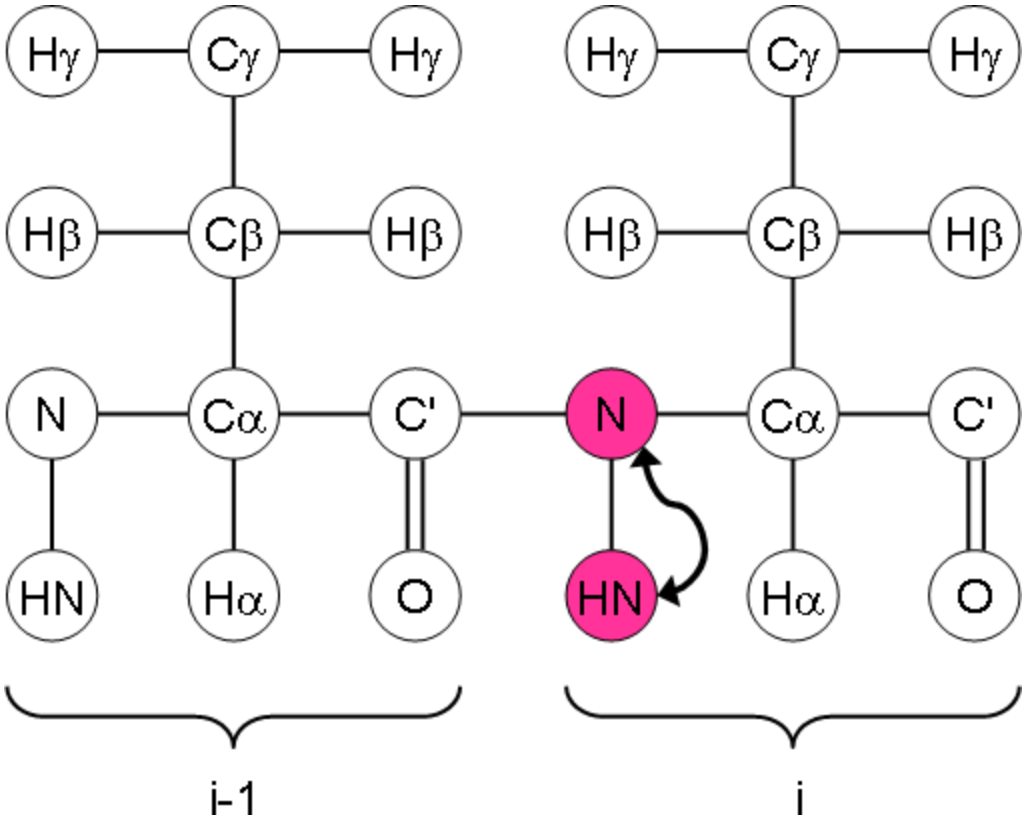


**Figure 1.3 Magnetization transfer as the name of the experiment depicts. The magnetization is transferred from the amide hydrogen to the nitrogen and back to the hydrogen. Figure is adapted from Higman (2012).**

HNCO

HNCO provides information on the backbone HN and CO of the proceeding amino acid and it is the most sensitive triple-resonance experiment (Higman, 2012). In HNCO, magnetization is transferred from the amide proton to the amide nitrogen and then to the carbonyl carbon via *J*-coupling based transfer mechanism, then the magnetization is transferred back to the proton for detection (Higman, 2012). The chemical shifts were recorded on $^{15}N$ and $^{13}C$ for indirect detection, and on $^{1}H$ for direct detection, which results in a three-dimensional spectrum. Combination of the HNCO and HN(CA)CO can provide sequential connections. Figure 1.4 presents the magnetization transfer for HNCO.

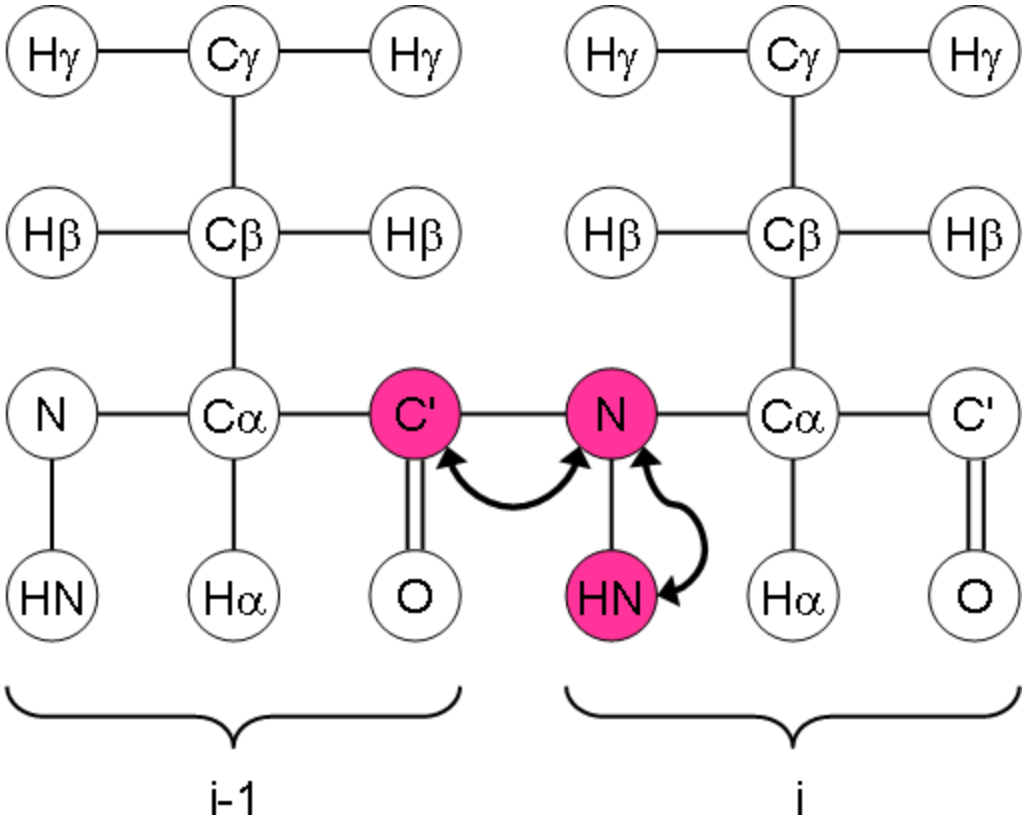


**Figure 1.4 Magnetization transfer for HNCO as the name of the experiment depicts. Figure is adapted from Higman (2012).**

HN(CA)CO

HN(CA)CO provides backbone assignment information when it is applied in conjunction with HNCA, HN(CO)CA and HNCO (Higman, 2012). In this experiment, magnetization is transferred from the amide hydrogen to the nitrogen and then via the Cα through J-coupling to the carbonyl carbon, then the magnetization is transferred back (Teng, 2013). As the amide nitrogen is coupled to the preceding residue, magnetization transfer also occurs for the previous residue. The chemical shift is recorded for $^{1}H$, $^{15}N$ and $^{13}CO$, bypassing $^{13}C\alpha$ as the magnetization transfer without chemical shift evolves (Higman, 2012). As both magnetization experiments produce a signal, the coupling in the present residue is stronger than the preceding residue, resulting in a stronger signal (Higman, 2012). Figure 1.5 represents the magnetization transfer in HN(CA)CO. Analyzing the information obtained in both HNCO and HN(CA)CO, chemical shifts of the residue and the previous residue can be achieved.

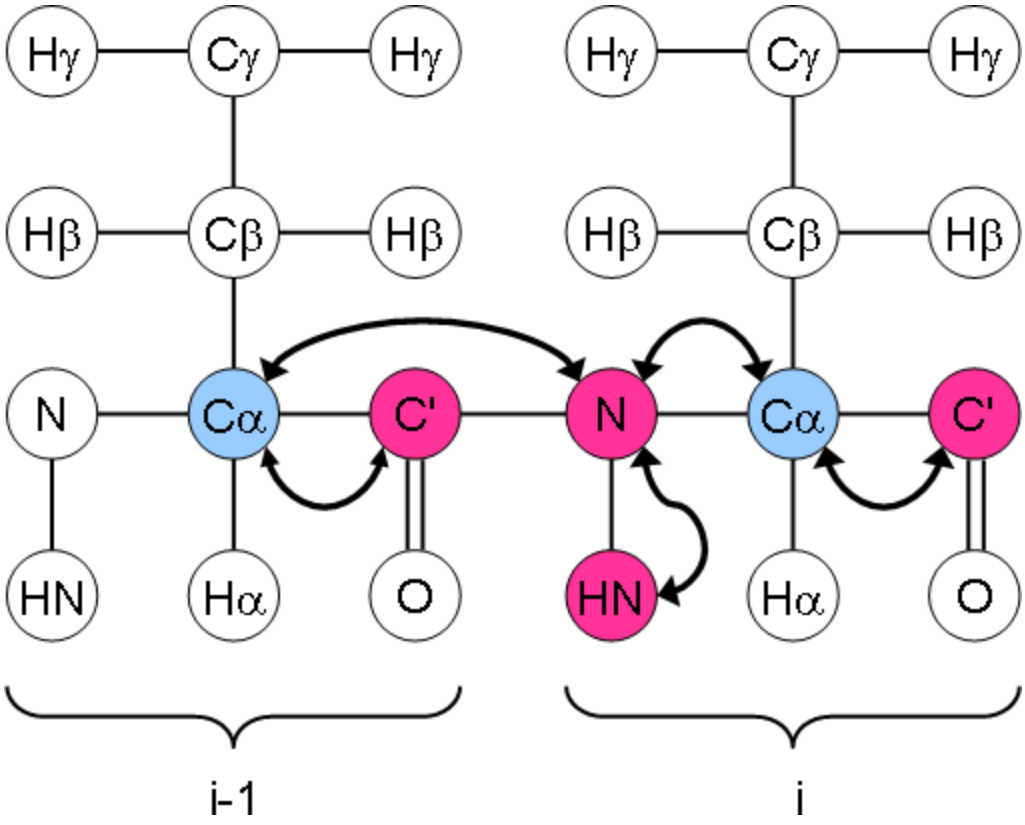


**Figure 1.5 Magnetization transfer for HN(CA)CO as the name of the experiment depicts. Figure is adapted from Higman (2012).**

HNCA

HNCA is a useful experiment for backbone resonance assignment by combining with HN(CO)CA in distinguishing between the Cα and the Cα of the preceding residue (Higman, 2012). In HNCA, magnetization is transferred from the amide hydrogen to the nitrogen, then to Cα and back for detection. As in HNCA, the amide nitrogen is coupled to the Cα and the Cα of the proceeding residue; both signals are visible on the spectrum (Higman, 2012). Figure 1.6 presents the magnetization transfer in HNCA.

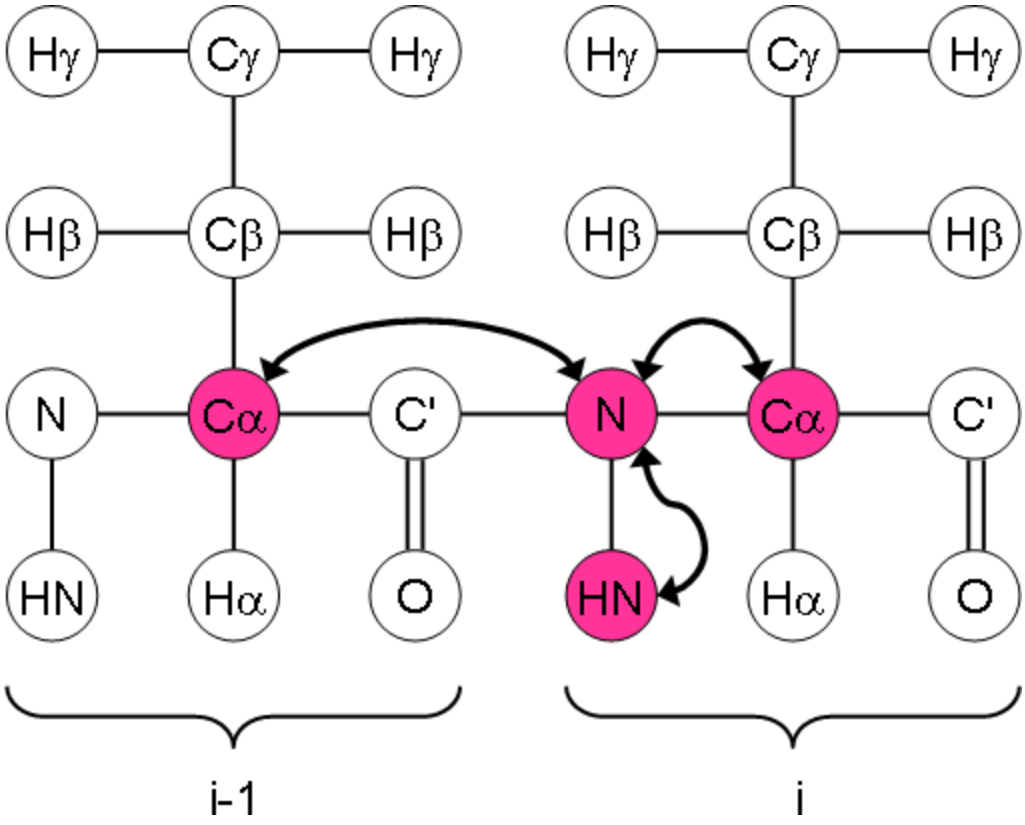


**Figure 1.6 Magnetization transfer for HNCA as the name of the experiment depicts. Figure is adapted from Higman (2012).**

HN(CO)CA

HN(CO)CA provides information of the chemical shift of Cα from the preceding residue. This information is useful for backbone assignment when it is combined with HNCA (Higman, 2012). In HN(CO)CA, the magnetization is transferred from the amide hydrogen to the nitrogen, bypassing the carbonyl carbon, and to the Cα of the proceeding residue and back for detection. The result provides the same information as in HNCA but it is selective for Cα of the previous residue (Teng, 2013). Figure 1.7 presents the magnetization transfer in HN(CO)CA.

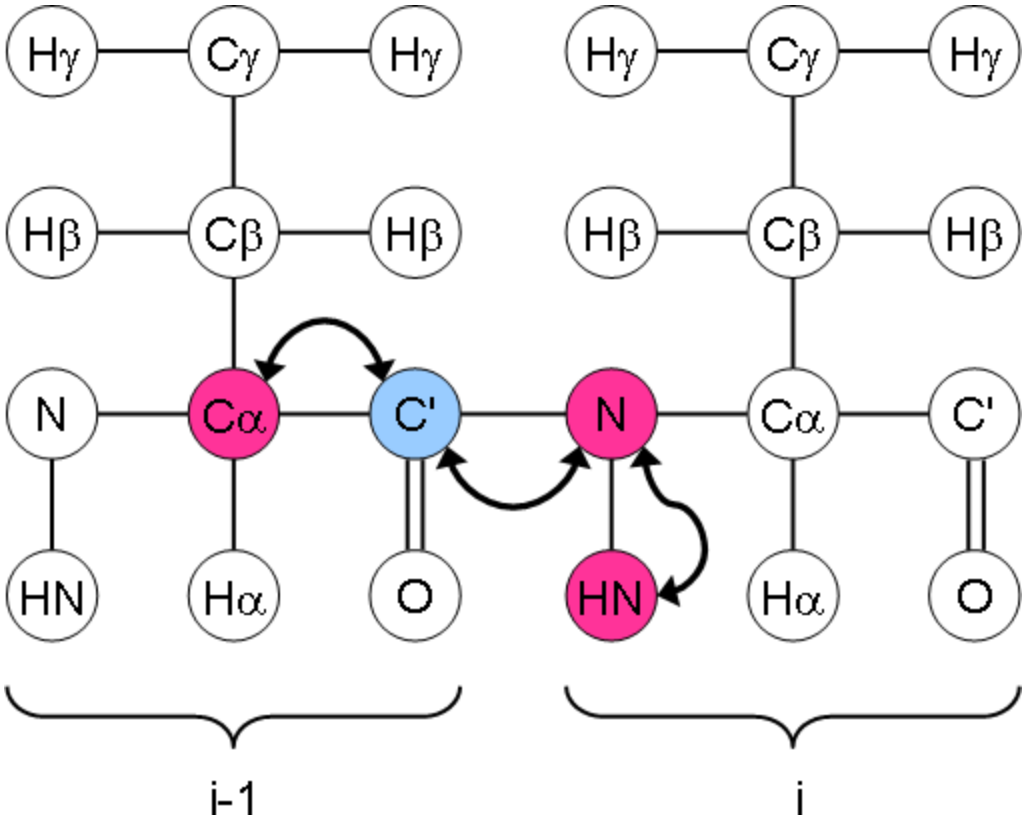


**Figure 1.7 Magnetization transfer for HN(CO)CA as the name of the experiment depicts. Figure is adapted from Higman (2012).**

CBCA(CO)NH/HN(CO)CACB

In the CBCA(CO)NH experiment, the Cα and Cβ chemical shifts can be obtained, by bypassing CO (Higman, 2012). First, magnetization is transferred from Hα and Hβ to the Cα and Cβ, respectively. Following, the magnetization is transferred from Cβ to Cα, then to CO, N and the amide hydrogen for detection. Figure 1.8 presents the magnetization transfer for CBCA(CO)NH. In large proteins, the signal-to-noise ratio might be poor for the CBCA(CO)NH experiment, other experiments including HNCA, HN(CO)CA, HNCO and HN(CA)CO may also be required.

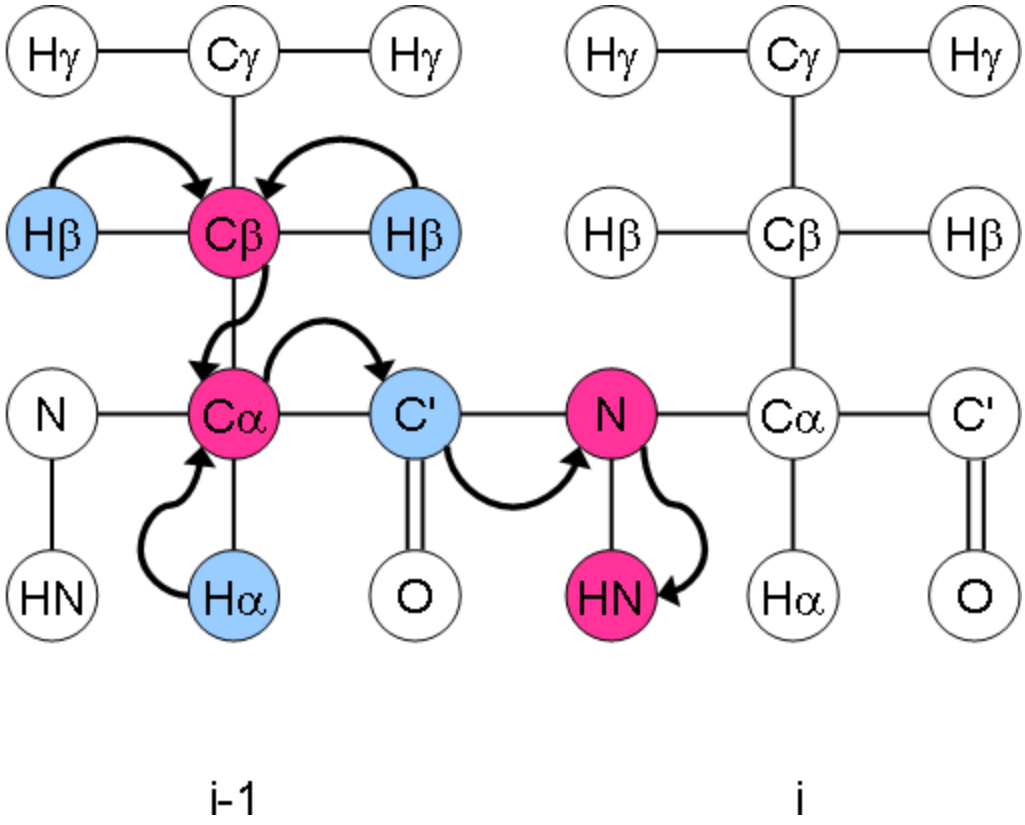


**Figure 1.8 Magnetization transfer for CBCA(CO)NH/HN(CO)CACB as the name of the experiment depicts. Figure is adapted from Higman (2012).**

HNCACB

The magnetization transfer of HNCACB is first transferred from HN to Cα of both the same residue and the preceeding residue, and then to Cβ, and transfer back for detection (Higman, 2012). In the HNCACB experiment, magnetization also reaches the preceding residue through the same pathway. Chemical shifts including Cα and Cβ of the residue and Cα and Cβ of the previous residue are obtained from this experiment. Figure 1.9 presents the magnetization transfer for HNCACB.

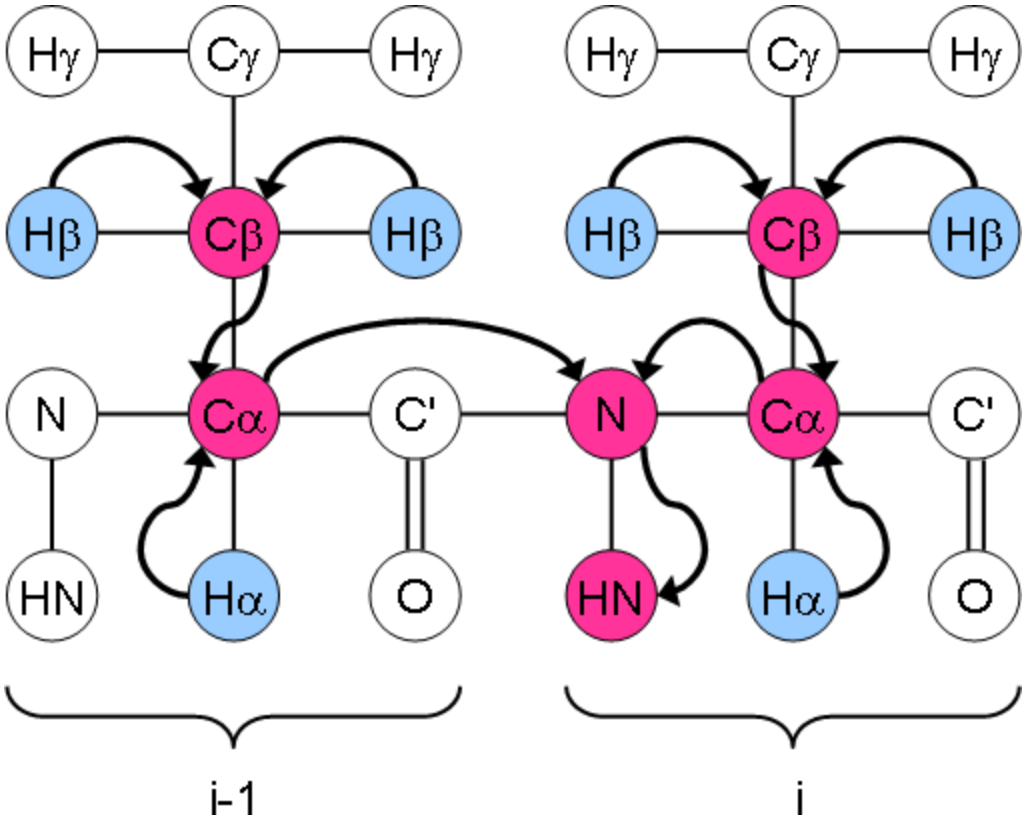


**Figure 1.9 Magnetization transfer for HNCACB as the name of the experiment depicts. Figure is adapted from Higman (2012).**

### 1.8.5 Relaxation

Relaxation measurements in NMR are powerful techniques in determining the overall and internal motions in proteins (Teng, 2013). Relaxation experiments for backbones usually include the $^{15}N$ longitudinal relaxation (Spin-Lattice, $T_1$), the $^{15}N$ transverse relaxation (Transverse, $T_2$) and the $^{1}H$-$^{15}N$ Heteronuclear NOE experiments.

Longitudinal relaxation presents the restoration of magnetization back to the Boltzmann equilibrium, after perturbing, i.e., a hard pulse. The longitudinal relaxation occurs in the *z*-direction and it occurs by transferring energy from the nuclear spin system to the neighboring molecule (Sattler, 2004; Aliev, 2014). Figure 1.10 shows the mechanism of longitudinal relaxation.

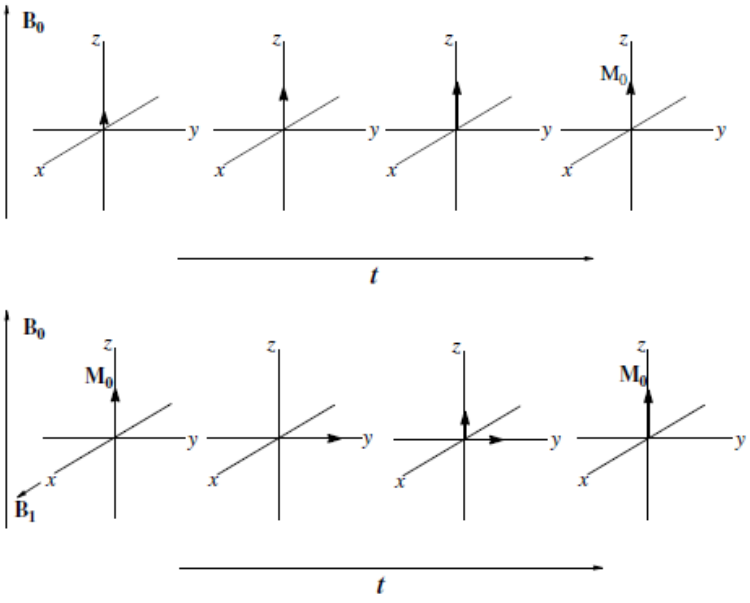


**Figure 1.10 Mechanism of longitudinal relaxation which occurs in the z-direction and leading to equilibrium. Figure is adapted from the Aliev (2014) lecture series.**

Transverse relaxation presents the decay of magnetization along the direction proportional to the direction of magnetic field. By applying a 90° pulse, the nuclear spins become phase coherent in one direction, but the alignment is gradually lost due to field heterogeneity or direct interactions between the spins without energy transfer to the lattice (Aliev, 2014). This quantifies the magnetization rate of decay in the *xy* plane. Figure 1.11 shows the mechanism of transverse relaxation.

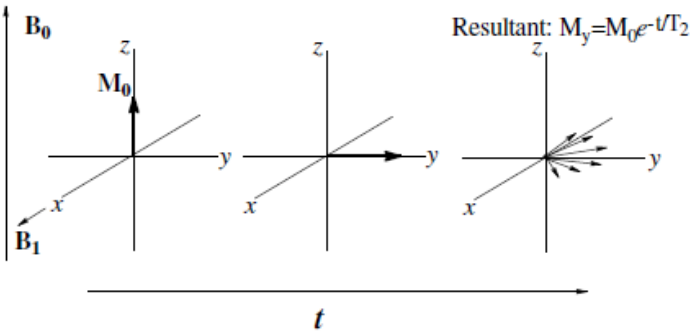


**Figure 1.11 Mechanism of transverse relaxation which occurs in the xy plane and leading to restoration.**

**Figure is adapted from the Aliev (2014) lecture series.**

The heteronuclear NOE is determined through comparing the change in intensity of the NMR signal of the heteronucleus in equilibrium to the saturated heteronucleus upon applying a pi-pulse (Teng, 2013). The resulting signal is extracted as an intensity ratio between individual cross-peaks on the NOE and non-NOE spectra. This gives information on the rigidity of local structure of the protein (Teng, 2013).

Relaxation measurements involved collecting a series of 2D $^{1}H$-$^{15}N$ HSQC experiments. In both the longitudinal and the transverse relaxation, the pulse sequences include a relaxation period inserted either before or after the $t_1$ evolution period. In contrast, the pulse sequence of the cross relaxation period (saturation period) in the heteronuclear NOE measurement is integrated into the preparation period of the 2D steady-state NOE sequence (Teng, 2013).

### 1.8.6 Hydrogen-Deuterium (H/D) Exchange

In the presence of deuterium water, Hydrogen-Deuterium (H/D) exchange can take place in the exchangeable protons (i.e. amide protons) of macromolecules. The mechanism of H/D exchange involves replacing a covalently bonded hydrogen atom with a deuterium atom, or vice versa (Kazazic et al., 2010). For example, in proteins, the hydroxyl or amine groups are usually exchangeable depending on the solvent accessibility and the strength of hydrogen bonding. Figure 1.12 provides a visual representation of H/D exchange. The H/D exchange rate depends on backbone conformation and dynamics; highly unstructured and unprotected regions can exchange rapidly, while the protons of hydrogen-bonded amide groups and protected regions will exchange much slower or are non-exchangeable (Chalmer et al., 2006). The rate of H/D exchange can characterize the protection factors and dynamics of local structures in protein. Thus, H/D exchange can provide significant insights into solvent accessibility of various parts of

a protein, characterizing protein interaction through regions of protection, and examining the protein conformational dynamics (He et al., 2007; Kazazic et al., 2010).

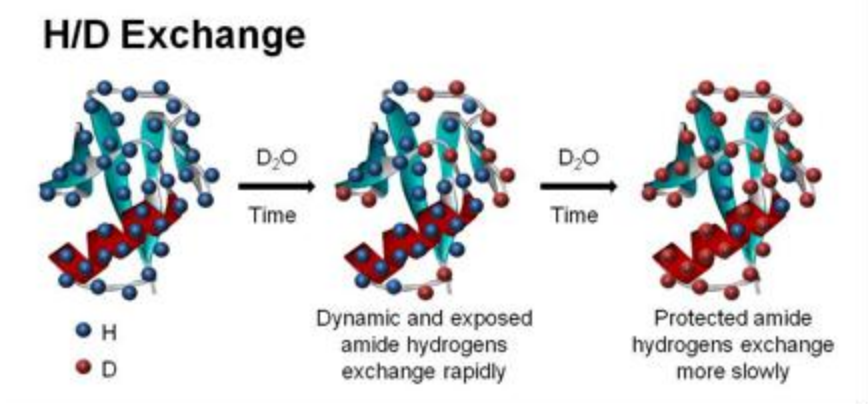


**Figure 1.12 Rationale of the exchangeable regions on a protein molecule. Figure adapted from McKenna (2015).**

Monitoring H/D exchange can be done through NMR spectroscopy as hydrogen and deuterium nuclei are different in magnetic properties. In a $^{1}H$ NMR spectrum, deuteron will not produce a signal; conversely, in a $^{2}H$ NMR spectrum, protons signals will not be observed (Chalmer et al., 2006). Conventionally, as HSQC is specific for hydrogen signals, it can be used to monitor the exchange rate of H/D at progressive time points. The presence of signal cross peaks will be suppressed drastically as hydrogen exchange with deuteron (Zhang et al., 2008). With a prior protein backbone assignment, H/D residue specific information can be obtained as each cross peak represents an amino acid.

### 1.8.7 Magnetization Transfer through the Proton-Proton Spin-Diffusion Technique

The inter protons spin-diffusion technique specifically detects membrane embedded segments of a protein (Huster et al., 2001). The mechanism involves transferring of magnetization from the methyl protons on the lipid to the center of the bilayer. Rapid spin diffusion can be observed as a protein with transmembrane domains has rigid segments close to the center of the liquid-crystalline bilayer. This facilitates the magnetization transfer from the lipid methyl protons to the protein protons, producing a strong signal (Huster et al., 2001). In contrast, slow spin diffusion is apparent when a protein only has surface-bound segments. Magnetization transfer is slower in this case as it has to pass through the lipid acyl chains before reaching the protein in a given time frame. The surface-bound protein receives very little magnetization transfer from the methyl protons as a result. Thus, weak signals will be produced (Huster et al., 2001). The magnetization transfer rate can be vastly different between a rigid macromolecule and a mobile lipid.

### 1.8.8 Molecular Interaction Using NMR

In all areas of biology, the ability for proteins to interact with membranes is of utmost importance for natural processes (Lipchock and Loria, 2009). NMR is an ideal tool to examine the molecular interaction of protein-protein and protein-ligands as it can complement the shortcomings in methods which may cause co-crystalization of complex due to low affinity or local disorder (Marion, 2013). In many cases, protein interaction can cause detectable changes which can be evaluated through chemical shift perturbation, paramagnetic relaxation enhancement, intermolecular NOE, H/D exchange rates and residual dipolar couplings (Marion, 2013). These methods can be employed in either solution state NMR or solid state NMR.

### 1.8.9 Structure Characterization

NMR spectroscopy and x-ray crystallography are two powerful techniques which can determine the structure of macromolecules with atomic resolution (Wider, 2000). In x-ray crystallography, a pure crystal is required for structural determination. This can result in limitations for molecules that could form a crystal. Unlike x-ray crystallography, NMR studies can be carried out in solution or in a solid state near physiological conditions, providing much wider applications (Wider, 2000). Every active nucleus in the macromolecule gives rise to a distinct signal in the spectrum for analysis (Wider, 2000). The process of structural determination through NMR requires a set of heteronuclear multidimensional experiments (Sattler, 2004) followed by extensive data analysis and computer calculations (Wider, 2000). The regular NMR spectra collection for structural calculation can be lengthy; employing a powerful cryoprobe can significantly reduce the time needed and improve on spectra sensitivity (Teng, 2013). Thus, the structure characterization through the use of NMR has become one of the most powerful techniques.

## 1.9 Conclusion

The review presented a wide range of topics providing the background information in order to examine the motion, dynamics, topology and interaction profile with phospholipids for the potato plant specific insert from aspartic proteases as part of a natural plant defense mechanism. As was reviewed, potatoes express a high level of aspartic proteases upon fungal infection, e.g., those that cause the late blight disease. The recombinant potato plant specific insert are bactericidal against human pathogens, and have membrane interaction and membrane permeabilization properties. The exploration of the natural plant defense response plays a critical role towards future innovative and food supply solutions.

## 1.10 Research Questions

Currently, the properties of *Solanum tuberosum* plant specific insert have not been elucidated through nuclear magnetic resonance spectroscopy. Information gathered from this thesis will provide important and novel insights into the interaction mechanism of the plant specific insert with phospholipid membranes and will provide a better understanding for the innate immunity in natural plant host defense response against pathogens. In addition, the research findings are expected to contribute new knowledge and understanding for environmentally friendly crop protection strategies for agricultural food business, food security, and the food supply chain. In this approach, several questions are formulated in examining the plant specific insert from *Solanum tuberosum.* The following research questions are proposed:

1. Can monomer-dimer equilibrium be observed by altering the pH and do they differ in protein dynamics?
2. Which segments of the PSI are critical for protein-membrane interaction?
3. What is the topology of protein-membrane interaction?

# Chapter 2: Hypotheses and Objectives

## 2.1 Hypothesis and Objective I

H1.1: Monomer-dimer equilibrium of PSI can be observed by varying the pH; dimers are predominant in the acidic pH, whereas monomers are predominant in neutral pH.

H1.2: Secondary structural elements of the PSI are similar in both the neutral and the acidic pH range and are predominantly α-helical.

O1.1: To elucidate pH dependent protein monomer-dimer equilibrium of PSI using solution state NMR.

O1.2: To obtain backbone assignments of the monomeric and the dimeric PSI using solution state NMR.

## 2.2 Hypothesis and Objective II

H2: PSI has rigid structure core containing four α-helices, flexible N-terminus, flexible C-terminus and a long loop connecting helices; longitudinal relaxation yields twice the relaxation time for PSI in pH 2 than in pH 7, whereas transverse relaxation yields twice the relaxation time in pH 7 than in pH 2.

O2: To measure the longitudinal relaxation ($T_1$), transverse relaxation ($T_2$) and $\{^1H\}$- $^{15}N$ NOE relaxation on PSI in pH 2.0 and pH 7.0.

## 2.3 Hypothesis and Objective III

H3.1: PSI-membrane interaction is pH dependent, interaction occurs in the acidic pH.

H3.2: Phospholipid interaction with PSI occurs through the phosphate head group.

O3.1: To examine the PSI-membrane interactions through titration in solution state NMR.

O3.2: To examine the interaction of phospholipid membrane upon PSI interaction.

## 2.4 Hypothesis and Objective IV

H4: Upon interaction, segments of the PSI are embedded within the acyl chains of the phospholipid membrane.

O4: To examine the PSI-membrane interaction and topology using solid state NMR

# Chapter 3: Materials and Methods

## 3.1 Materials

All reagents, peristaltic variable speed pump, HisPur™ Ni-NTA Resin column, and 6,000-8,000 Da cut-off dialysis tubing used in protein expression and purification were purchased from Fisher Scientific. Ammonium chloride ($^{15}N$, 99%) and D-glucose (U-$^{13}C_6$, 99%) were obtained from Cambridge Isotopes Laboratories, Inc. (Tewksbury, MA). All synthetic phospholipids and natural pig brain phospholipids were purchased from Avanti Polar Lipids (Alabaster, AL). Water used in this study was filtered with a Millipore Milli-Q Plus system with a resistance higher than 18 mΩ/cm.

## 3.2 Microbial Strain

Incorporation of the *Solanum tuberosum* plant specific insert gene into the pET32b(+) plasmid was previously performed by Bryksa et al. (2011). The construction vector was made for the expression of thioredoxin-PSI protein in *E.coli* Rosetta-gami B (DE3) pLysS. The stock culture was maintained with glycerol and stored at -80 °C. This cloned microbial strain was used for the recombinant expression of the plant specific insert (Bryksa et al., 2011).

## 3.3 Recombinant Protein Expression

*E.coli* Rosetta-gami B (DE3) pLysS cells transformed with pET-32b was used to inoculate 50 mL of sterilized Luria-Bertani (LB) media with 50 µg/ml ampicillin, 12.5 µg/ml tetracycline, 15 µg/ml kanamycin, and 34 µg/mL chloramphenicol as the initial overnight culture. The culture was inoculated in a 500 mL baffled flask and incubated at 37°C with vigorous agitation overnight (250 rpm). The cells were harvested by centrifugation in two sterile 50 mL conical tubes at 4,000 x g for 5 minutes and the supernatant was discarded. The pellet was then washed with 10 mL of sterilized M9 minimal media and subsequently resuspended in

another 10 mL of sterilized M9 minimal media. The resuspended culture was divided in two 2 L baffled flasks containing 500 mL of M9 minimal media each. For isotopic labeling, $^{15}NH_4Cl$ and $^{13}C_6$-D-Glucose were used as the sole nitrogen and carbon sources, respectively. The cells were incubated at 37°C with vigorous agitation until an $OD_{600}$ of 0.8 was reached (approximately 6.5 hours) and cooled to room temperature. The induction was performed by adding isopropyl β-d-1-thiogalactopyranoside (IPTG) to a final concentration of 0.5 mM. After an overnight incubation at 30 °C, the cells were spun down by centrifugation at 5,000 x g for 5 minutes at 4 °C and frozen in -20 °C for later use. The pellets were thawed at room temperature and resuspended with 5 mL of 20 mM of Tris buffer at pH 7.4 for every 100 mL of culture. The re-suspension was incubated at room temperature for 15 minutes and 1 μL of Benzonase-Nuclease was added for every 5 mL of lysate. The suspension was left on ice for 1 hour for lysis to fully occur and the resulting cell lysates were centrifuged at 5,000 x g for 20 minutes at 4°C. The resulting supernatant was immediately centrifuged at high speed 20,500 x g for 30 minutes at 4 °C to remove insoluble matter. The final supernatant was obtained as the crude protein.

### 3.4 Protein Purification

Protein purification was performed using a peristaltic variable speed pump (Watson Marlow Inc.). The cell lysate soluble fraction was applied to one 5 mL HisPur™ Ni-NTA Resin column (Pierce Biotechnology Inc.) and equilibrated with 20 mM Tris-Cl, 300 mM NaCl, and 10 mM Imidazole in pH 7.4 (binding buffer) followed by washing with 20 mM Tris-Cl, 300 mM NaCl, and 30 mM Imidazole in pH 7.4 (wash buffer) for 10 column volumes. The isolation of thioredoxin-PSI fusion protein was eluted by 20 mM Tris-Cl, 300 mM NaCl, and 300 mM Imidazole in pH 7.4. The fusion protein was then dialyzed in 20 mM Tris-Cl in pH 7.4 to remove the imidazole. Thrombin was added to the dialysate at a 1:1000 mass ratio and incubated at 37°C

for at least 12 h with mild agitation for the hydrolysis of fusion protein to separate thioredoxin from PSI. The PSI was collected in the flow through from reapplication of the affinity chromatography in room temperature using HisPur™ Ni-NTA Resin columns and 20 mM Tris-Cl three times consecutively at 1 mL/min to remove the thioredoxin fusion tag. PSI was then dialyzed against 6 x 2L de-ionized water to remove elution buffer using 6,000-8,000 Dalton molecular mass cut-off dialysis tubing. Subsequently, the sample was lyophilized to the powder form and stored dry at -80 $^{o}$C for long term storage. Figure 3.1 shows the sequential steps of PSI expression and purification on a SDS gel. Purity was approximately 90% as measured with NMR cross-peak intensity.

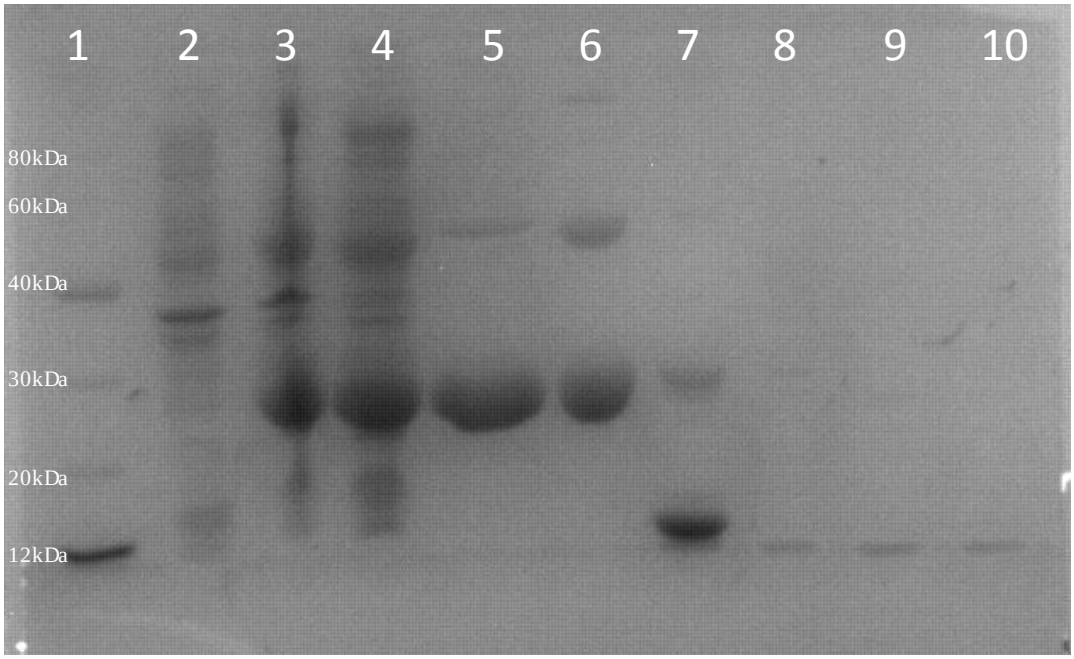


**Figure 3.1 The PSI expression and purification steps against a molecular marker on the SDS gel- lane 1: molecular marker; lane 2: before IPTG induction; lane 3: expression after 6 hours; lane 4: overnight expression; lane 5: post Ni affinity chromatography of thioredoxin fusion protein tag with PSI; lane 6: post dialysis for removal of Imidazole and salt; lane 7: post thrombin cleavage for free PSI and thioredoxin fusion protein; lane 8: post Ni affinity chromatography eluent of pure PSI; lane 9: post Ni affinity chromatography eluent of pure PSI- second time; lane 10: post Ni affinity chromatography eluent of pure PSI- third time. Each lane contained 10 µL of sample.**

### 3.5 Preparation of Phospholipids

Phospholipids were prepared with mixing phosphatidylcholine (PC), phosphatidylethanolamine (PE) and phosphatidylserine (PS) in a molar ratio of 1:1:1. The phospholipid suspension was mixed at room temperature for 2 hours in a round bottom flask and dried under $N_2$ flush for 30 minutes. The dried phospholipids were then lyophilized for 3 hours and resuspended with 27 mM Na-$H_3PO_4$ and 140 mM NaCl pH 2.0 buffered solution. The Na-$H_3PO_4$ was prepared by adjusting the pH of phosphoric acid with NaOH to the desirable pH. To obtain a uniform phospholipid mixture, the suspension was incubated at 37 °C for 45 minutes with periodic vortexing. The prepared phospholipids were stored in 4 ° Celsius. This preparation of phospholipid solutions was used for all experiments.

An additional phospholipid mixture from naturally extracted pig brain was prepared using the same procedures as above. The naturally extracted phospholipids were used for $^{31}P$ spectra only.

### 3.6 Solution State NMR Sample Preparation

#### 3.6.1 Protein Dynamic Studies

Lyophilized $^{15}N$-labled or $^{13}C$, $^{15}N$-labled PSI were solubilized in buffers depending on the desired pHs in the experiments. Samples of 0.5 mM $^{13}C$, $^{15}N$-labeled PSI in 20 mM Tris-Cl at pH 7.0 containing 10% $D_2O$ and samples of 0.3 mM $^{13}C$, $^{15}N$-labeled PSI in 27 mM Na-$H_3PO_4$ at pH 2.0 containing 10% $D_2O$ were used for backbone assignment in solution state NMR. Samples of 0.1mM with $^{15}N$-labeled PSI at pH 2.0, 3.0, 4.5, 5.4 and 7.0 (27 mM Na-$H_3PO_4$ for pH 2.0 and 3.0; 20 mM Na-Acetate for pH 4.5 and 5.4; and 20 mM Tris-Cl for pH 7.0) were used for examining monomer-dimer equilibrium. Protein concentration was determined by measuring the UV absorbance at 280 nm. All samples for solution NMR were measured using Wilmad NMR sample tubes.

### 3.6.2 Protein Self-Protection by $D_2O$ Exchange

For a better understanding of protein interaction, protein self-protection was examined. To test for protein self-protection, lyophilized $^{15}N$-labeled PSI was dissolved in $D_2O$ buffer at pH 7.0 buffer ($D_2O$ 20 mM Tris-Cl, 140 mM NaCl) and at pH 2.0 buffer ($D_2O$ 27 mM Na-$H_3PO_4$, 140 mM NaCl). The protein concentration was 0.1 mM $^{15}N$-labeled PSI for both the cases. A series of $^{15}N$ HSQC were collected over 24 hours to examine the deuterium/$H_2O$ exchange.

### 3.6.3 Protein Titration Studies

Samples of 0.2 mM $^{13}C$, $^{15}N$-labeled PSI at pH 7.0 (20 mM Tris-Cl, 140 mM NaCl) and pH 2.0 (27 mM Na-$H_3PO_4$, 140 mM NaCl) were used for phospholipid titration. All samples for solution NMR titration were measured in a Wilmad NMR sample tube.

## 3.7 Solid-state NMR Sample Preparation

Samples of 0.8 mM and 0.3 mM $^{13}C$, $^{15}N$-labeled PSI in pH 2.0 (27 mM Na-$H_3PO_4$, 140 mM NaCl) were used for the solid-state NMR based protein-membrane interaction and the $^{31}P$ NMR studies, respectively. To examine the PSI-phospholipid interaction, the $^{13}C$, $^{15}N$-labeled PSI sample was mixed with phospholipid in a molar ratio of 1:30 for 1 hour with gentle agitation at room temperature. The proteoliposome was then ultracentrifuged at 900,000 x g at 4 $^{\circ}C$ for three hours in a Hitachi Micro Ultracentrifuge CS150NX. The collected proteoliposomes for solid-state NMR were packed in a 3.2 mm rotor.

## 3.8 Solution State NMR Assignment

Solution state NMR data were collected at 298 K on a 0.5 mM $^{13}C$, $^{15}N$-labeled PSI sample in 20 mM Tris-Cl at pH 7.0 containing 10% $D_2O$ and on a 0.3 mM $^{13}C$, $^{15}N$-labeled PSI sample in 27 mM Na-$H_3PO_4$ at pH 2.0 containing 10% $D_2O$. All solution state NMR experiments for backbone assignment were performed in a 500 MHz Bruker Ultrashield$^{TM}$ spectrometer

equipped with a cryogenic triple resonance probe $^{1}H/^{15}N/^{13}C$ (NMR Center, Peking University). Backbone assignment was assigned with the experiments: $^{15}N$-HSQC, HNCA, HNCOCA, CBCACONH, HNCACB and HNCO. The spectra data were processed by Bruker TopSpin 2.1 and analyzed using the Computer Aided Resonance Assignment (CARA) Program. The protein secondary structural elements were predicted using chemical shift index (CSI) (Wishart and Sykes, 1994).

### 3.9 Protein Monomer-Dimer Equilibrium and Phospholipid Titration

The monomer-dimer equilibrium was monitored with $^{15}N$-HSQC immediately upon sample preparation and after 24 hours in a 600 MHz Bruker Ascend™ spectrometer with 0.1 mM $^{15}N$-labeled PSI at pH 2.0, 3.0, 4.5, 5.4 and 7.0 (27 mM Na-$H_3PO_4$, at pH 2.0 and 3.0; 20 mM Na-Acetate at pH 4.5 and 5.4; and 20 mM Tris-Cl at pH 7.0). Phospholipid protein interactions were performed at pH 7.0 and pH 2.0. 0.3 mM PSI and 0.3 mM PC/PE/PS (1:1:1) phospholipids mixture were used in the interaction studies. Protein-phospholipid interaction was monitored using $^{15}N$-HSQC.

### 3.10 $^{15}N$ Backbone Relaxation Measurements

The $^{15}N$ longitudinal relaxation rates $R_1$, transverse relaxation rates $R_2$, and steady-state heteronuclear $^{1}H$-$^{15}N$ NOE values of the of PSI at pH 7.0 and pH 2.0 was measured following the pulse sequence from Farrow et al. (1994). Relaxation experiments were performed with 0.3 mM $^{15}N$-labeled PSI samples at both pH 7.0 and pH 2.0. All the relaxation experiments were collected at 298K on a Bruker Ultrashield™ spectrometer at 500 MHz. For $R_1$ and $R_2$ measurements, complex data points of 1024 ($^{1}H$) and 80 ($^{15}N$) were collected with 16 transients per increment and a recycle delay time of 3.0 seconds. The relaxation delay used in the $R_1$ experiments were 20, 100, 200, 300, 400, 600, 800, 1000, 1600 and 2000 ms. For the $R_2$

experiments, the relaxation delays were 7.94, 15.88, 31.76, 47.64, 63.52, 95.28, 127.04, 158.8, 190.56 and 238.20ms. The relaxation rate constants were obtained by fitting with mono-exponential function (Fushman et al., 1997). The $^{1}H$-$^{15}N$ NOE experiments were performed in the presence of a 3.0 s pre-saturation period prior to $^{15}N$ excitation pulse with recycle delays of 5.0 seconds, respectively (Markley et al., 1971). A reference spectrum of 1H-15N NOE experiment (non-NOE) was collected identically to the NOE experiments with the exception of running the pre-satureation pulse train. Each experiment was collected with 32 transients.

### 3.11 Solid-state NMR Interaction Protein Topology

PSI-phospholipid complex containing approximately 4.0 mg of $^{13}C$, $^{15}N$ uniformly labeled PSI was packed into a 3.2 mm rotor for solid-state NMR studies. Solid-state NMR measurements were acquired on a Bruker Avance III Spectrometer at 600.23 MHz equipped with a 3.2 mm E-free $^{1}H/^{13}C/^{15}N$ probe (Bruker USA, Billerica, MA). The rotor spinning frequency was set to 12.0 kHz and the effective sample temperature was maintained at 298 K for all experiments. The temperature was calibrated externally by $T_1$ relaxation time of $^{79}Br$ of KBr powder (Thurber and Tycko, 2009). Typical $\pi/2$ pulses were 2.5 μs for $^{1}H$, 4.0 μs for $^{13}C$, and 5.0 μs for $^{15}N$, respectively. All experiments utilized SPINAL64 (Fung et al., 2000) of 100 kHz for $^{1}H$ decoupling during both direct and indirect chemical shift evolution.

The 2D experiment for $^{15}N$-$^{13}C\alpha$ correlation spectra were collected on the $^{13}C$, $^{15}N$ uniformly labeled PSI- phospholipid complex, the $^{1}H/^{15}N$ cross-polarization (CP) was set with 2 ms contact time and with a constant radio-frequency (r.f.) field of ~50 kHz on nitrogen (proton r.f. intensity ramped linearly around the n=1 Hartmann-Hahn condition). $^{15}N$-$^{13}C\alpha$ band-selective SPECIFIC CP (Baldus et al., 1998) was implemented with a contact time of 5.5 ms, with nitrogen r.f. field of ~42 kHz, while carbon r.f. field ramped (10% ramp) linearly around

~30 kHz. The $^{1}H$ CW decoupling during $^{15}N$-$^{13}C\alpha$ CP transfer was 100 kHz. 200 scans were recorded with a recycle delay of 1.8 s for each experiment, resulting in a total NMR time of 20 hours.

The PSI-phospholipid complex was buffer exchanged with $D_2O$ to observe the change in signals of the unprotected, hydrophilic regions of the protein. All NMR data was processed using NMRpipe (Delaglio et al., 1995) and analyzed using the CARA program.

PSI exchanged in D2O buffers directly followed the same procedures as above. Comparison of NMR spectra provided evidence for protein topology.

### 3.12 Solid State NMR $^{31}P$ Phospholipid Spectra

The $^{31}P$ NMR spectra were measured on a Bruker Avance III Spectrometer at 600.230 MHz using a 4.0 mm DVT H/X/Y probe. The PSI-phospholipid complex sample was packed into a 4.00 mm rotor and the $^{31}P$ NMR spectra were recorded through direct polarization with $^{1}H$ decoupling using a 4μs $\pi/2$ for $^{31}P$ and a 4-s recycle delay. A total of 256 scans were taken for the $^{31}P$ NMR spectra.

### 3.13 Magnetization Transfer

Magnetization transfer experiments were conducted on the PSI-phospholipid complex on a Bruker Avance III Spectrometer at 600.23 MHz and equipped with a 3.2 mm E-free $^{1}H/^{13}C/^{15}N$ probe at 298 K as per Huster et al. 2002. In summary, the $^{1}H$ spin-diffusion technique initiated the magnetization transfer of protons from the acyl lipid chain terminus to the protons of the protein. Subsequently, the magnetization transferred from the proton of the protein to the carbon of the protein (Huster et al., 2002). Signals were generated from the magnetization transfer.

# Chapter 4: Results and Discussion

## 4.1 pH Dependent PSI Monomer-Dimer Equilibrium

The aggregation state changes from monomer to dimer of the StAP PSI were largely dependent on the pH (Bryksa et al., 2011). From the present study, PSI monomer-dimer equilibrium was examined by recording the $^{1}H$-$^{15}N$ HSQC spectra of 0.1 mM PSI solution. The same number of scans was set for the experiments at pH 1.0, 2.0, 3.0, 4.5, 5.4 and 7.0 at 298K, as shown in Figure 4.1. Changing the environmental conditions such as the pH would cause structure alterations or dissociation of oligomeric proteins, which produce chemical shift variations (de Alba et al., 2003). Comparing the $^{15}N$ HSQC spectra from pH 1.0 to 7.0, shifts in cross peaks of many residues were observed. From Figure 4.1, comparison of spectra patterns of PSI at pH 7.0 and at pH below pH 7.0, the cross peaks demonstrated noticeable chemical shifts. Also the spectral quality is poor at acidic pH when compared to the neutral pH. The $^{1}H$-$^{15}N$ HSQC spectra demonstrated a change of cross peak intensities and a mixture of different states of proteins as the pH was lowered. This suggested that a conformation change occurred upon pH alteration. These results were in agreement with the sedimentation equilibrium analytical ultracentrifuge data collected by Bryksa (2016). The molecular weight of the PSI increased as the pH lowered and reached almost double the molecular weight at pH 3.0 compared to the neutral pH (Bryksa, 2016). This suggested the presence of monomer-dimer equilibrium. Taking together, the StAP PSI changed state as the pH altered from neutral to acidic. Similarly in the mature saposins A and C, changes in confirmations were achieved as the environmental pH was lowered from neutral to acidic (John et al., 2006). Saposin A demonstrated cross peak aggregation in acidic pH as compared to the neutral pH, and saposin C showed monomer-dimer equilibrium by altering the pH (John et al., 2006). Comparing to the present study, these saposin

like proteins (SAPLIP) have similar behaviours. Conversely, saposin B and saposin D were not as strongly affected by altering the pH environment. This could be due to the difference in sequence of the proteins (John et al., 2006).

The isoelectric point for the StAP PSI is at 4.6; at around this pH, samples prepared in high concentration were very unstable and they precipitated out of the solution which caused broad NMR spectral signals (John et al., 2006; Bryksa, 2016). From the current study, it was found that at pH 3.0 and 4.5, the PSI solution state NMR samples precipitated out of the solution over time at 0.1 mM. The StAP PSI had limited solubility under acidic conditions. Supporting these results, Bryksa (2016) was unable to conduct sedimentation equilibrium analytical ultracentrifuge experiments at pH 4.5 even with a much lower concentration of 80 μM compared to the 34 mg/mL in the neutral condition. Additionally, in the mammalian saposin C, broad spectra and weak signals were observed using high concentrations between the pH range of 3.0 to 4.5 (de Alba et al., 2003; John et al., 2006). Sample aggregation in this pH range caused problems for NMR $^{15}$N HSQC data collection. To improve upon the sample conditions, the temperature of the sample or the concentration can be altered (John et al., 2006). However, it was not suggested to use higher temperatures as was our present research because of the difference to physiological conditions and subsequent experimental plans. Further, concentrations below 0.1 mM were not suggested for data collection due to low sensitivity and long NMR spectra acquisition time (de Alba et al., 2003; Teng, 2013). Thus, working around the isoelectric point presented difficulties for spectra collection. Figure 4.1 (C, D) showed faint and aggregated spectra which could not be validated. Thus, PSI was examined at lower pH.

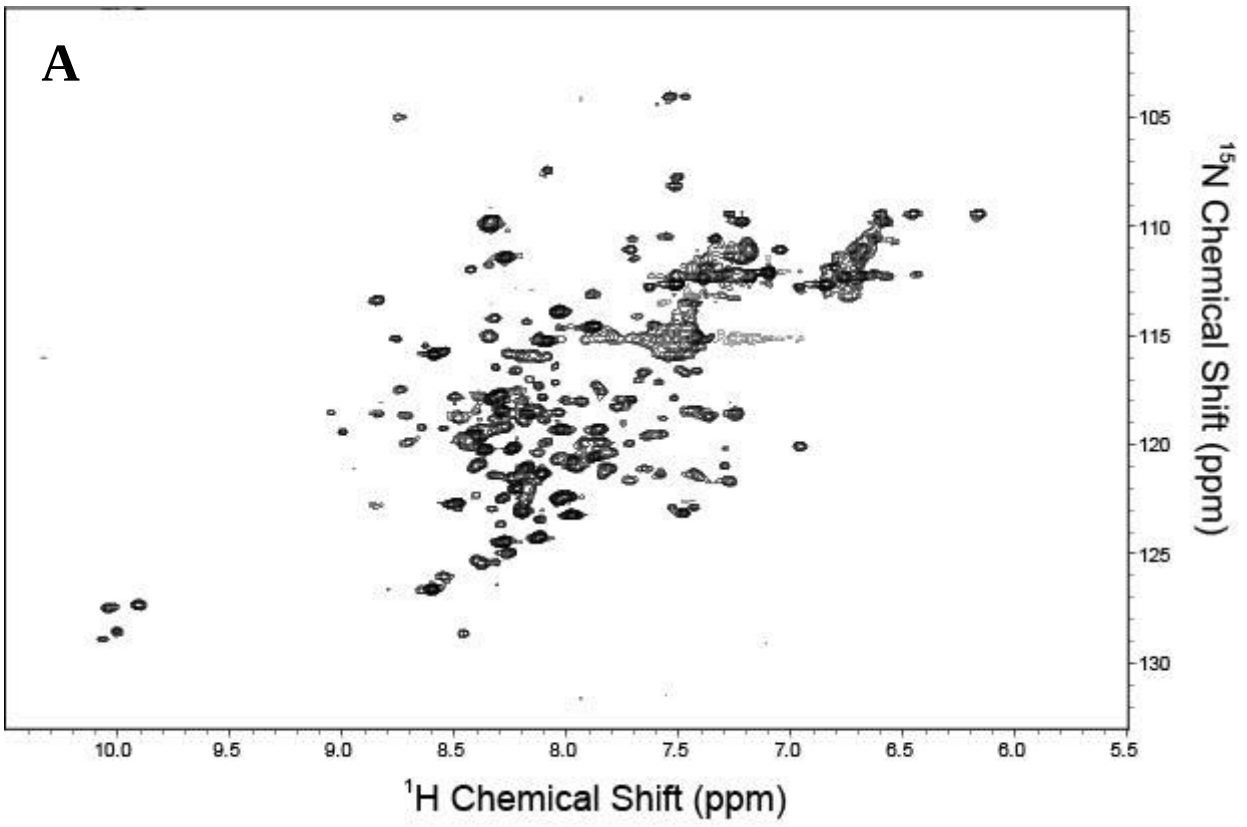
A
105
110
115
120
125
130
$^{15}$N Chemical Shift (ppm)
10.0
9.5
9.0
8.5
8.0
7.5
7.0
6.5
6.0
5.5
$^{1}$H Chemical Shift (ppm)

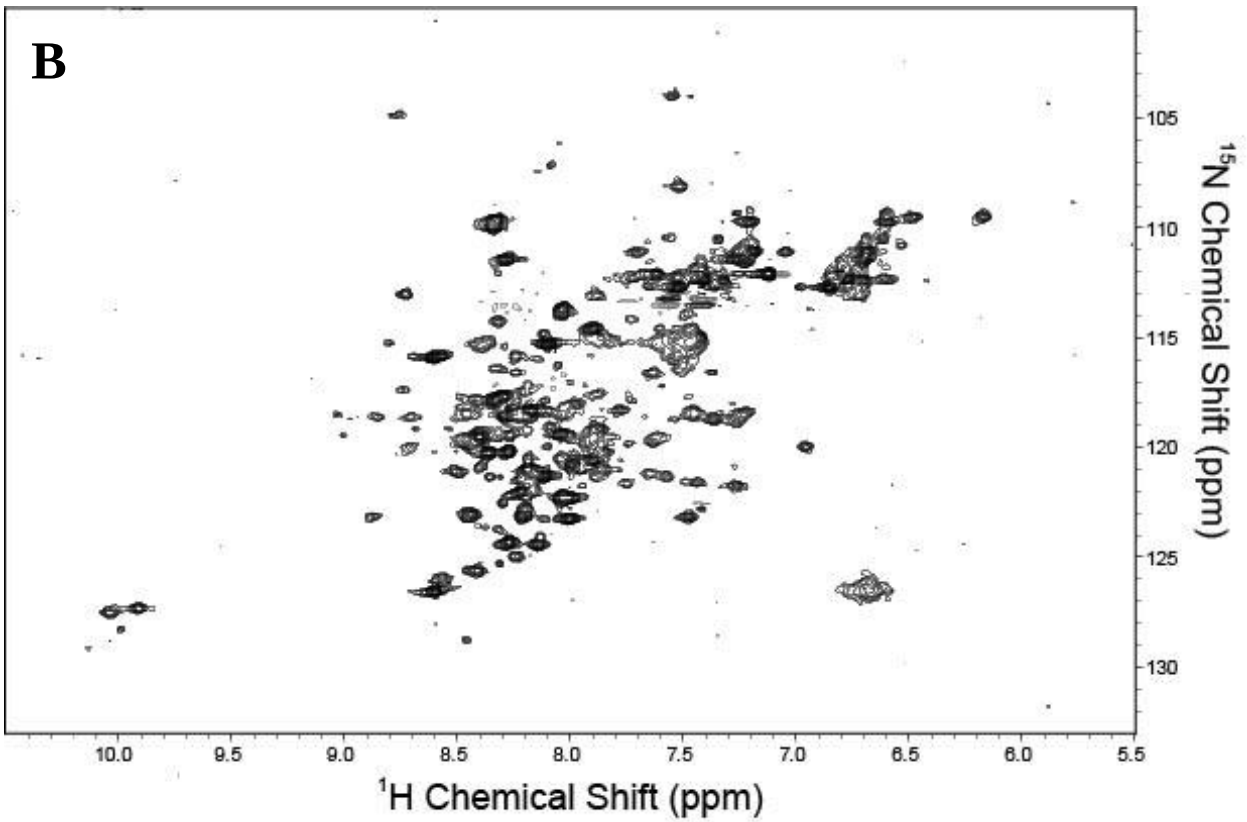
B
105
110
115
120
125
130
$^{15}$N Chemical Shift (ppm)
10.0
9.5
9.0
8.5
8.0
7.5
7.0
6.5
6.0
5.5
$^{1}$H Chemical Shift (ppm)

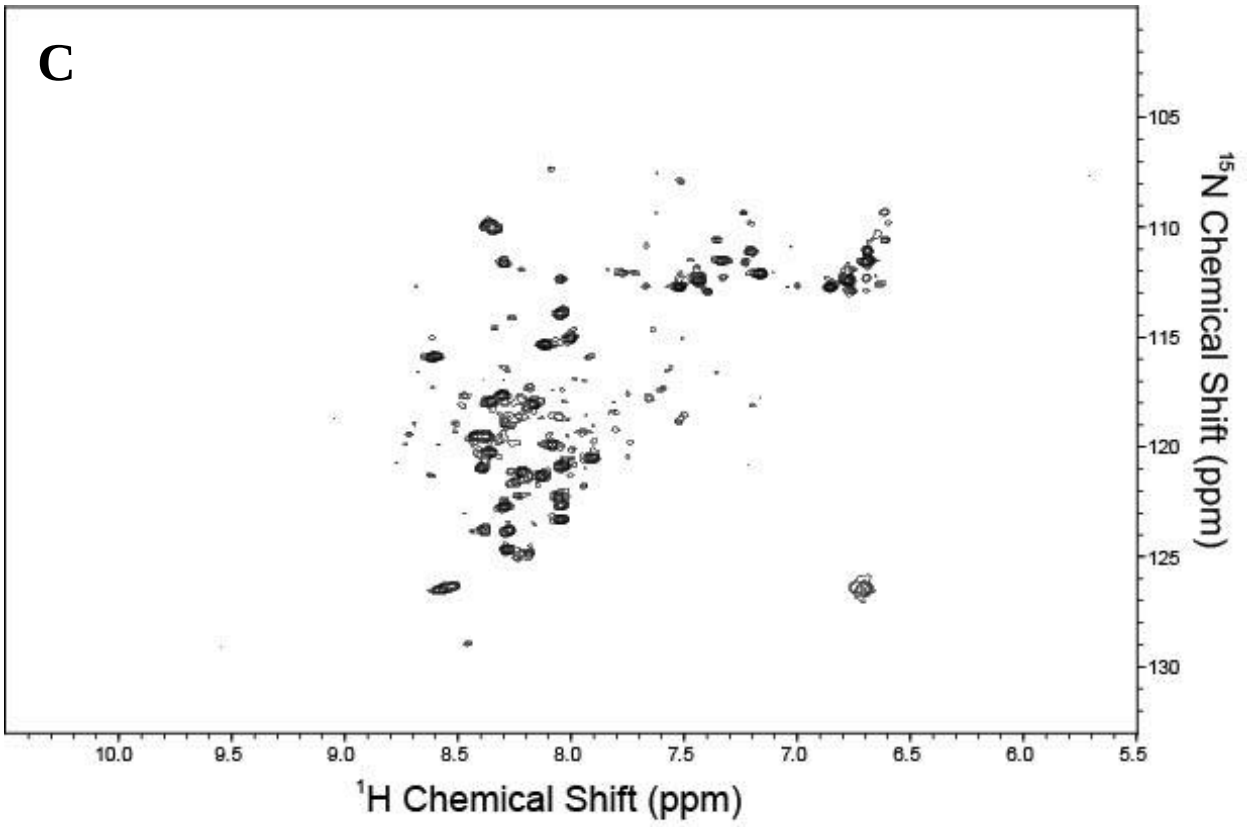
C
105
110
115
120
125
130
15N Chemical Shift (ppm)
10.0
9.5
9.0
8.5
8.0
7.5
7.0
6.5
6.0
5.5
1H Chemical Shift (ppm)

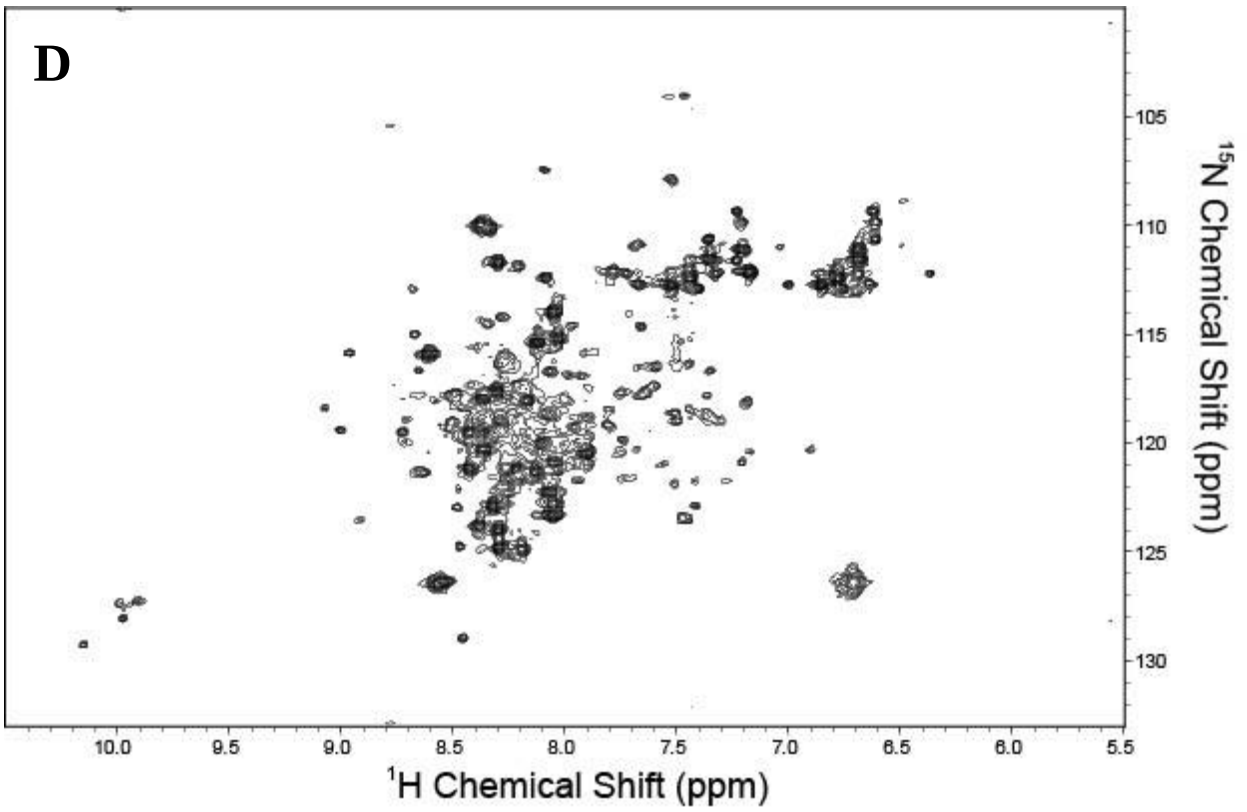
D
105
110
115
120
125
130
$^{15}$N Chemical Shift (ppm)
10.0
9.5
9.0
8.5
8.0
7.5
7.0
6.5
6.0
5.5
$^{1}$H Chemical Shift (ppm)

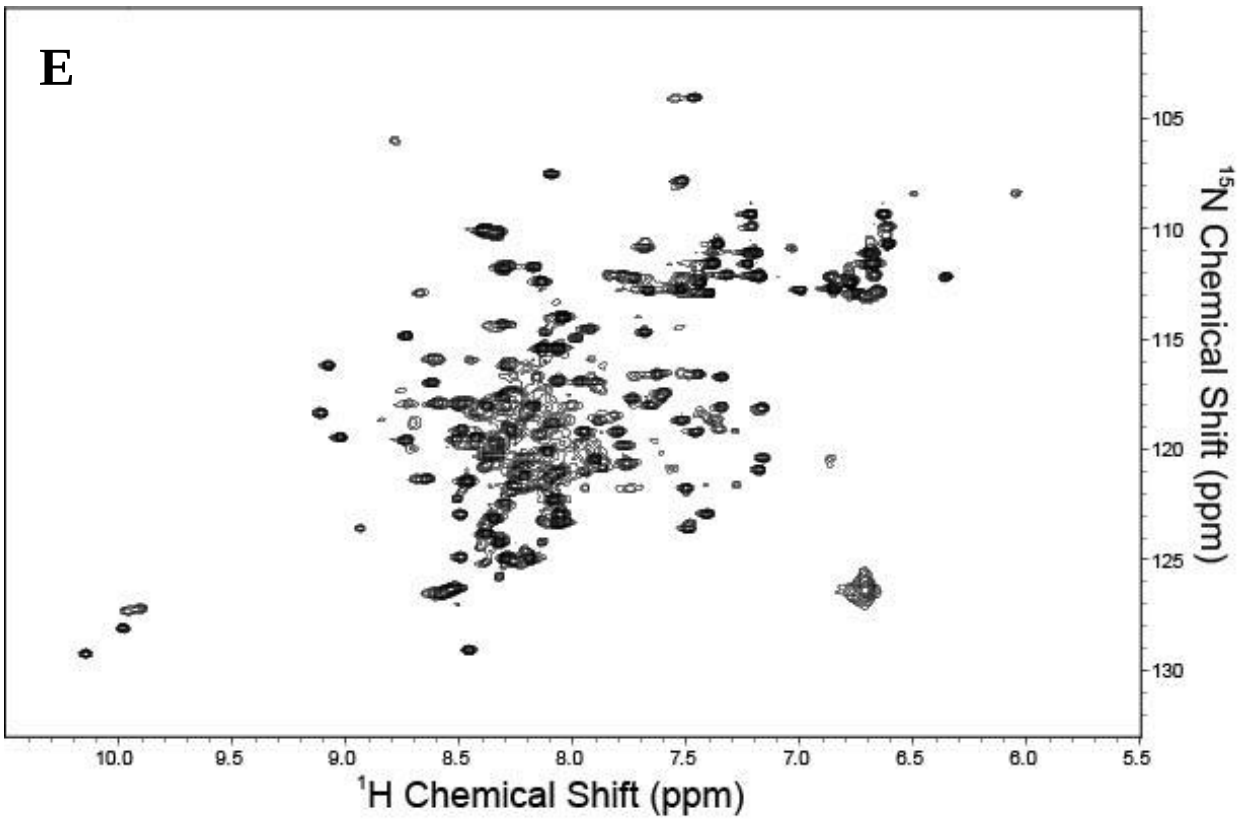
E
105
110
115
120
125
130
$^{15}$N Chemical Shift (ppm)
10.0
9.5
9.0
8.5
8.0
7.5
7.0
6.5
6.0
5.5
$^{1}$H Chemical Shift (ppm)

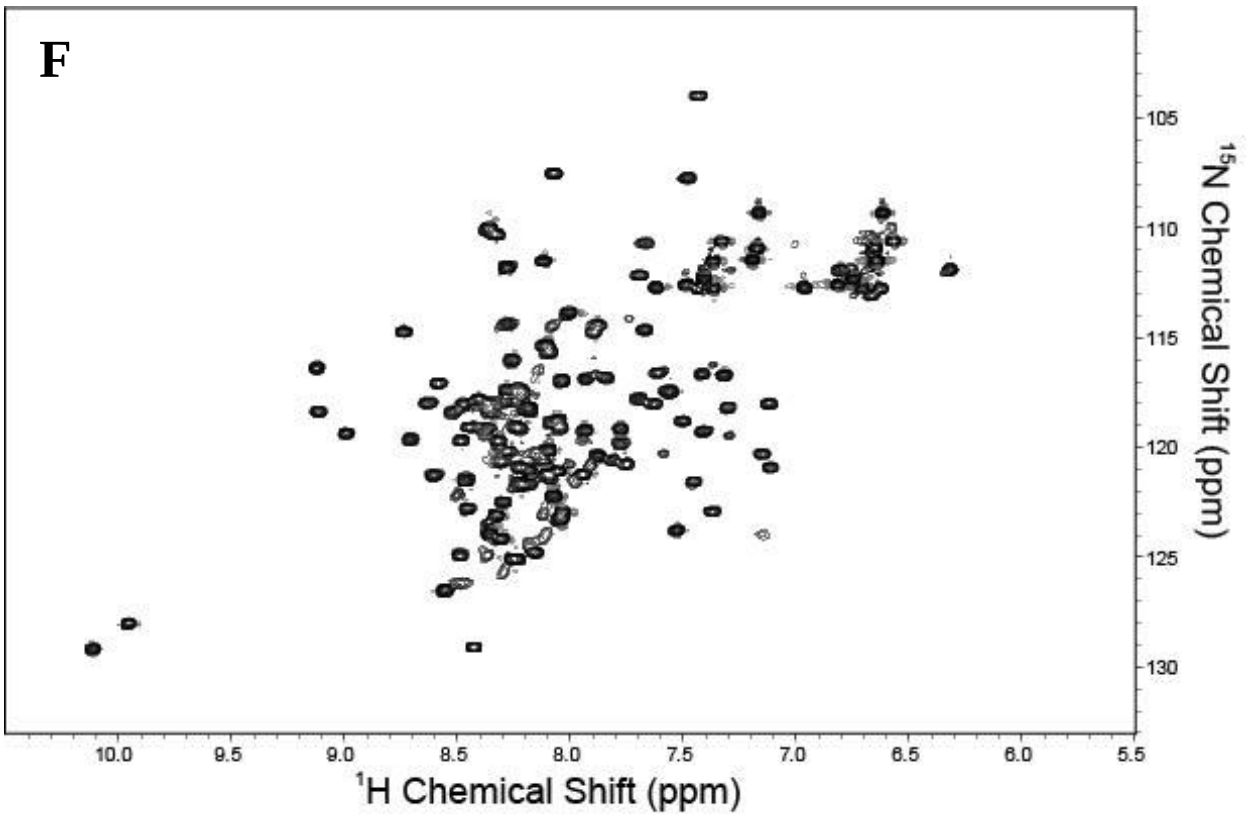


**Figure 4.1 $^{1}$H-$^{15}$N HSQC spectra of StAP PSI, recorded on a 500 MHz spectrometer, 298K, 16 scans and at (A) pH 1.0, (B) pH 2.0, (C) pH 3.0, (D) pH 4.5, (E) pH 5.4, and (F) pH 7.0. Samples were prepared to contain 0.1 mM and compatible buffer conditions with respect to the pH. $^{1}$H chemical shift in ppm is labeled on the x-axis and $^{15}$N chemical shift in ppm is labeled on the y-axis.**

By overlapping the most significant shifts in the $^{1}H$-$^{15}N$ HSQC spectra at pH 2.0 and 7.0 shown in Figure 4.2, notable cross peak relocations were present. Location of the predicted side chains at $^{1}H$ chemical shift of around 10 ppm and $^{15}N$ chemical shift between 125-130 ppm demonstrated relocation as distinguished by the red and blue cross peaks at pH 2.0 and 7.0, respectively. Additionally, the cross peak which represents Glycine 40 clearly showed a chemical shift variation between the different pHs. Moreover, dramatic changes in chemical shifts were observed in the center of the spectra. These shifts in the cross peaks suggested that either conformational or chemical exchanges could be present in the PSI (de Alba et al., 2003). The superimposed $^{1}H$-$^{15}N$ HSQC spectra not only demonstrated chemical shifts from the amide signals, but they also showed signal line broadening in the center of the spectra where major shifts occurred. This indicated that in addition to conformation change, protein aggregation caused by the decrease in pH also occurred (de Alba et al., 2003; John et al., 2006). Further supporting these results was the visual appearance of the precipitated sample over time in the acidic pH (image not shown). A slight white precipitate was present upon data collection in room temperature in acidic pH (pH 2.0). Subsequent experiments such as backbone assignment and relaxation were required in order to confirm the secondary structure at a residue level and monomer-dimer states of the PSI, respectively.

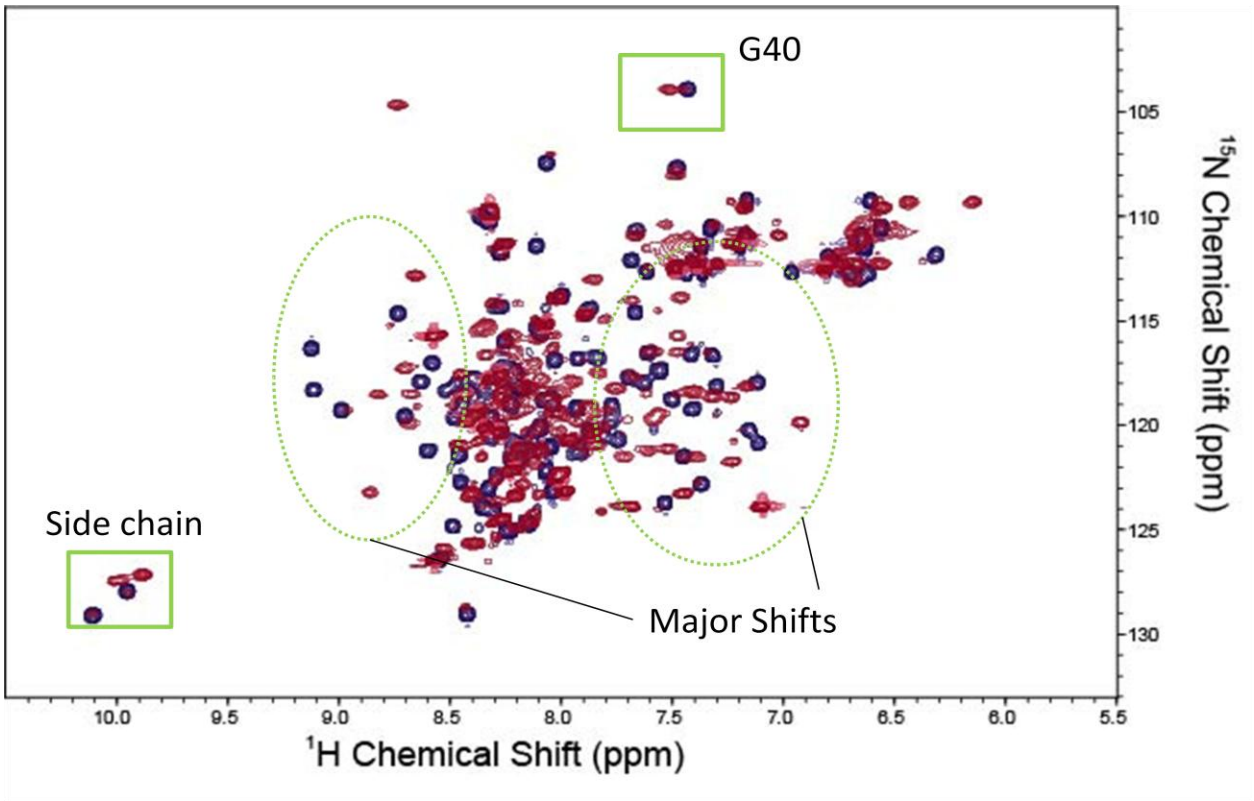


**Figure 4.2 Overlapped $^{1}H$-$^{15}N$ HSQC spectra of StAP PSI of pH 2.0 and 7.0 were recorded on a 500 MHz spectrometer, 298K and with 16 scans. Samples were prepared to 0.1 mM and compatible buffer conditions with respect to the pH. $^{1}H$ chemical shift in ppm is labeled on the x-axis and $^{15}N$ chemical shift in ppm is labeled on the y-axis. pH 7.0 is represented with blue cross peaks and pH 2.0 is represented with red cross peaks.**

## 4.2 Secondary Structural Analysis and Backbone Assignment Using Solution State NMR

Backbone assignments for the StAP PSI at pH 7.0 and pH 2.0 were completed using the following experiments: $^{1}H$-$^{15}N$ HSQC, HNCA, HNCOCA, CBCACONH, HNCACB and HNCO. Assignments for both pH conditions were performed. Depending on the sample condition, concentration and purity, spectra collection typically required one to two weeks and assignment would take another one to two weeks (John et al., 2006). In the current study, spectra acquisition and assignment for PSI at pH 7.0 took one week each, while PSI at pH 2.0 required two weeks.

PSI at pH 7.0 yielded much desirable H-N correlations map (Figure 4.3-A-i) than at pH 2.0 (Figure 4.3-B-i). The H-N correlations map from pH 2.0 demonstrated limited dispersion as the cross peaks were broad and partly overlapping. The PSI at pH 2.0 did not show confirmation homogeneity, traces of cross peaks were still present as retrieved from the neutral condition. In the backbone assignment of PSI at pH 7.0, 98 out of the 108 residues were assigned as shown in Figure 4.3-A-i; and in pH 2.0, 79 out of the 108 residues were assigned as shown in Figure 4.3-B-i. The unassigned cross peaks could be attributed to the flexible N-terminus, broad peaks from rigid sections, aggregated cross peaks and prolines which do not produce a signal (O'Connell et al., 2009; Higman, 2012). The poor quality of the HSQC spectra in the acidic pH is due to protein aggregation and self-association in the dimeric state. Similar phenomenon was observed by de Alba et al.(2003) and John et al. (2006). Similarly, varying the environmental temperature or introducing interacting substances such as phospholipids affect the secondary structure of the PSI (Munoz et al., 2014). Aggregation and self-association of protein resulted in heavily overlapped peaks which would be excluded from the relaxation analysis in the subsequent sections as ambiguity arises. Information obtained from backbone assignment are important

towards defining the secondary structure (Sattler, 2004) which would be useful for dynamic measurements (Marion, 2013), structural calculations (Wider, 2000), and determining protein interaction profile (O'Connell, 2009).

The secondary structural predictions were achieved using the chemical shift index (CSI) equation [4.1]:

$$Chemical\ Shift\ Index = [C\alpha - C\alpha(ref)] - [C\beta - C\beta(ref)]$$

This calculated the difference between the Cα against a reference value and the Cβ against a reference value (Wishart and Sykes, 1994). Due to the limited spectrum resolution in StAP PSI at pH 2.0, only Cα against a reference value was used to calculate the chemical shift index. The chemical shift index equation used for pH 2.0 only took consideration of Cα as shown in equation [4.2]:

$$Chemical\ Shift\ Index = [C\alpha - C\alpha(ref)]$$

The resulting chemical shift indexes were plotted against residue numbers in Figure 4.3-A-ii and Figure 4.3-B-ii for pH 7.0 and pH 2.0, respectively. In the chemical shift index plot, alpha-helical regions were shown in the positive scale (Yang et al., 2007) and beta sheets, twists, turns, or random coil were shown in the negative scale (Yang et al., 2007). The secondary structural prediction performed by NMR was able to examine the characteristics of each backbone amino acid at a residue level. Under both pH 7.0 and 2.0, the StAP PSI does not present alpha-helical structure between residues 40 to 70, leaving the rest of the backbone structure mainly alpha-helical. These results are in accordance with the crystal structure elucidated by our research group (Bryksa et al., 2011). Comparing the StAP PSI with other

alpha-helical rich (approximately 54%) SAPLIP, similar secondary structures were found (Anderson et al., 2003; de Alba et al., 2003; Brunh et al., 2005; Munoz et al., 2011).

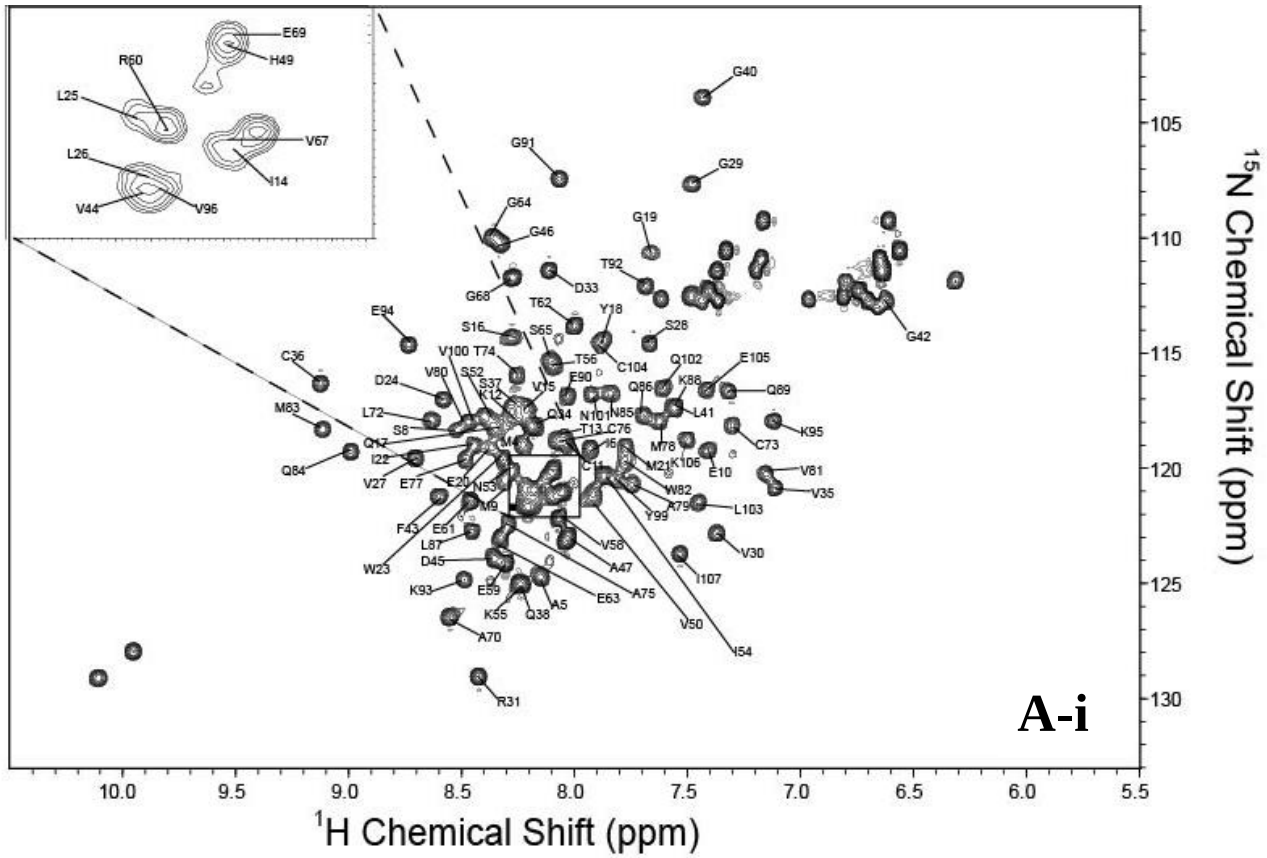
E69
H49
R60
L25
V67
L26
I14
V44
V96
G40
G91
G29
G64
G46
G19
T92
D33
G68
T62
Y18
S28
G42
E94
S16
S65
V100 T74
T56
C104
Q102
E105
C36
D24
V80
S52
S37
E90
Q86
K86
Q89
M63
L72
S8
T13 C76
L41
K95
Q84
I22
V27
E77
E20
N53
M78
K105
E10
C73
V81
V35
W82
A79
L103
Y99
F43
E61
M9
V58
V30
L87
W23
D45
A47
I107
K93
E59
E63
A75
A5
K55
Q38
V50
A70
I54
R31
A-i
10.0
9.5
9.0
8.5
8.0
7.5
7.0
6.5
6.0
5.5
$^{1}$H Chemical Shift (ppm)
105
110
115
120
125
130
$^{15}$N Chemical Shift (ppm)

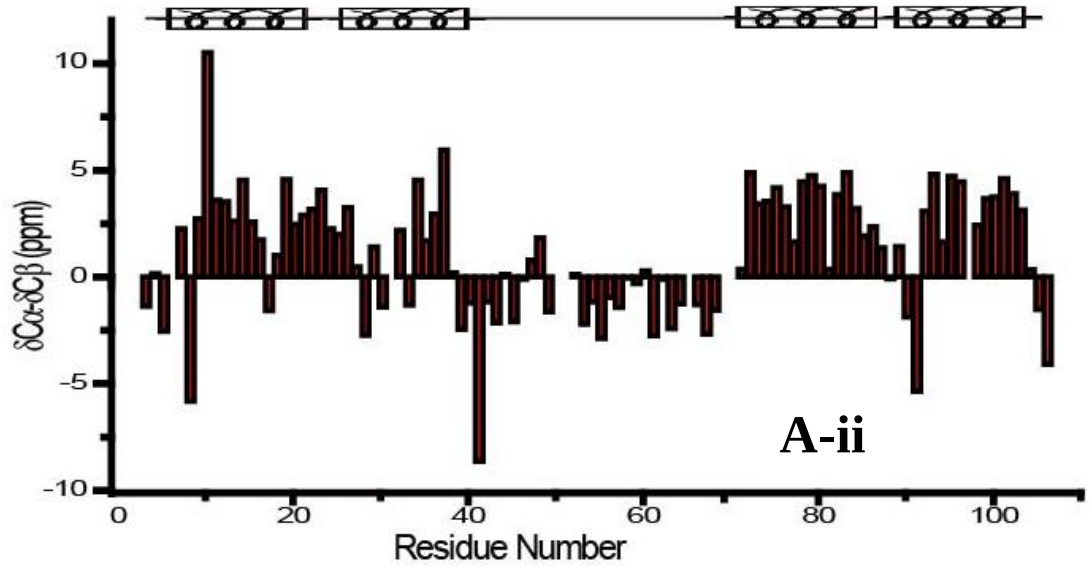
10
5
0
-5
-10
δCα-δCβ (ppm)
A-ii
0
20
40
60
80
100
Residue Number

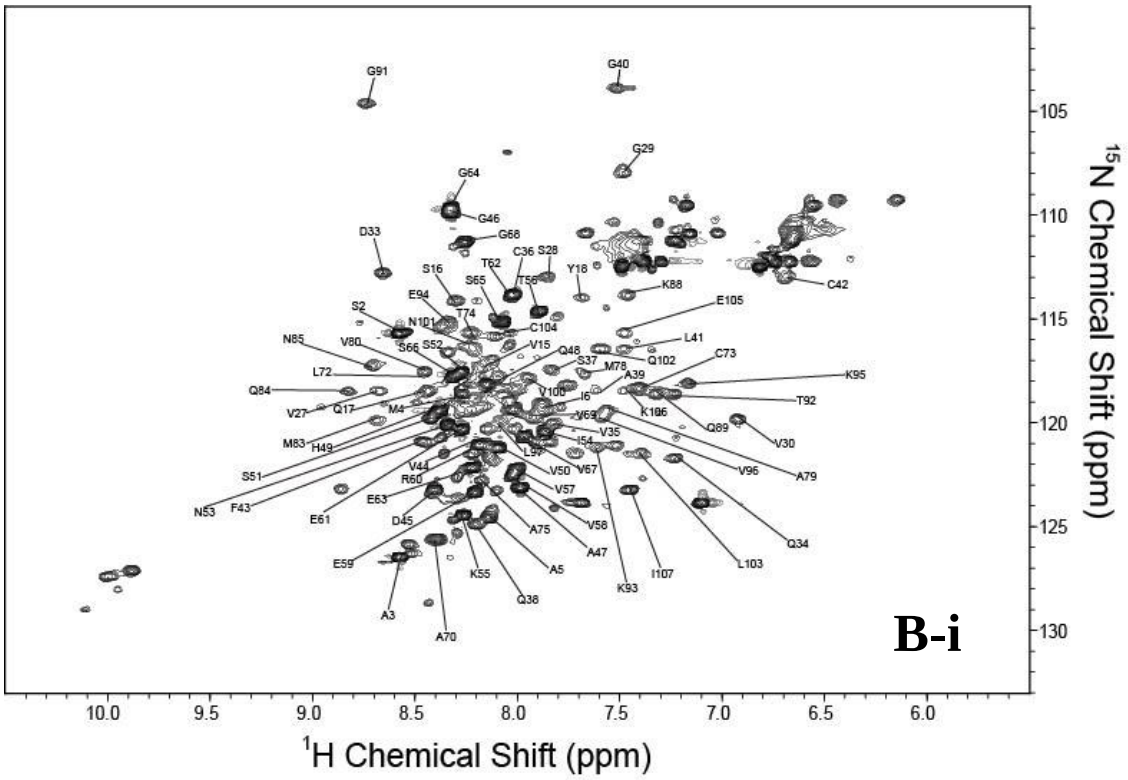


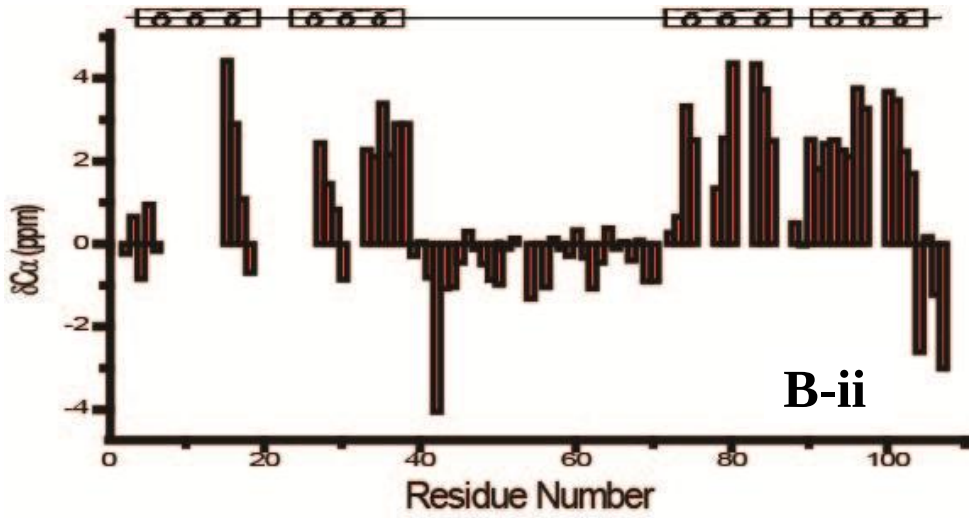


**Figure 4.3 Backbone assignment of the StAP PSI collected on a 500 MHz Bruker Ultrashield™ spectrometer at 298K and chemical shift index plotted against residue numbers. A-i) Backbone assignment of StAP PSI in pH 7.0, A-ii) Chemical shift index of StAP PSI in pH 7.0, B-i) Backbone assignment of StAP PSI in pH 2.0, A-ii) Chemical shift index of StAP PSI in pH 2.0.**

Previously, using Circular Dichroism (CD), Bryksa et al. (2011) elucidated the four helices of PSI independently (H1: residues 1-24, H2: residues 27-34, H3: residues 66-82, and H4: residues 85-99). These four helices were stabilized by three disulfide bonds (H1 to H4 via $Cys^{6}$ and $Cys^{99}$, H3 to H2 via $Cys^{51}$ and $Cys^{71}$, and $Cys^{57}$ and $Cys^{68}$) which led to an open, boomerang shaped tertiary structure, imperative for its functions. Another study performed by Munoz et al. (2014) examined the secondary structure of StAP PSI with IR spectroscopy in which high degree of stability was observed in solution. Although not studied in the current NMR measurements, Munoz et al. (2014) found that the secondary structure of the StAP PSI altered with different temperatures. Low temperatures change the mixture of helical and unordered structures to a mixture of helical structures, whereas high temperatures form unordered and aggregated structures (Munoz et al., 2014). Likewise, structural changes for the StAP PSI were expected as the pH is lowered from neutral to acidic (Bryksa, 2011). The chemical shift perturbation is calculated as per equation [4.3]:

$$Chemical\ Shift\ Perturbation = \sqrt{[(\Delta H)^2 + \frac{(\Delta N)^2}{25}]/2}$$

Changes from the PSI secondary structure is shown in Figure 4.4. These regions 1-2 and 3-4 were found to be the helical segments on the PSI structure. Acidification to the environment can possibly increase the hydrophobicity of Glu and Asp residues in the helical regions (Rafalski et al., 1991), reaching neutralization of the carboxylate groups (de Alba et al., 2003). Similar mechanisms occur in saposin C which leads hydrophobic side chains to become solvent exposed as the saposin fold opens (John et al., 2006). Thus, in StAP PSI, lowering the pH from neutral to pH 2.0 can result in charge alteration on residues which may be critical for the structure. In

contrast, from both the pH 7.0 and pH 2.0 PSI, the unchanged region approximately between residues 37 and 67 matched the crystal structure where no electron density was found (Bryksa et al., 2011).

Due to the high sequence similarity of PSI with other proteins in the SAPLIP family, comparable secondary structures were expected, which gave rise to similar tertiary structures (Bryksa et al., 2011). The overall fold of the StAP PSI is comparable to saposin C and could also be superimposed with the phytepsin PSI; all resulting in a V shaped, open confirmation in the dimer form (Hawkins et al., 2005).

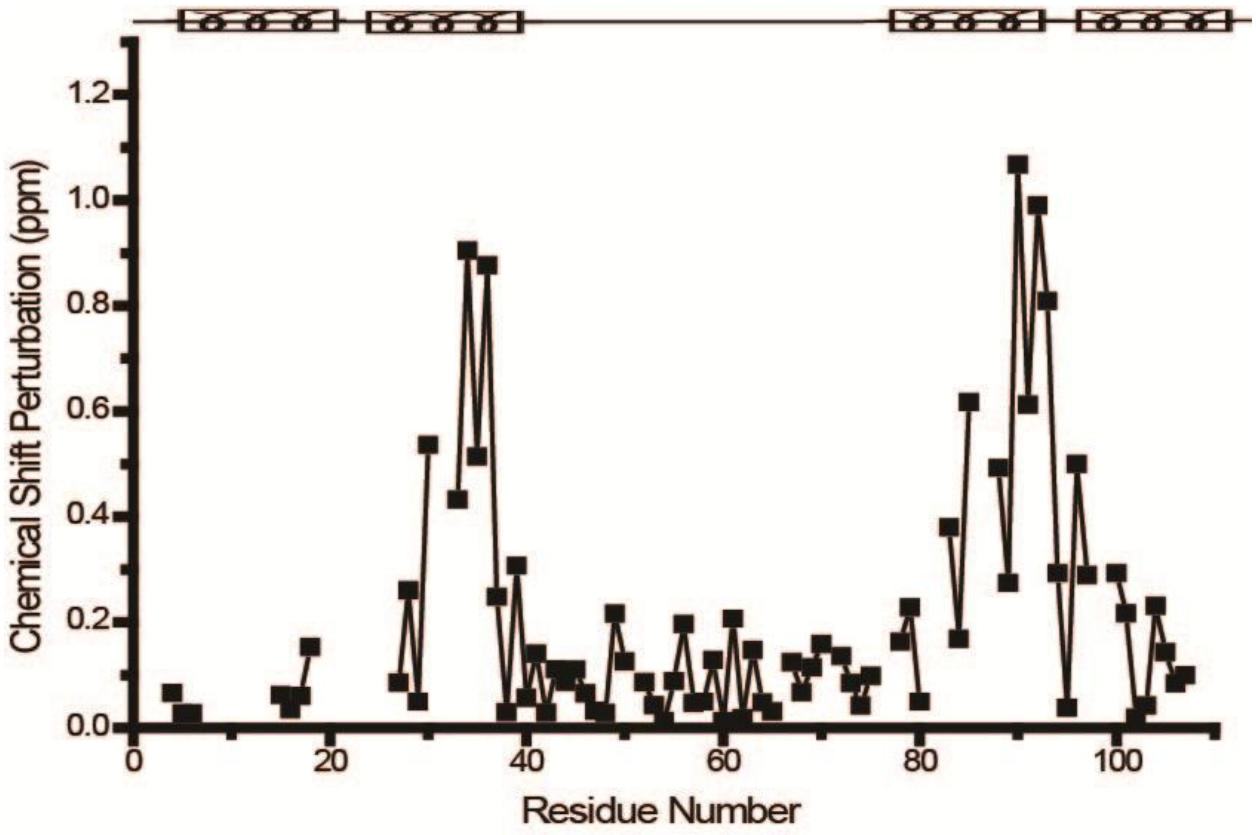


**Figure 4.4 Chemical shift perturbation of the StAP PSI for pH 2.0 and pH 7.0 plotted against the residue numbers.**

## 4.3 $^{1}$H- $^{15}$N NOE Relaxation, Longitudinal Relaxation, Transverse Relaxation

Information on protein dynamics can be obtained from NMR relaxation measurements (de Alba et al., 2003).The $^{15}$N backbone relaxation measurements for the StAP PSI in both pH 7.0 and 2.0 were conducted. Relaxation measurements were collected in both pH 7.0 and pH 2.0 at 298K on a Bruker Ultrashield$^{TM}$ spectrometer at 500 MHz. The data were collected using spectral width for $^{1}$H and $^{15}$N was 6009.615 Hz and 1368.459 Hz, respectively, with a total scan number of 32 per transient.

The NOE was measured as a ratio of NOE and NONOE by applying a pulse signal. This calculated ratio was then plotted against residue numbers of the primary sequence of the PSI. In $^{1}$H- $^{15}$N NOE measurements, ratio of above 0.7 signifies extreme rigidity (Hu et al., 2006), flexibility is related to ratios near zero or in the negative range (Hu et al., 2006)). In both pH 7.0 and 2.0 in Figure 4.5-A and B, respectively, most helical segments of the PSI were rigid, whereas the N-terminus, C-terminus and the loop connecting helices were very flexible. The rigid segments correspond to the helices of the PSI, namely H1 to H4; and the flexible region corresponds to the extended loop between H2 and H3. Residues which had weak signals or overlapping signals displayed poor data quality. Therefore, these residues were excluded from the relaxation analysis. The rigid segments of the PSI demonstrated chemical shift perturbation from pH 7.0 to 2.0 in Section 4.2. The changes in chemical shift suggested that these regions were related to the structural change of the PSI. Likewise in the SAPLIP, a high degree of mobility in saposin C was observed in its short loops, and the N-and C-termini, whereas the regular secondary structure regions were extremely rigid (de Alba et al., 2003). The backbone physical characteristic similarities between SAPLIP were expected as they have high sequence homology and the saposin fold (Bryksa et al., 2011).

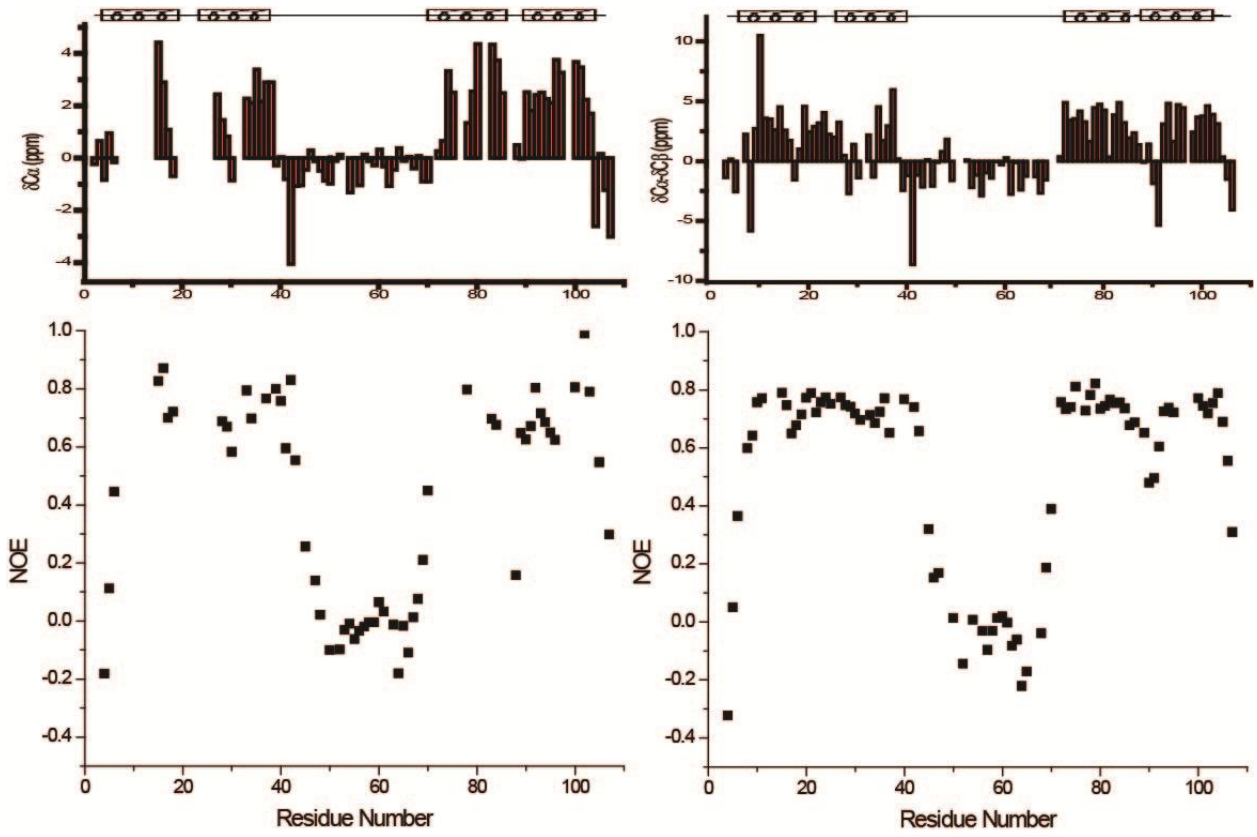


**Figure 4.5 Nuclear Overhauser Effect (NOE) of the StAP PSI collected at A) pH 2.0, B) pH 7.0.**

Longitudinal and transverse relaxation methods were used to characterize the dynamics of PSI. From our previous results, it is suspected that monomer and dimer equilibrium existed by varying the pH conditions. As shown in Figure 4.6-A and B, longitudinal relaxation of the StAP PSI at pH 7.0 and 2.0, respectively, PSI at pH 7.0 tumbled at a different rate than at pH 2.0. The average time of the longitudinal relaxation at pH 7.0 was 0.53 ± 0.03 s and at pH 2.0 was 0.99 ± 0.18 s. The average tumbling time of PSI at pH 7.0 was half of when it was at pH 2.0. This confirmed that the PSI at pH 7.0 is a monomer, whereas PSI at pH 2.0 is a dimer. The flexible loop moved at a faster rate than the rest of the protein and it was excluded from the calculation of average relaxation rates. On the other hand, small molecules in longitudinal relaxation tumble fast, whereas large molecules tumble slowly (Teng, 2013). In transverse relaxation, the average time at pH 7.0 was 108 ± 14 ms, and at pH 2.0, the average relaxation time was 48 ± 9 ms. Figures 4.7 A and B shows the transverse relaxation of the StAP PSI at pH 7.0 and 2.0, respectively. The average tumbling time of PSI at pH 2.0 was almost half of when it was at pH 7.0. This further confirmed that the PSI at pH 7.0 is a monomer and at pH 2.0 is a dimer. Like in longitudinal relaxation, the flexible loop moved at a different rate than the rest of the protein, thus, excluded from the calculations. $^{15}$N relaxation measurements examined the monomer-dimer equilibrium of PSI at a residual level. These findings agreed with Bryksa's (2016) analytical ultracentrifugation results in examining the monomer-dimer equilibrium of PSI. Analytical centrifugation measurements presented that the molecular mass of PSI at pH 7.4 was 12.5 kDa, whereas 21.7 kDa in pH 3.0. The fluorescence emission were also taken for pH 6.4 and 4.5, similar signals were found between pH 6.4 and pH 7.4 and different from at pH 4.5 and 3.0 (Bryksa, 2016). The StAP PSI is a monomer in neutral pH and dimer in the acidic pH.

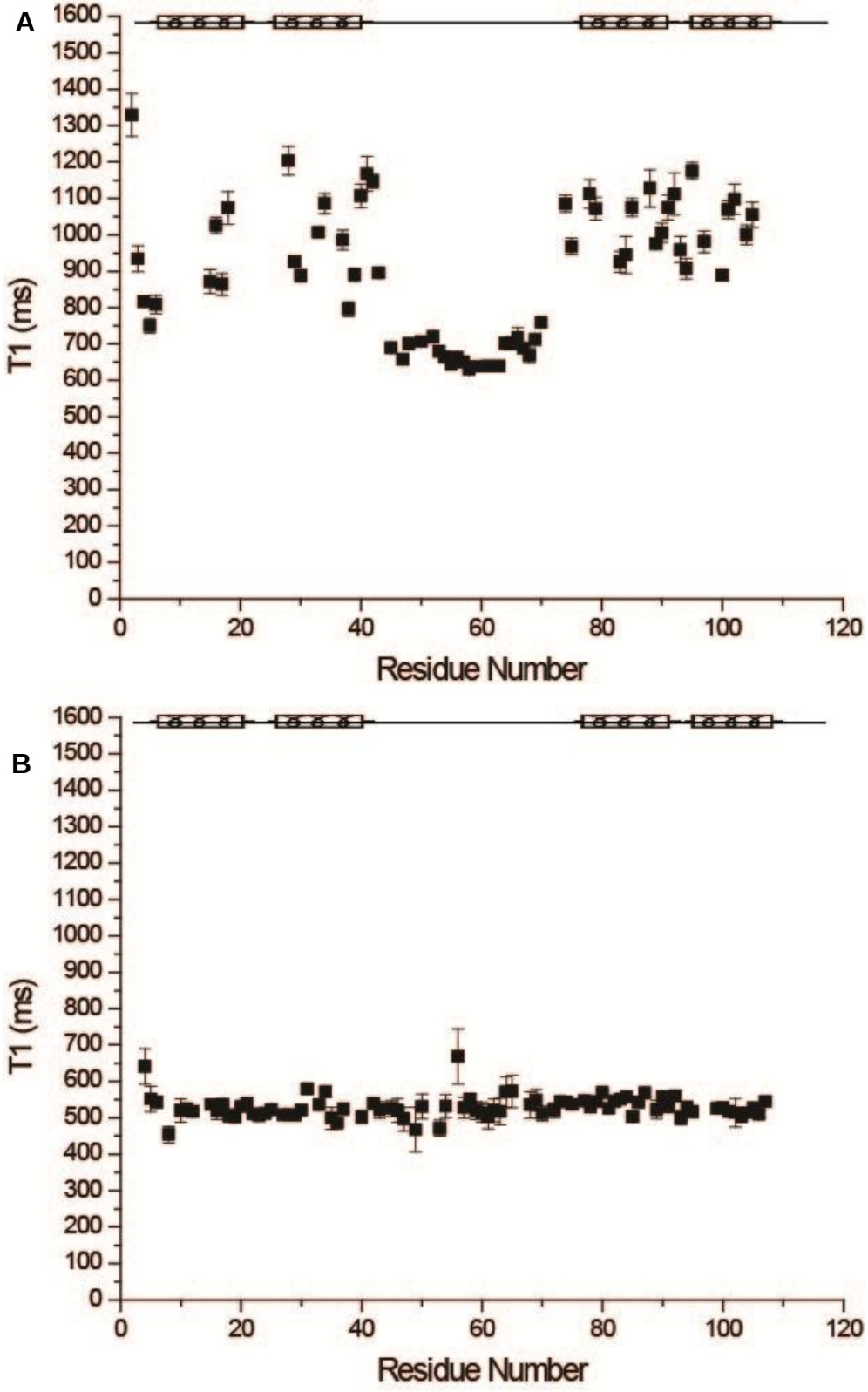


**Figure 4.6 Longitudinal relaxation collected for the $^{15}$N StAP PSI at A) pH 2.0, B) pH 7.0.**

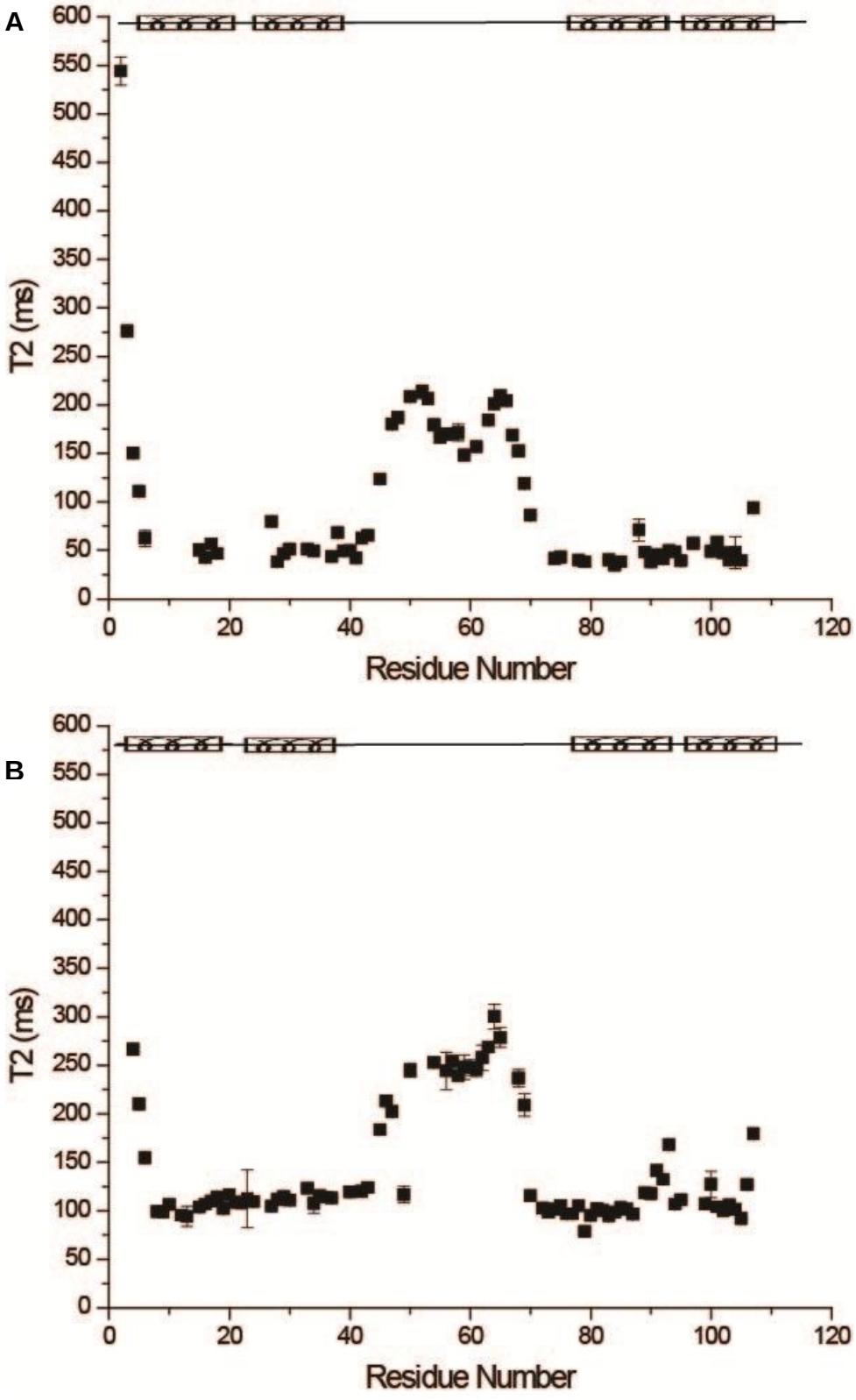


**Figure 4.7 Transverse relaxation of the $^{15}$N StAP PSI collected at A) pH 2.0, B) pH 7.0.**

Although the StAP PSI is sequentially related to the mature saposins, especially in saposin C (Munoz et al., 2010; Bryksa et al., 2011), remarkable differences were found for their behaviour in solution with different pHs. The behavior of saposins A-D at pH 4.0 and pH 7.0 were summarized by John et al. (2006) in Table 4.1. From these results, only saposin C shared common conformation as the StAP PSI. Changes with pH were observed in all mature saposins except for in saposin D (John et al., 2006). These findings suggested that the mechanism of action would be different for the SAPLIPs.

| Protein | pH 4.0 | pH 7.0 |
|---|---|---|
| Saposin A | Strongly aggregated | Monomeric, multiple confirmations |
| Saposin B | Dimeric, multiple conformations | Dimeric, multiple conformations |
| Saposin C | Monomeric, dimeric | Monomeric |
| Saposin D | Monomeric, two conformations | Monomeric, two conformations |

**Table 4.1 Human saposins A-D in solution. The behaviour of human saposins A-D in solution are summarized in Table 1, adapted from John et al., 2006.**

## 4.4 PSI-Membrane Interaction with pH in Solution State NMR

Previously our research group (Bryksa et al., 2011) determined that PSI has membrane disruption activities which can cause vesicle leakage in the acidic pH range depending on the phospholipid composition (Bryksa et al., 2011). To gain information on the PSI-phospholipid interaction as a function of pH at a residual level, solution state NMR was employed. $^{1}H$-$^{15}N$ HSQC were collected for PSI at pH 2.0 and pH 7.0 with and without the addition of phospholipids (PC/PE/PS at 1:1:1) as shown in Figure 4.8. From these spectra, $^{1}H$ and $^{15}N$ chemical shift changes were observed to identify the presence of change at a residue level upon condition changes (de Alba et al., 2003). The StAP PSI at pH 7.0 did not show any conformation or chemical change as the phospholipid mixture was added to the protein sample. All NMR signals from the HSQC spectrum were identical for both the PSI at pH 7.0 and when the phospholipid was added to the sample at pH 7.0. This suggested that the PSI does not interact with phospholipids under neutral pH. In contrast, the HSQC of StAP PSI at pH 2.0 demonstrated dramatic difference upon mixing with liposomes. Upon the addition of the phospholipid mixture, the majority of the signals disappeared. This signified that PSI was active at pH 2.0 and interaction with the phospholipid mixture was apparent. As the PSI binds with phospholipid in solution, the overall complex size increases, causing slower tumbling rate. This phenomenon caused the signals on the HSQC spectrum to broaden and disappear as larger sizes of complex cannot be observed in solution state NMR (Teng, 2013). By overlapping the HSQC spectra of PSI-phospholipid in pH 2.0 and pH 7.0 as in Figure 4.9, a clear difference can be observed at the two different pHs. A similar result was found with saposin C upon binding with phospholipids, slow molecular tumbling causing unobservable signals (de Alba et al., 2003).

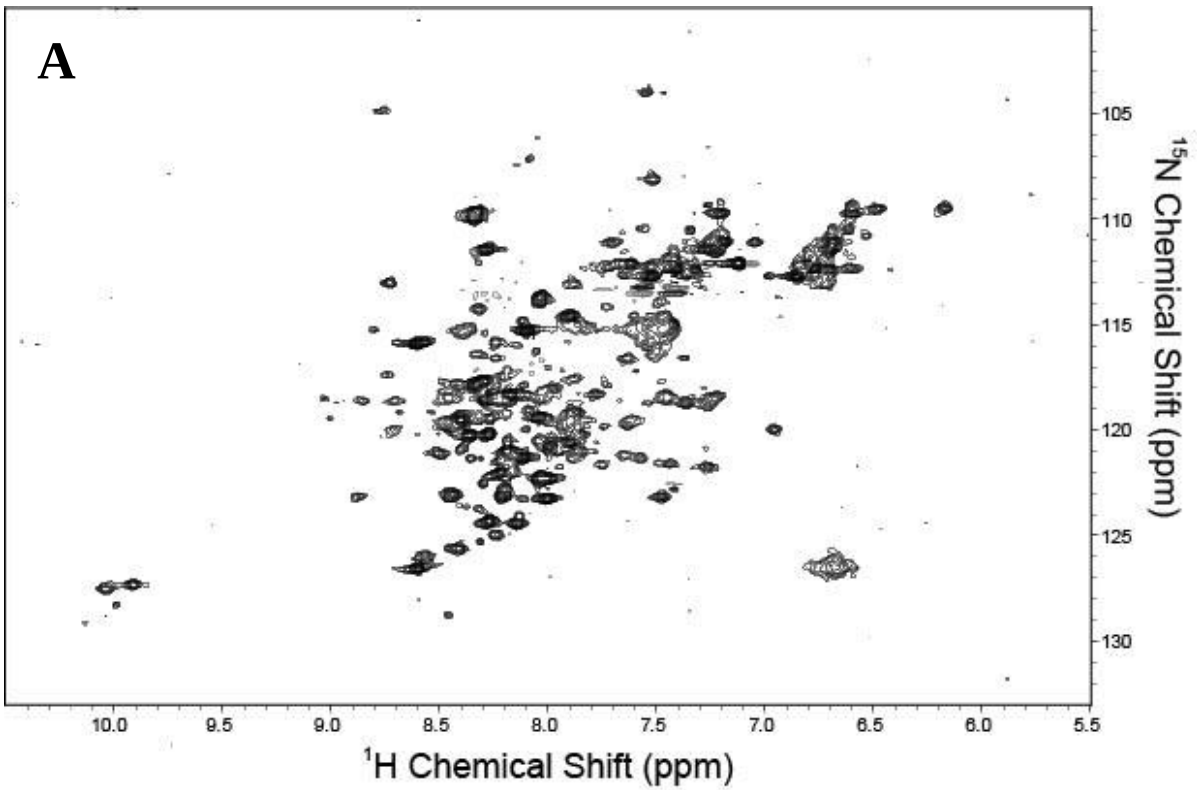
A
105
110
115
120
125
130
$^{15}$N Chemical Shift (ppm)
10.0
9.5
9.0
8.5
8.0
7.5
7.0
6.5
6.0
5.5
$^{1}$H Chemical Shift (ppm)

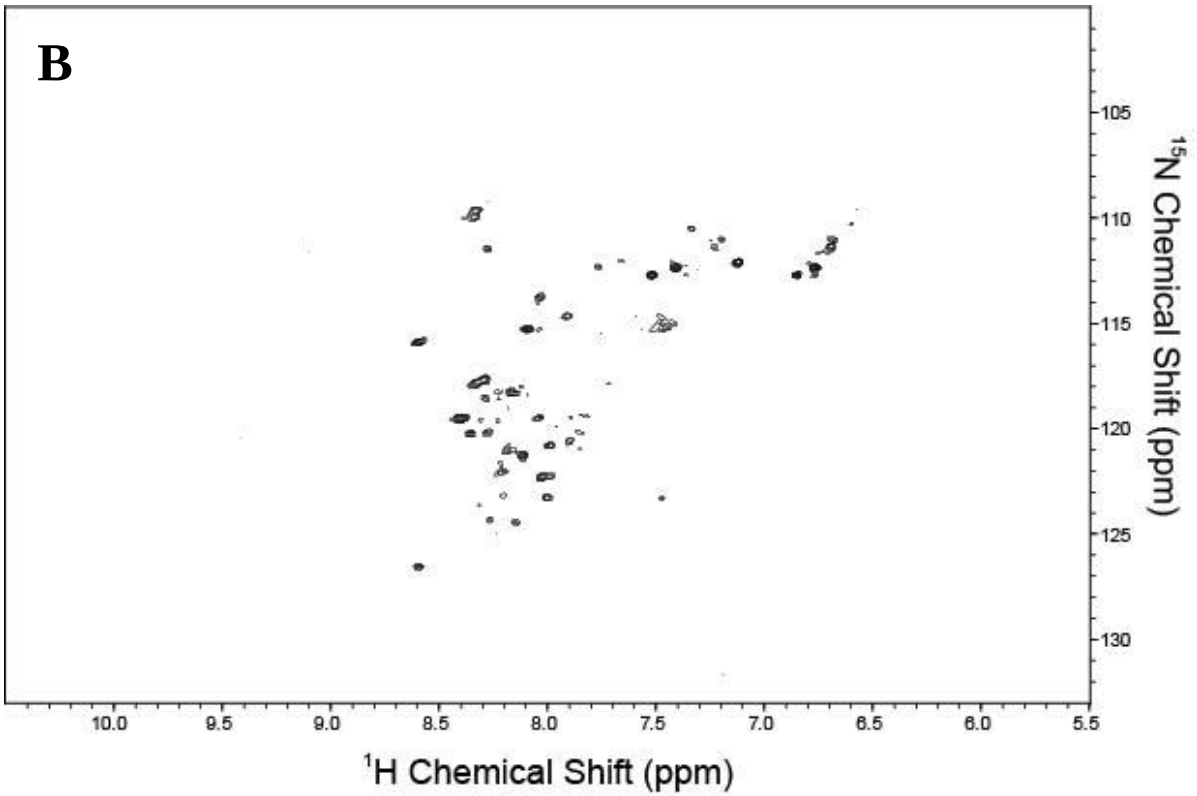
B
105
110
115
120
125
130
$^{15}$N Chemical Shift (ppm)
10.0
9.5
9.0
8.5
8.0
7.5
7.0
6.5
6.0
5.5
$^{1}$H Chemical Shift (ppm)

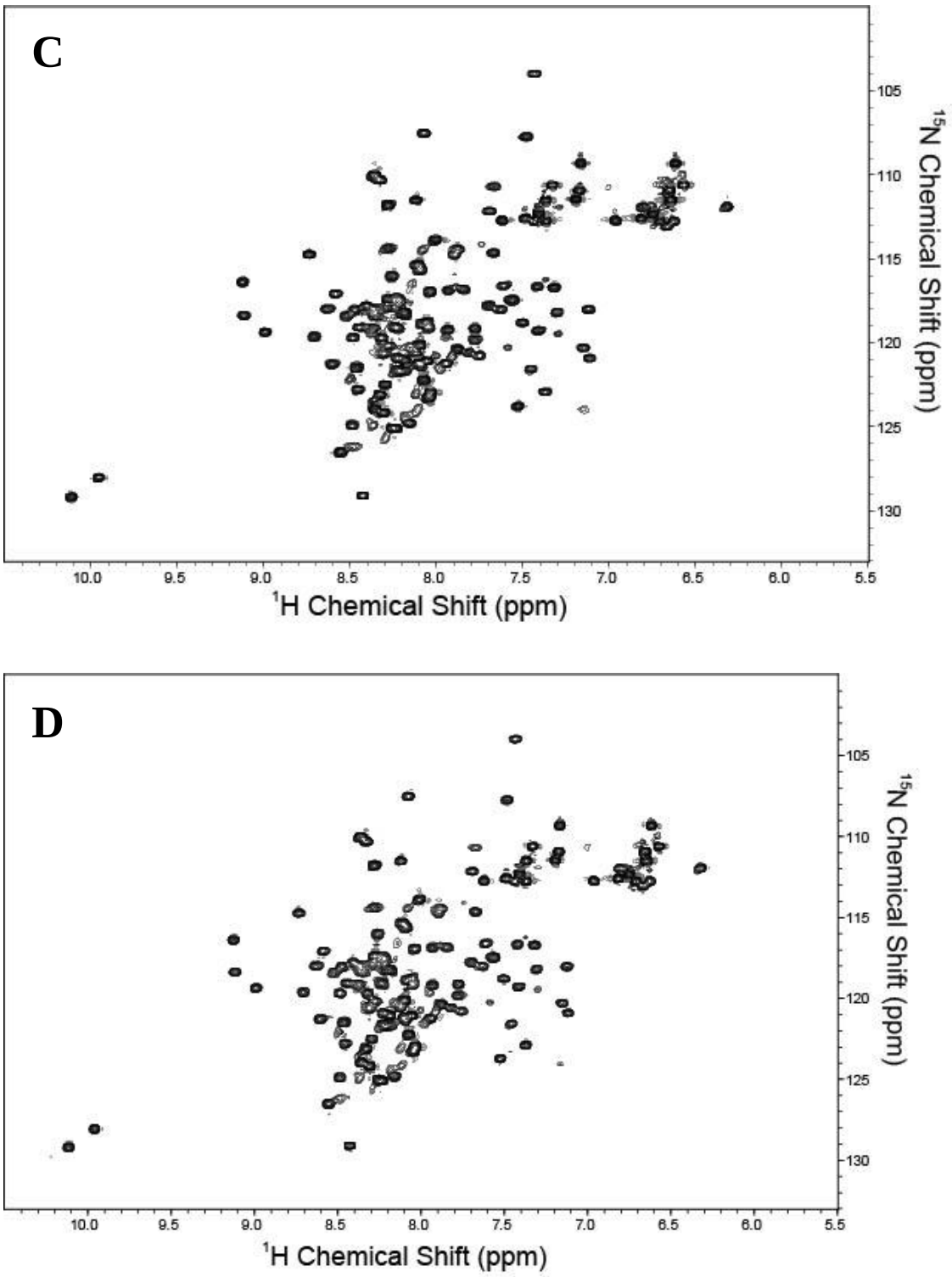


**Figure 4.8 PSI Titration of the StAP PSI. A) PSI in pH 2.0 without phospholipids, B) PSI in pH 2.0 with phospholipids, C) PSI in pH 7.0 without phospholipids, D) PSI in pH 7.0 with phospholipids.**

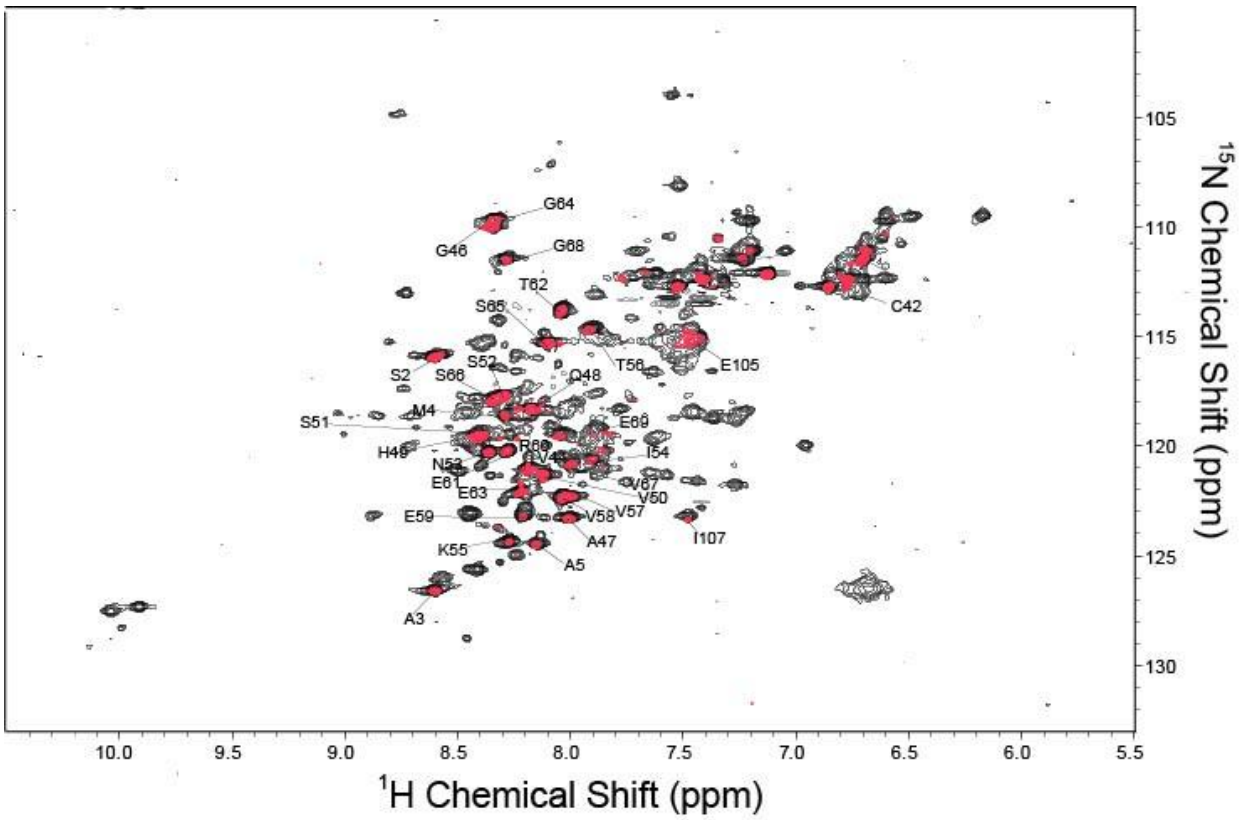


**Figure 4.9 Overlapping titration of the StAP PSI from pH 2.0 and pH 7.0 both with phospholipids (Red represents pH 2.0).**

From the backbone assignment, the remaining signals of PSI on the HSQC spectra after interacting with liposomes represented the flexible loop of the PSI. This result suggested that only the helical segments of the PSI were active in the interaction with phospholipids. This is in accordance with results reported above where chemical perturbations were the most significant in helical regions of the PSI. From the crystal structure of StAP PSI, the tertiary structure of one monomer from the dimers is organized such that one side is enriched with polar residues and the other side is composed of hydrophobic residues (Bryksa et al., 2011). The organization of residues suggested that interaction with the phospholipid membrane would occur from the hydrophobic side. Likewise in saposin C, charged amino acid side chains were solvent exposed, while the hydrophobic phase was partially or completely buried in the protein core (de Alba et al., 2003). Saposin C formed a negative potential from the high content of negatively charged residues and their location on the exterior. The solvent exposed positively charged residues corresponded to lysines on the surface (de Alba et al., 2003). Critical amino acids on the hydrophobic regions of the protein have an important role in the interaction with membrane in the acidic pH.

The StAP PSI membrane interaction depends on pH and membrane compositions. By examining phospholipid bilayer disruption activity using large unilamella vesicles containing self-quenching fluorophore, Bryksa et al. (2011) suggested that any PL combination cannot be disrupted in the neutral pH and that neutral vesicle combination such as PC/PE did not show any disruption activity at any concentration. On the other hand, notable activity was achieved in equimolar combination of PS/PC/PE (Bryksa et al., 2011). Additionally, AFM revealed pronounced acidic PL bilayer rearrangement in the same conditions as disruption activity. The hydrophobic regions on the StAP dimer could be responsible for these activities. Recently,

Munoz et al. (2011; 2014) further examined the change of StAP PSI secondary structure upon lipid membrane interaction using IR spectroscopy. The PSI exhibit self-association and it interacts with both uncharged and negatively charged phospholipids by partitioning and burying in the membranes based on the presence of negatively charged phospholipids (Munoz et al., 2011; Munoz et al., 2014). In both Bryksa (2011) and Munoz's (2011; 2014) research, PSI interaction occurs in the acidic environment through neutralization of Glu and Asp, which lead to increased hydrophobicity (Munoz et al., 2014). This stabilizes the α-helices (Rafalski et al., 1991), and as determined by NMR, the rigid segments of PSI enhance membrane binding (Vacarro et al., 1999; Egas et al., 2000).

Similarly, in other SAPLIP including saposins A, C and D, the overall hydrophobicity increase upon acidification (Vacarro et al., 1995; Vacarro et al., 1999). The hydrophobic domains on the affected saposins are within the α-helices which trigger phospholipid membrane binding; this activity is dependent on the disulfide bridges (Vacarro et al., 1999). In contrast, saposin B remains unchanged from acidification (Vacarro et al., 1995; Vacarro et al., 1999). In general, saposin C and D were found to have similar hydrophobic residues and they exhibit stronger interaction with the phospholipids in the acidic pH when compared to saposin A (Vacarro et al., 1995; Vacarro et al., 1999). In particular, saposin C exhibited the strongest interaction. NMR studies on saposin C supported these findings by examining the conformational change at a residue level. Dramatic chemical shift perturbation occurred in the acidic pH and that binding was reversible between neutral and acidic conditions (de Alba et al., 2003). Additionally, composition of the phospholipids is critical for binding. Saposin D has no membrane binding activity in the absence of PS, whereas in saposin C, the binding is still present. However, in the presence of PS, membrane destabilization is increased (Vacarro et al.,

1994; Vacarro et al., 1995) in comparison to the absence of PS in a mixture. These results indicated that under acidic pH, saposin C is capable of destabilizing and cause fusion activities by altering the permeability of membranes containing PS (Vacarro et al., 1994).

### 4.5 Examining PSI-Membrane Interaction from Phospholipids

The effects of PSI on phospholipid membranes was studied using the $^{31}$P NMR spectra recorded on the Bruker Avance III Spectrometer at 600.230 MHz using direct polarization with $^{1}$H decoupling. The spectra records activities which are related to the phosphate group. Two types of phospholipids were examined for the interaction with PSI, including a mixture of PC/PE/PS with equal molar amount and a natural pig brain phospholipid mixture, as shown in Figure 4.10 and 4.11, respectively.

The MAS spinning $^{31}$P NMR spectra for the control in Figure 4.10-A showed the presence of three different spectral components. This is due to the three phospholipids in the mixture giving rise to the different $^{31}$P chemical shift. The control phospholipid mixture displayed sharp peaks in the spectra. When the phospholipids were scanned separately and individually, different chemical shifts were apparent as compared to the mixture (results not shown). Thus, we were unable to conclude which peak belonged to which phospholipid. Phospholipids can have intermolecular interactions and microscopic miscibility when combined in a mixture, so that strong inter-polar head group interactions (hydrogen bonding) could occur (Shin et al., 1995). This would cause a change in the chemical shift in the phospholipid mixture. Upon addition of the PSI to the phospholipid mixture, changes in spectral resolution were manifested by the broadened peaks shown in Figure 4.10-B. The disappearance of sharp peaks suggested that PSI-membrane interaction occurred via the phosphate head group. By superimposing the phospholipid mixture spectra and the spectra upon addition of PSI in Figure

4.10-C, changes in the sharpness of two of the three peaks were noticeable. The unaffected peak suggested that the perturbation at the head group was not apparent in that particular phospholipid type. Similar to PSI, Abu-Baker et al. (2005) observed interactions at the phospholipid head group with saposin C.

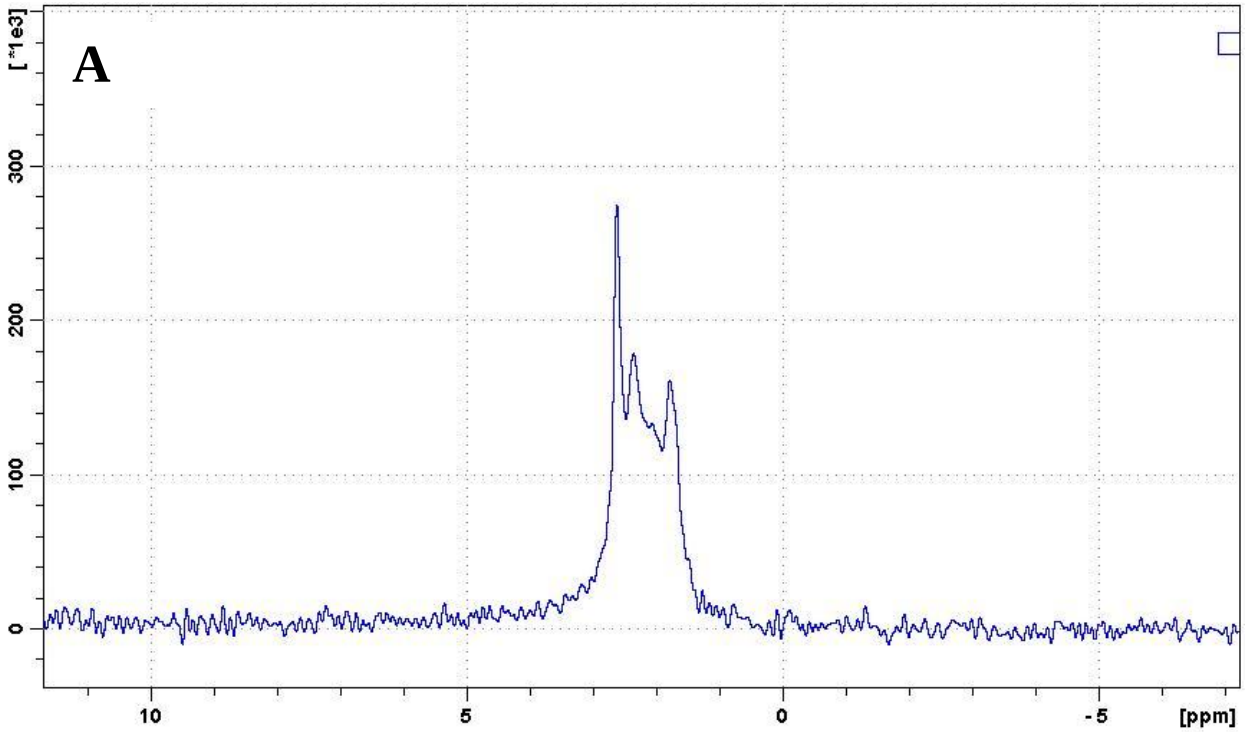
A
[*1e3]
300
200
100
0
10
5
0
-5
[ppm]

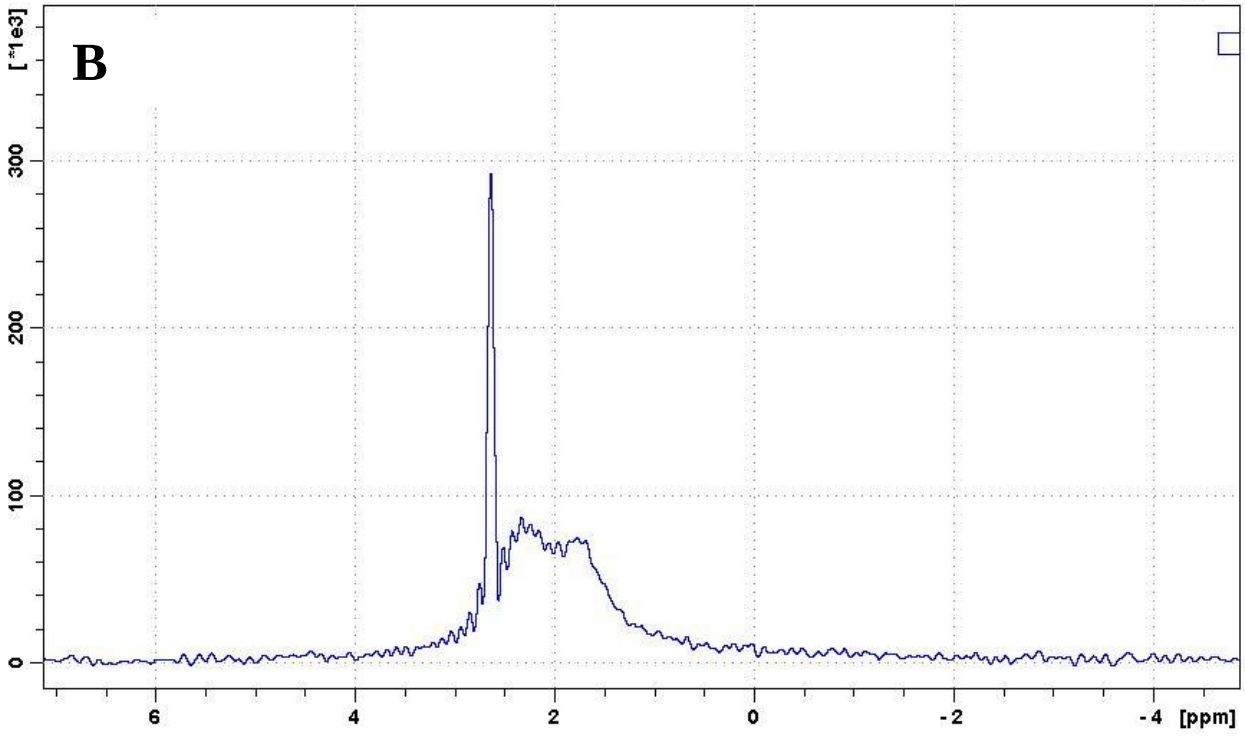
B
[*1e3]
300
200
100
0
6
4
2
0
-2
-4
[ppm]

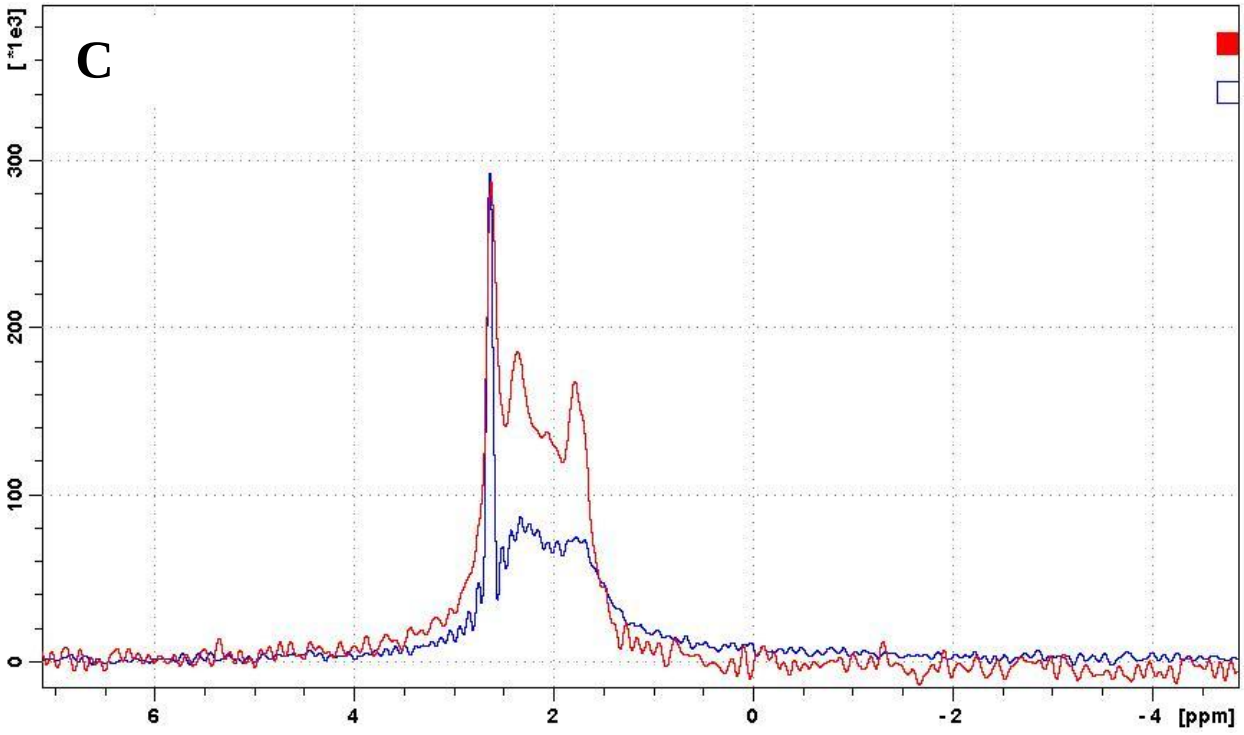


**Figure 4.10 PSI and PC/PE/PS phospholipid mixture interaction on $^{31}$P spectrum in pH 2.0. A) Phospholipids only, B) Phospholipids with PSI, C) Overlap of phospholipid and phospholipid-PSI spectrum.**

As PSI-membrane interaction occurs in natural systems, it was of our interest to examine the interaction relative to the physiological system through an extracted natural mixture of pig brain phospholipids. The natural pig brain phospholipid mixture was scanned independently in Figure 4.11-A, again resulting in sharp peaks. Upon adding the PSI to the natural phospholipid mixture in Figure 4.11-B, the spectra broadening was similar to the synthetic PC/PE/PS phospholipid mixture. However, peak broadening is not as significant as shown in Figure 4.11-C, superimposing the spectra of natural phospholipids alone and with PSI. This suggested that the PSI-membrane interaction capacity could be due to the phospholipid composition.

Taken together, the StAP PSI is confirmed for membrane interaction (Munoz et al., 2010; Bryksa et al., 2011), and the interaction occurs at the phosphate head group. The composition of the phospholipids affects the overall charge on the membrane bilayer; PSI had no effect on the combination of 1:1 PC/PE neutral vesicles at any concentration (Bryksa et al., 2011). With other membrane compositions PSI induced bilayer disruption with order of leakage rates: PE/PS>PC/PS>PE/PC/PS (Bryksa et al., 2011). Thus, we predict that the unaffected peak on the $^{31}$P spectra to be the PC from the mixture.

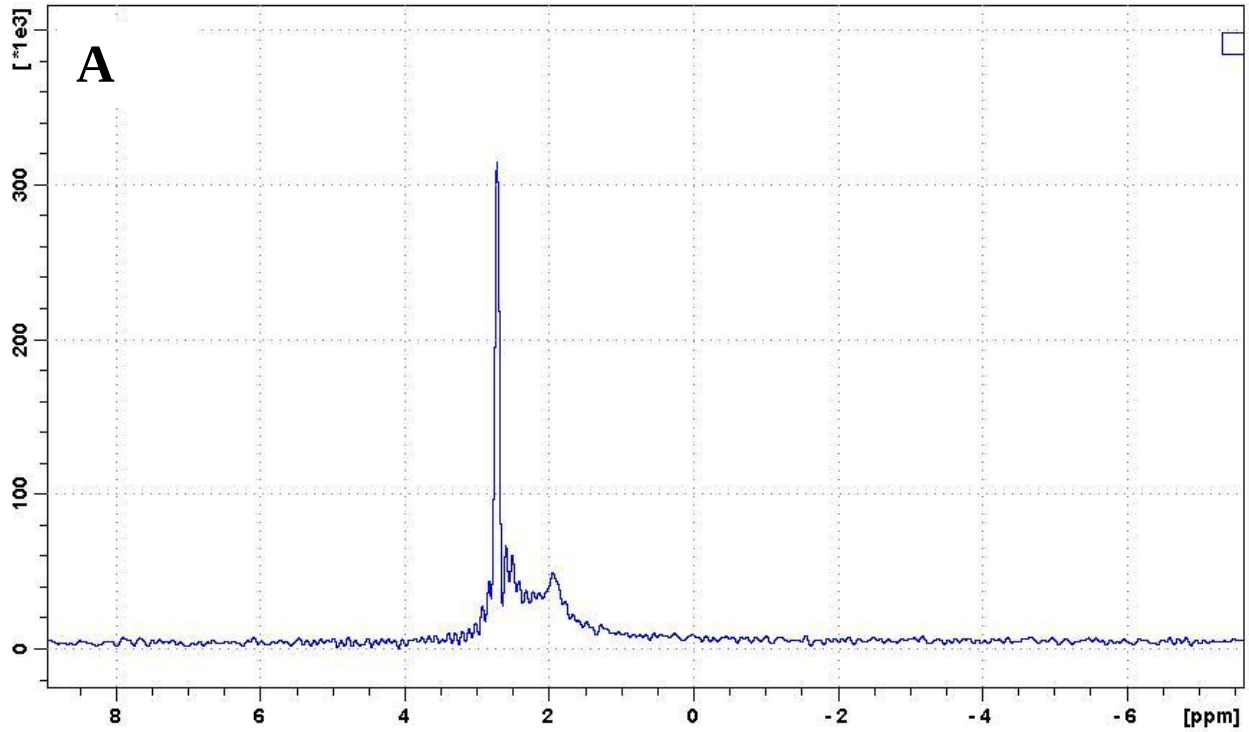
A
[*1e3]
300
200
100
0
8
6
4
2
0
-2
-4
-6
[ppm]

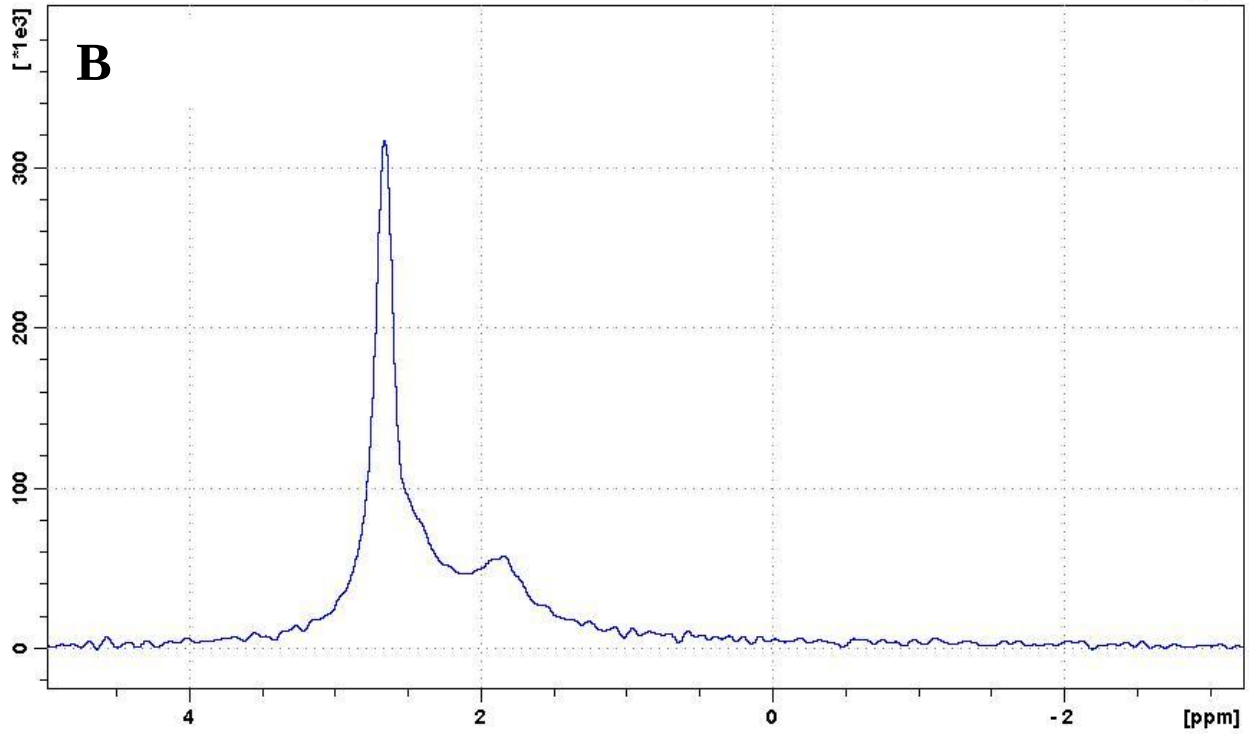
B
[*1e3]
300
200
100
0
4
2
0
-2
[ppm]

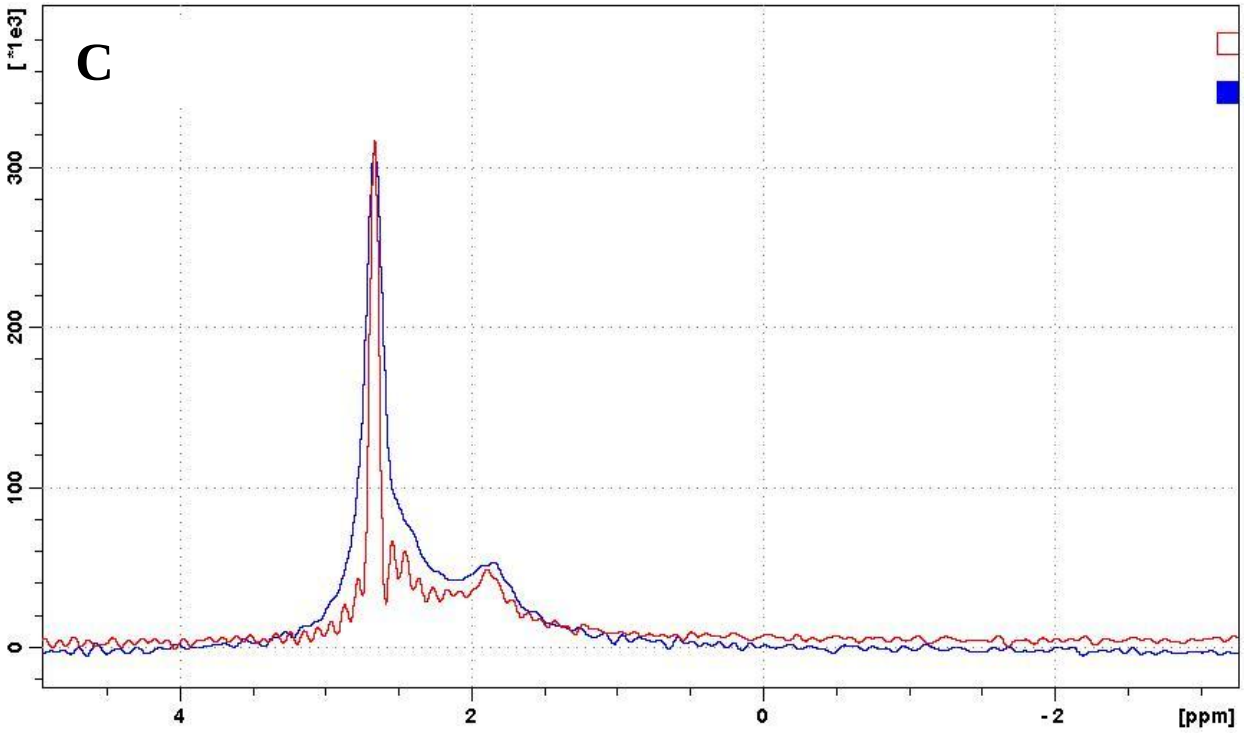


**Figure 4.11 PSI and pig brain phospholipid mixture interaction on $^{31}P$ spectra in pH 2.0. A) Phospholipids only, B) Phospholipids with PSI, C) Overlap of phospholipid and phospholipid-PSI spectra.**

## 4.6 PSI Topology Upon Membrane Interaction

The StAP PSI-phospholipid membrane interaction resulted in white aggregates, as shown in Figure 4.12. The aggregates were ultracentrifuged and packed into a 3.2 mm solid state NMR rotor for spectra collection.

To elucidate the topology of PSI upon membrane interaction, a series of HSQC were collected on PSI in deuterium buffer at pH 7.0 and 2.0 over 24 hours to examine the extent of protein self-protection. The mechanism of H/D exchange involves replacing a covalently bonded hydrogen atom with a deuterium atom, or vice versa (Kazazic et al., 2010). Figure 4.13 illustrated the PSI H/D exchange for protein self-protection at pH 7.0. A $H_2O$ buffered PSI HSQC spectra in Figure 4.13-A demonstrated all cross peaks which appeared from the protein in monomer as a control. By immediately mixing the lyophilized PSI sample with deuterium buffer at pH 7.0, the fast exchangeable residues disappeared leaving the non-exchangeable/slow exchangeable residues as shown in Figure 4.13-B. After 24 h, Figure 4.13-C presented the remaining cross peaks for the PSI at pH 7.0, which were either very slowly exchangeable or non-exchangeable. These cross peaks represented residues which were protected in the monomer form of the StAP PSI. According to the StAP PSI (PDB code: 3RFI), these slowly exchangeable/non-exchangeable regions at residues 22-36 and 78-84 were around the connecting turns between helix 1-2 and helix 3-4, respectively. This result suggested that the protection of protein is strongly related to the folding of the PSI. The majority of helical segments of PSI in pH 7.0 were exchangeable.

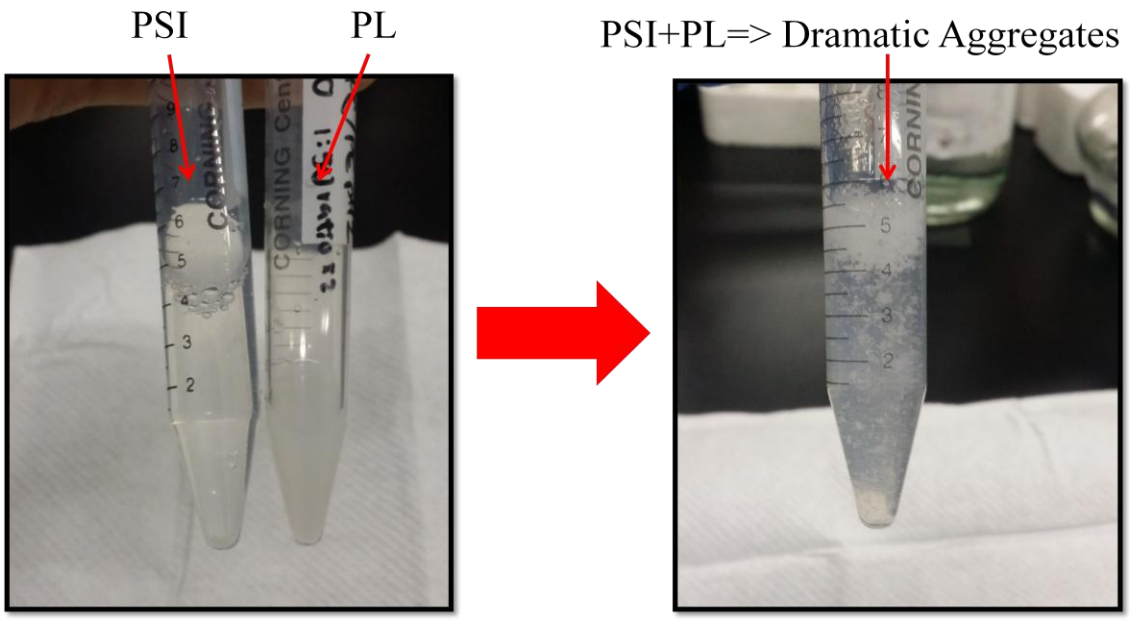


**Figure 4.12 Visual representation of phospholipids and PSI before and after reaction, A) PSI and phospholipids before reaction, B) PSI and phospholipids upon interaction.**

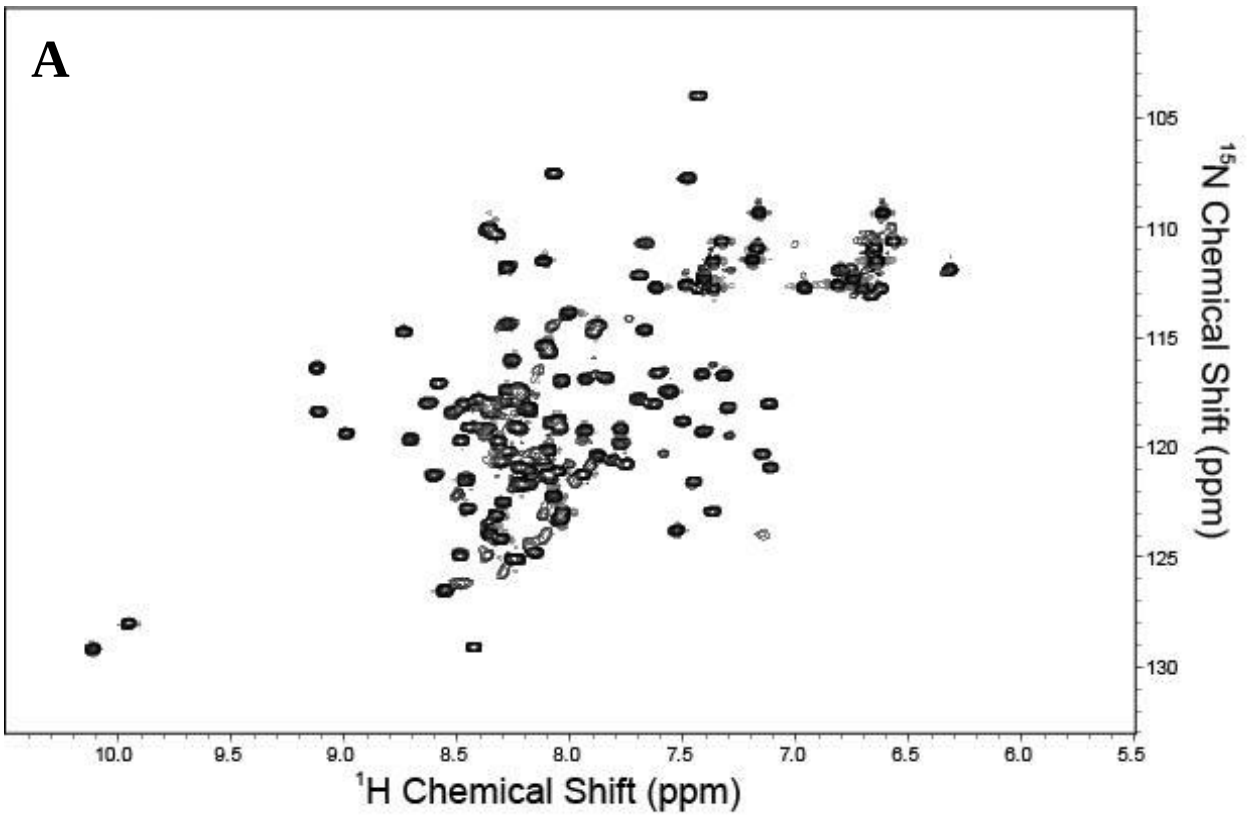
A
105
110
115
120
125
130
$^{15}$N Chemical Shift (ppm)
10.0
9.5
9.0
8.5
8.0
7.5
7.0
6.5
6.0
5.5
$^{1}$H Chemical Shift (ppm)

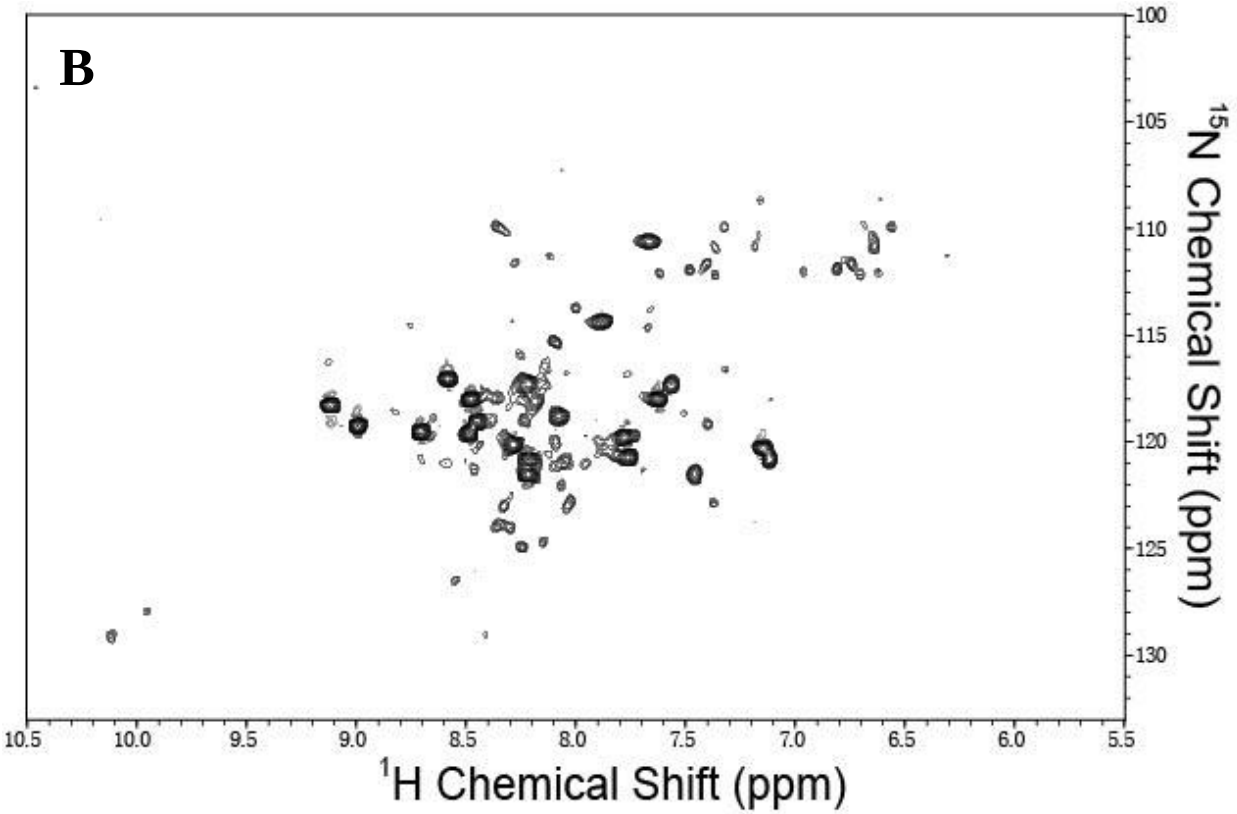
B
100
105
110
115
120
125
130
15N Chemical Shift (ppm)
10.5
10.0
9.5
9.0
8.5
8.0
7.5
7.0
6.5
6.0
5.5
1H Chemical Shift (ppm)

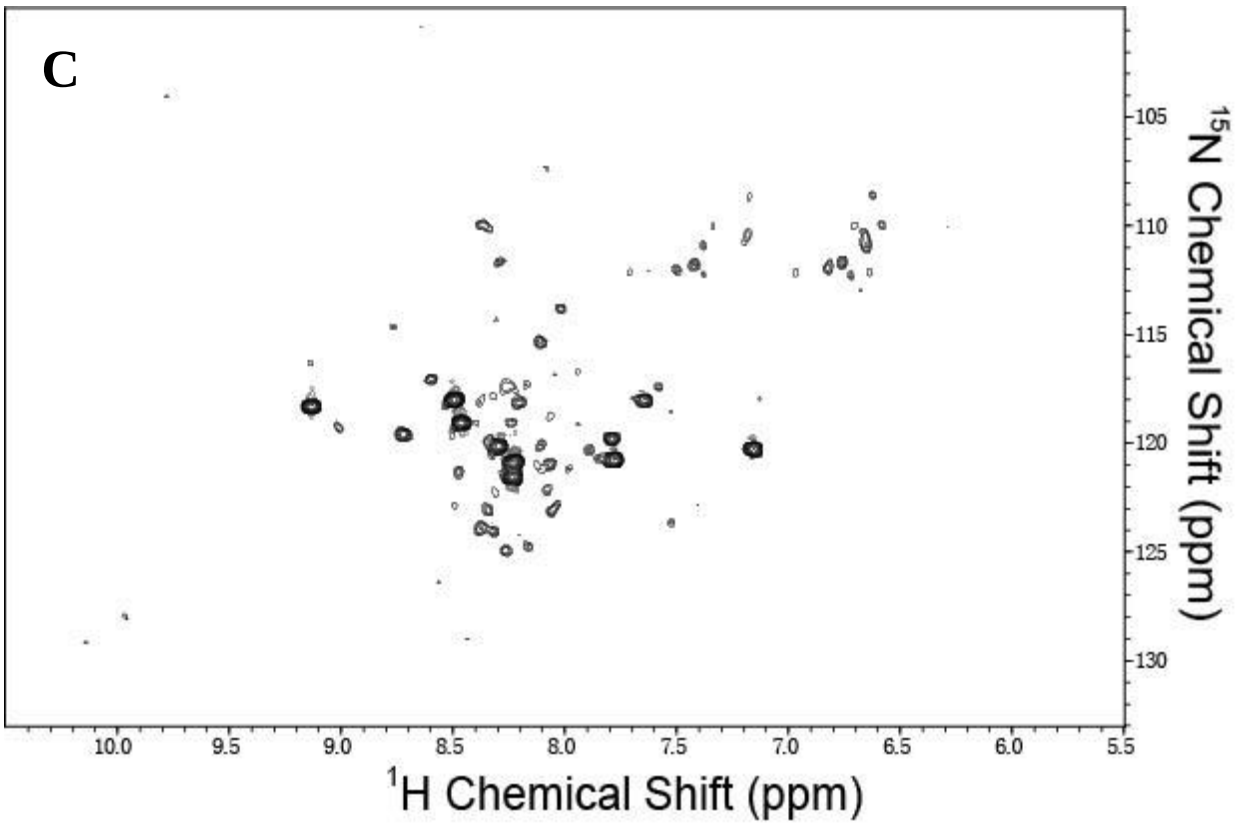


**Figure 4.13 PSI self-protection shown through $D_2O$ exchange in pH 7.0. A) PSI in pH 7.0 buffer, B) PSI in pH 7.0 $D_2O$ buffer immediately, C) PSI in pH 7.0 $D_2O$ buffer after 24 hours.**

Similar procedures were performed for the StAP PSI in pH 2.0 shown in Figure 4.14 to examine protein self-protection in the dimer form. The HSQC spectra of PSI, in $H_2O$-based buffer, in Figure 4.14-A demonstrated all cross peaks which appeared from the protein in dimer as a control. Upon the immediate mixing of the lyophilized PSI with pH 2.0 deuterium buffer, similar to that seen at pH 7.0, the fast exchangeable residues disappeared, leaving the non-exchangeable/slow exchangeable residues as shown in Figure 4.14-B. A decrease in the number of detected cross peaks was apparent on the HSQC spectra. After 24 h, the remaining cross peaks for the PSI at pH 2.0 (Figure 4.14-C) which were either very slowly exchangeable or non-exchangeable. These cross peaks represented residues which were protected in the dimer form on the StAP PSI. From the StAP PSI sequence and assignment which had identifiable residues, the slowly exchangeable/non-exchangeable regions are comprised of residues 15-20, 30-40, 77-84 and at 100. These segments include the connecting turn as identified from the monomer H/D exchange experiments. The rate of this exchange depends on the protein backbone confirmation and dynamics; highly unstructured and unprotected regions can exchange rapidly, hydrogen-bonded amide hydrogen and protected regions will exchange much slower or are non-exchangeable (Chalmer et al., 2006). The rate of H/D exchange characterizes the structure and dynamics of a protein. Thus, the results obtained from H/D exchange aid in the understanding of PSI-membrane interaction topology.

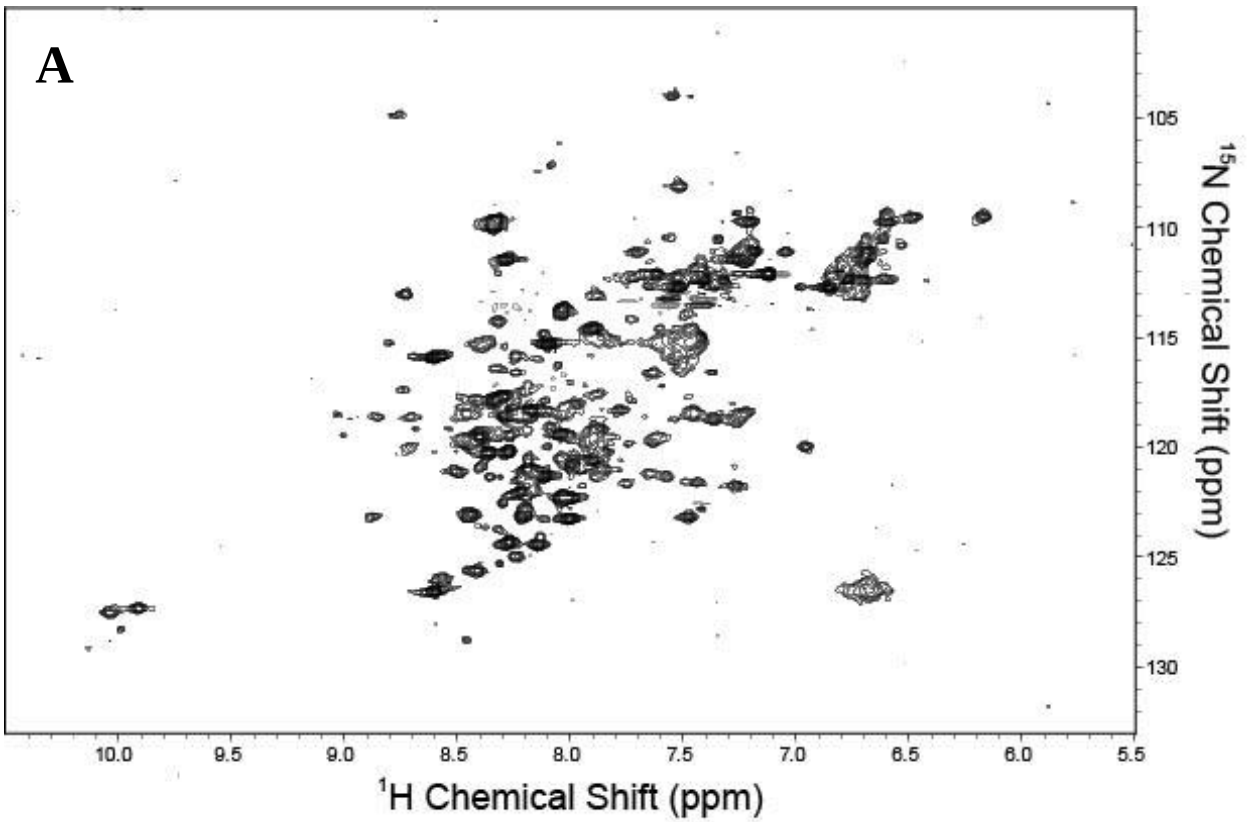
A
105
110
115
120
125
130
$^{15}$N Chemical Shift (ppm)
10.0
9.5
9.0
8.5
8.0
7.5
7.0
6.5
6.0
5.5
$^{1}$H Chemical Shift (ppm)

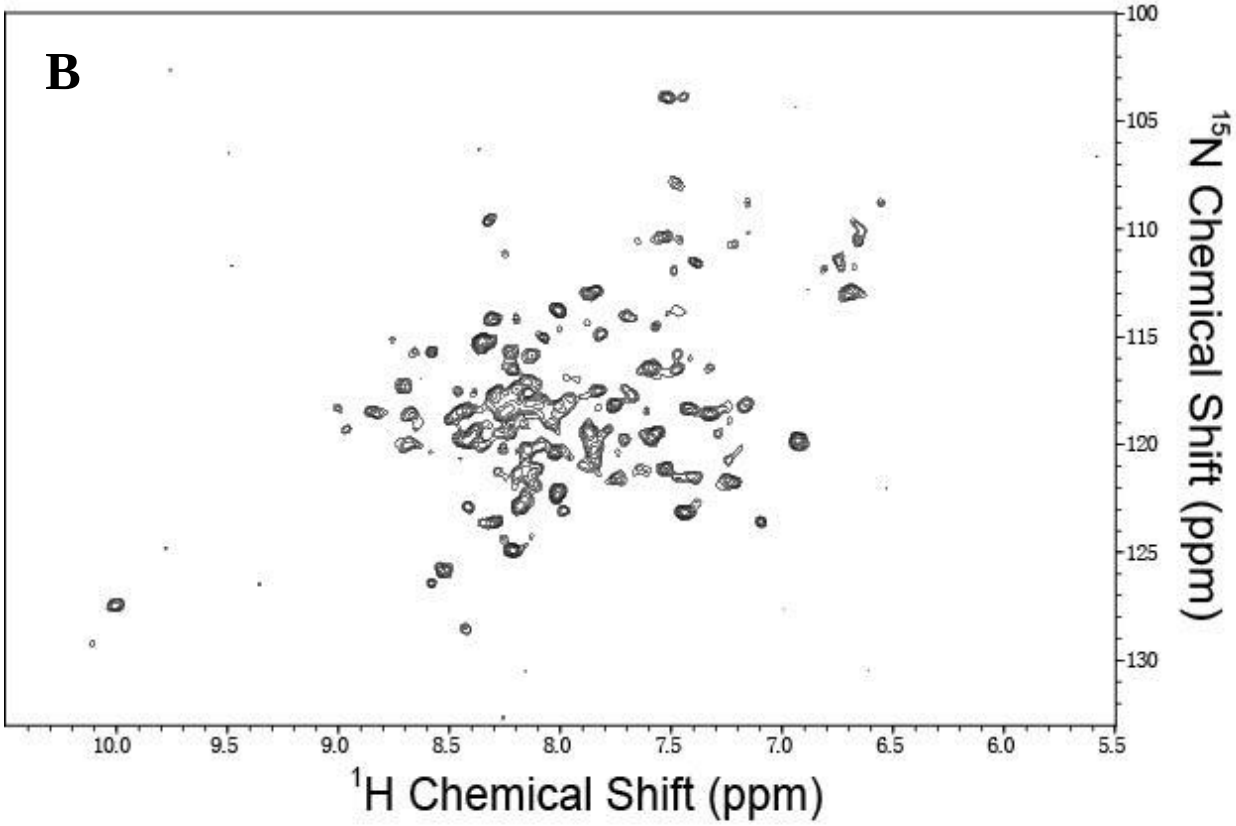
B
100
105
110
115
120
125
130
$^{15}$N Chemical Shift (ppm)
10.0
9.5
9.0
8.5
8.0
7.5
7.0
6.5
6.0
5.5
$^{1}$H Chemical Shift (ppm)

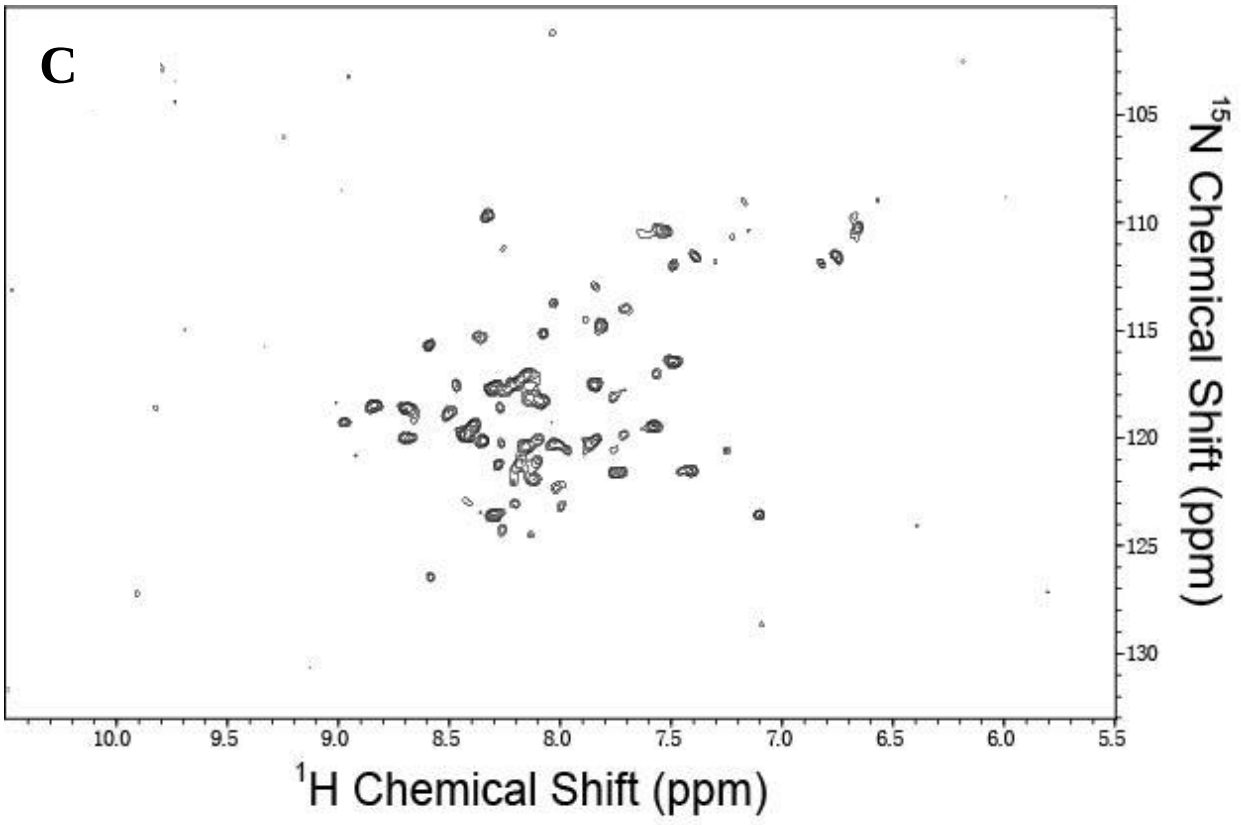


**Figure 4.14 PSI self-protection shown through $D_2O$ exchange in pH 2.0. A) PSI in pH 2.0 buffer, B) PSI in pH 2.0 $D_2O$ buffer immediately, C) PSI in pH 2.0 $D_2O$ buffer after 24 hours.**

PSI-membrane interaction was examined in solid-state NMR to elucidate the PSI interaction topology in the active dimer form. NCA experiments were collected under the same conditions for all spectra. Due to the aggressive PSI-membrane interaction which resulted in non-homogenous samples, PSI-membrane complex produced broad signals on solid-state NMR (Figure 4.15). The spectrum of PSI-membrane complex in the $H_2O$ pH 2.0 buffer is presented in Figure 4.15-A, and the spectrum of this complex exchanged into the $D_2O$ pH 2.0 buffer in Figure 4.15-B. Overlapping both of the spectra in Figure 4.15-C, cross peaks which diminished represented the exchangeable regions which were not protected by the phospholipid or self-protected by the protein. This result gave the first indication of which protein is within the phospholipid membranes.

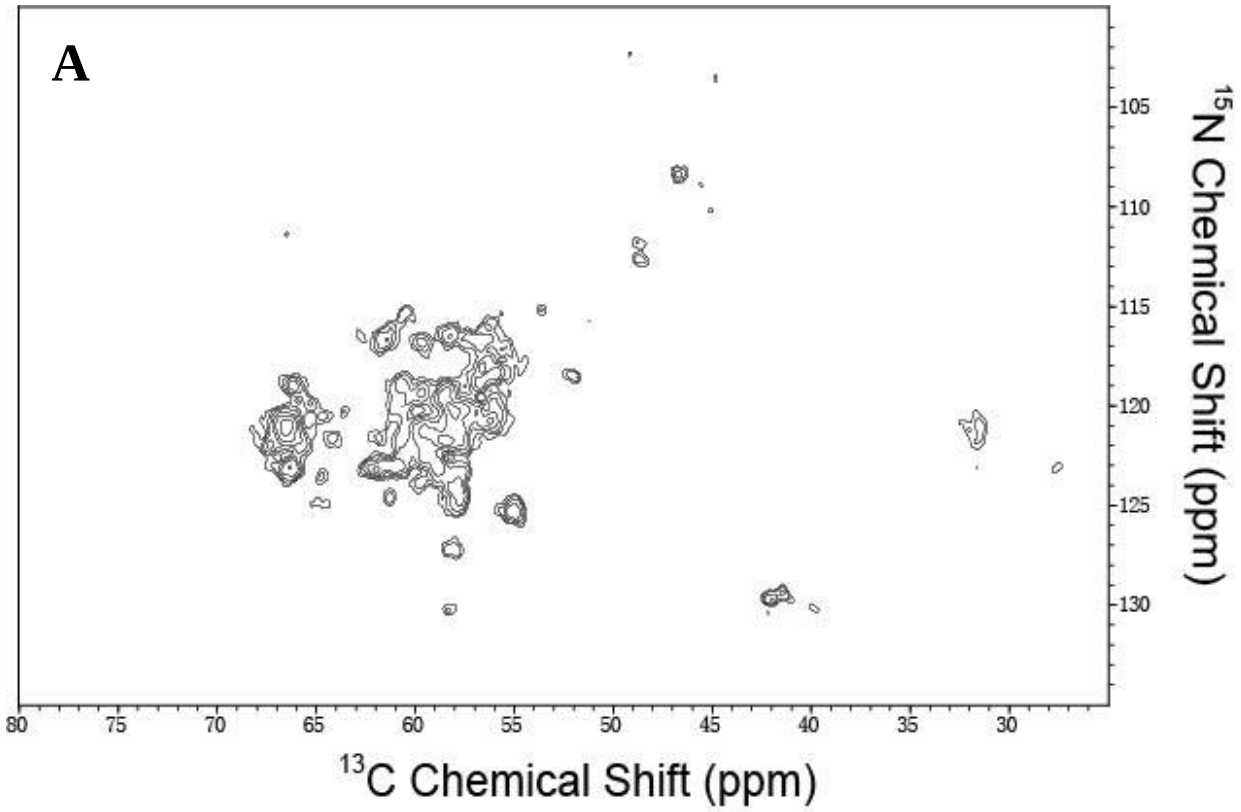
A
105
110
115
120
125
130
$^{15}$N Chemical Shift (ppm)
80
75
70
65
60
55
50
45
40
35
30
$^{13}$C Chemical Shift (ppm)

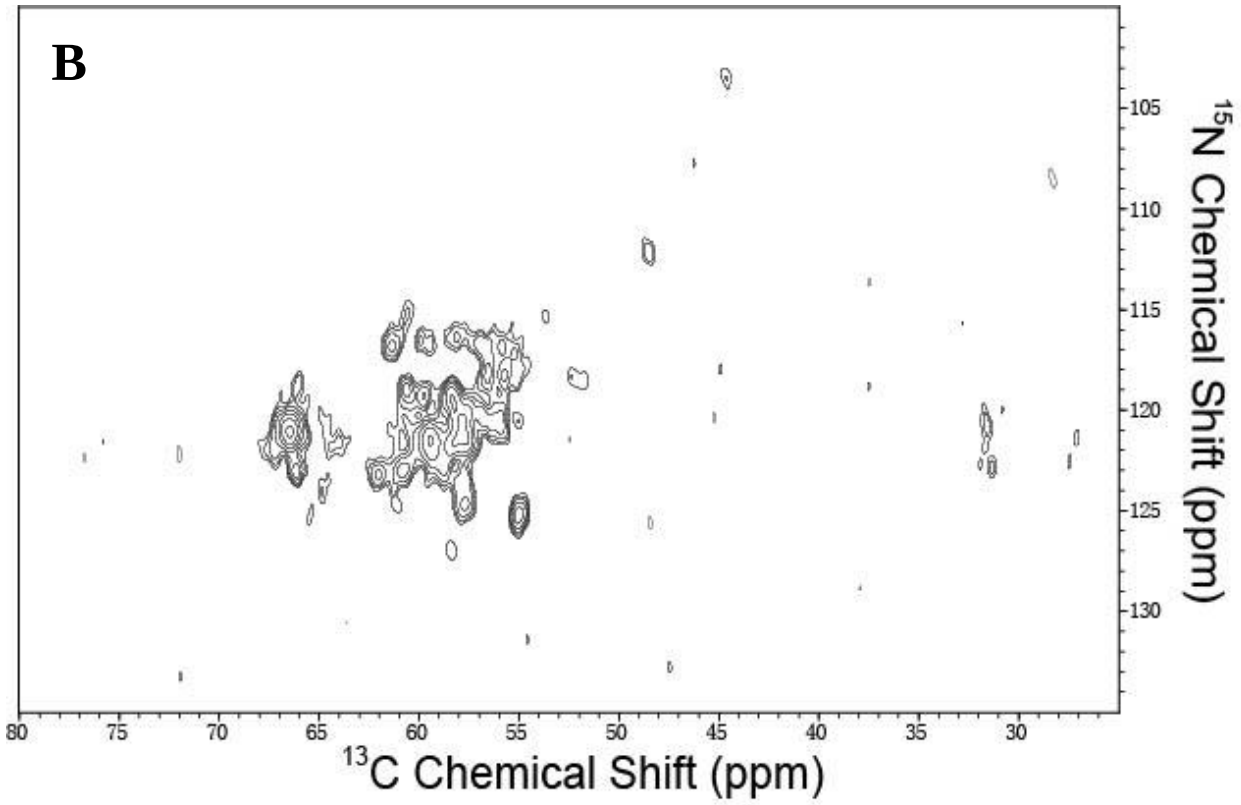
B
105
110
115
120
125
130
$^{15}$N Chemical Shift (ppm)
80
75
70
65
60
55
50
45
40
35
30
$^{13}$C Chemical Shift (ppm)

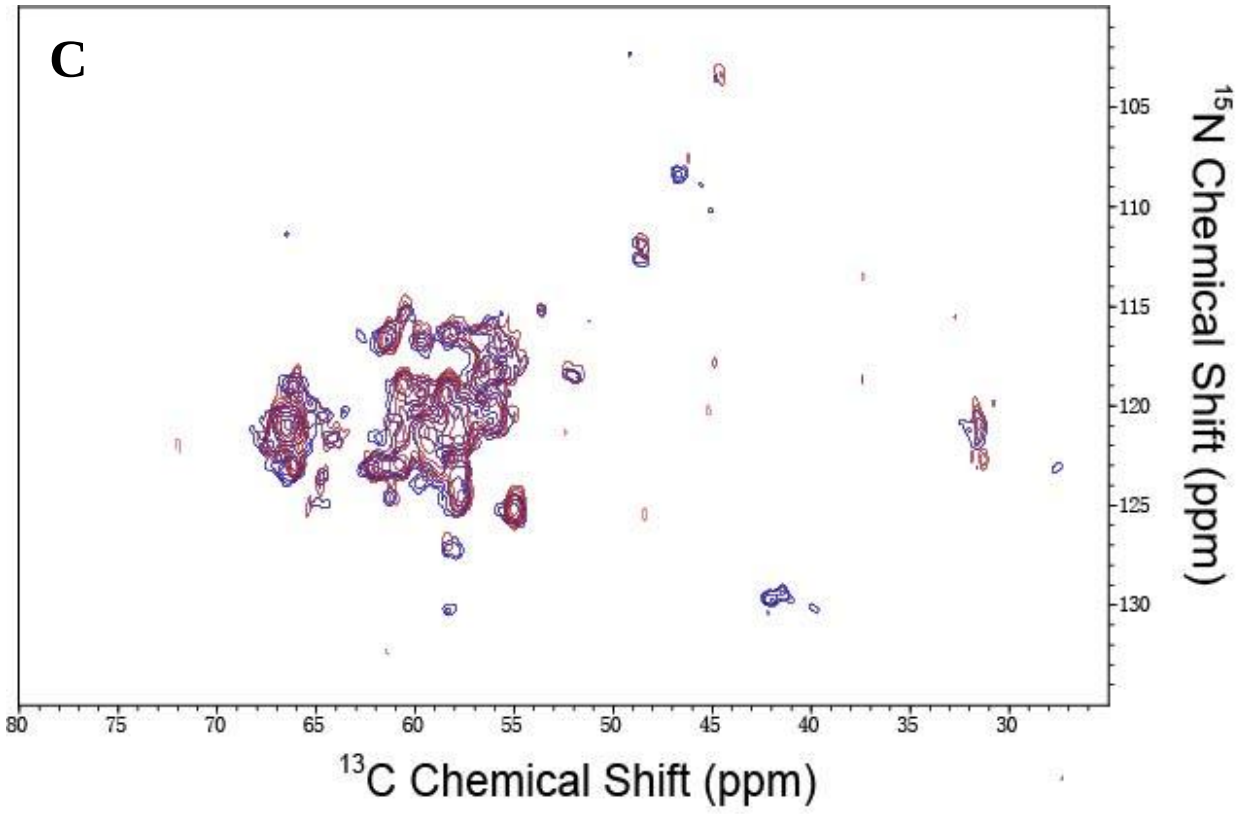


**Figure 4.15 PSI-Membrane interaction in pH 2.0 A)PSI-membrane interaction in pH 2.0 buffer, B) PSI-membrane interaction exchanged into $D_2O$ pH 2.0 buffer, C) Overlap of PSI-membrane interaction of pH 2.0 buffer (blue) and $D_2O$ exchange (red).**

Further, the NCA spectra of PSI-membrane complex, exchanged in $D_2O$ pH 2.0 buffer, was recorded as shown in Figure 4.16-A. Regions on the PSI which were apparent on the spectrum were either protected by the phospholipid membrane or self-protected from the protein. Comparing the cross peaks produced from PSI-membrane complex exchanged in $D_2O$ buffer with $D_2O$ buffer reacted PSI-membrane complex, the cross peaks which were not present in both spectra suggested that they were protected by the phospholipid (Figure 4.16-B).

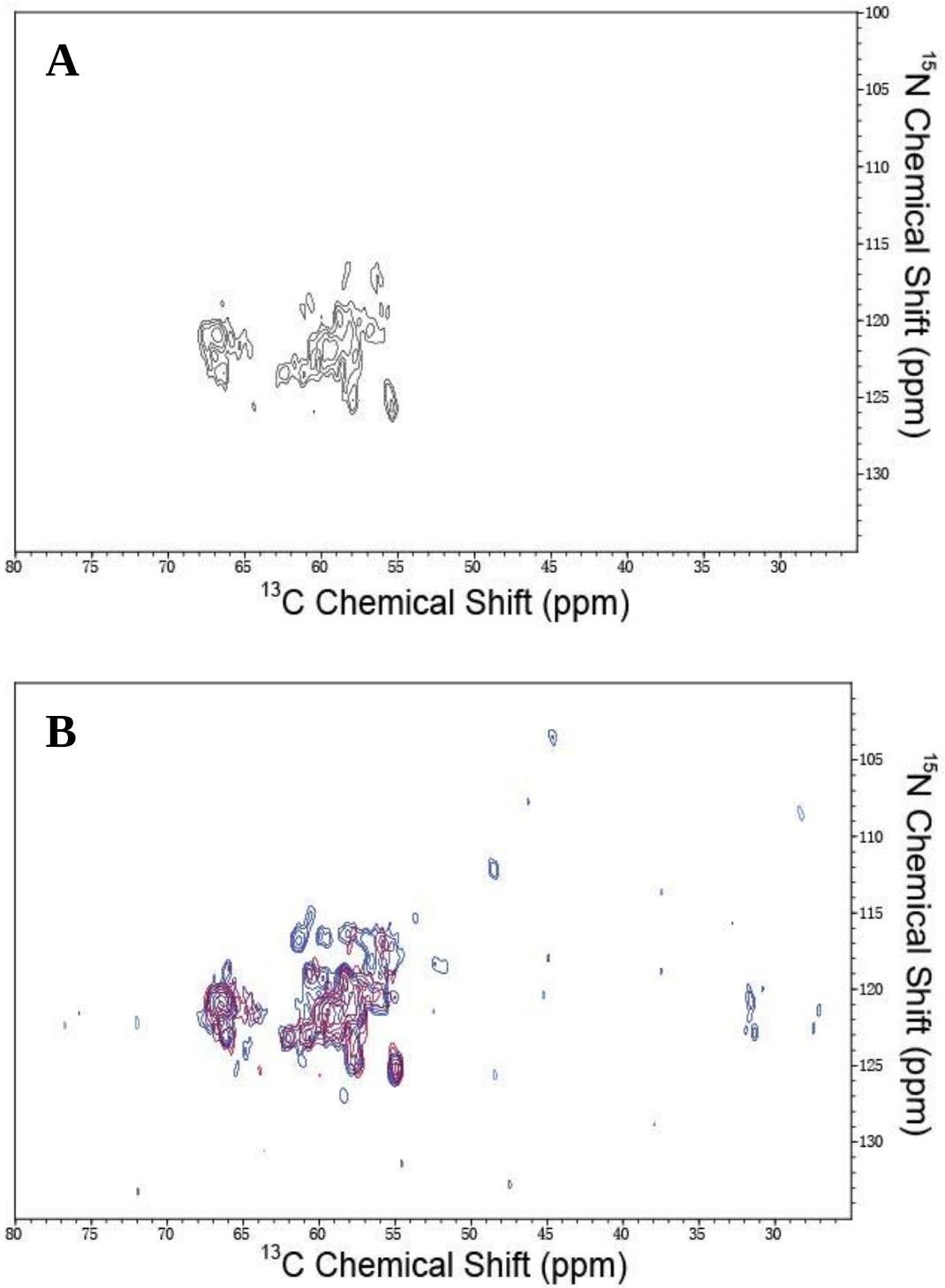


**Figure 4.16 PSI-membrane interaction in pH 2.0 $D_2O$ buffer A) PSI-membrane interaction in pH 2.0 $D_2O$ buffer, B) Overlap of PSI-membrane interaction of pH 2.0 $D_2O$ buffer (red) and $D_2O$ exchange (blue)**

To further confirm that PSI is embedded within the phospholipid upon interaction, lipid-protein magnetization transfer was employed. Magnetization was transferred through the proton of the acyl chains from phospholipids to a proton of the PSI and subsequently transferred to a carbon, producing a signal on the spectrum. In Figure 4.17-A, strong signals were presented around 4 ppm and weak signals were presented between 7 and 8 ppm. By overlapping the 1-D spectra in Figure 4.17-B, the signals produced around 4 ppm were from the acyl chains on the phospholipids, which suggested that magnetization transfer occurs between lipids chains and the protein . The signals produced between 7 and 8 ppm were from water. As stronger signals were observed from the acyl chains than from water, it revealed that signals were produced from the magnetization transfer from the lipid acyl chains to the protein. This confirmed that the PSI is embedded within the phospholipid membranes. However, the orientation or critical residues for interaction could not be observed.

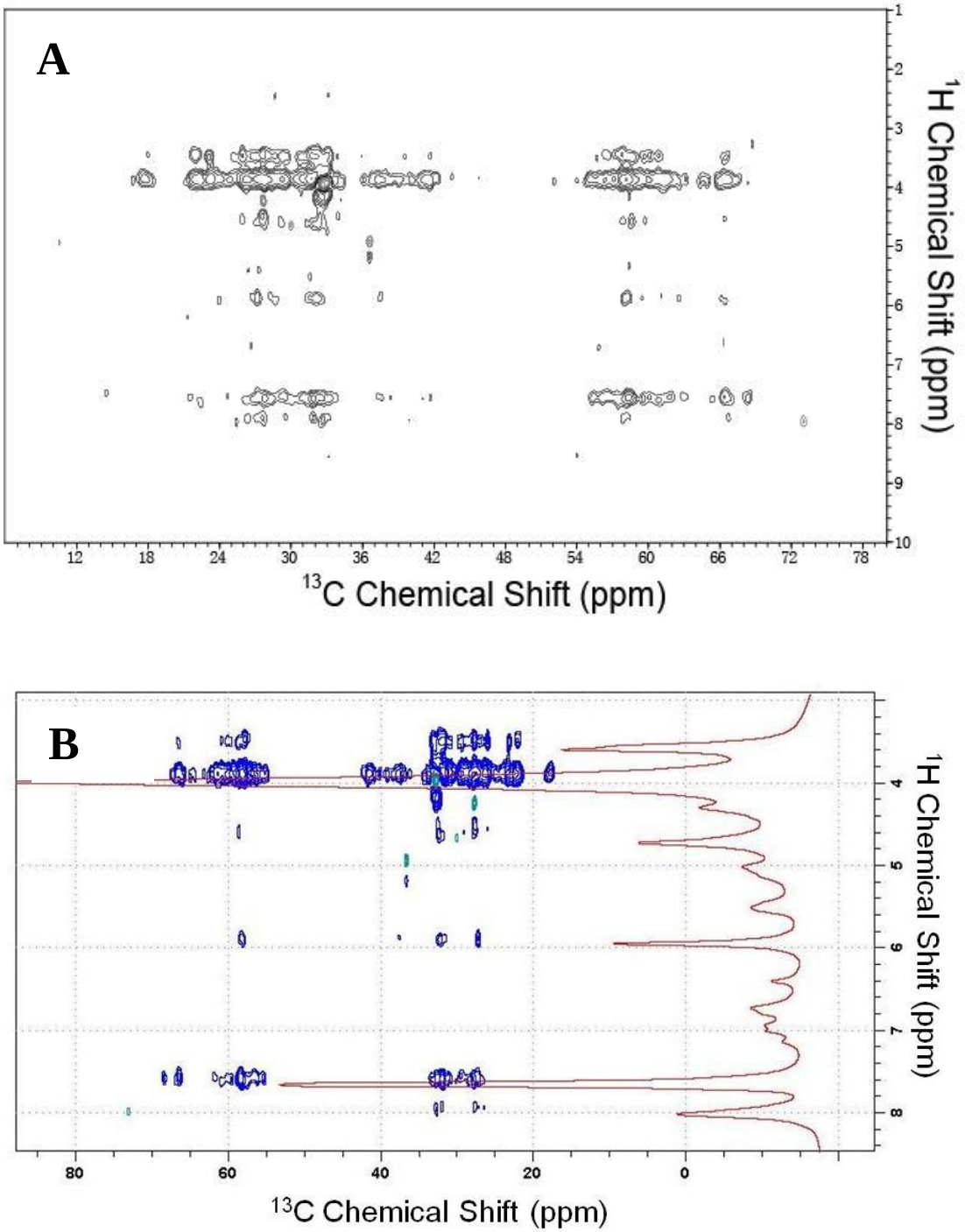


**Figure 4.17 PSI-membrane magnetization transfer A) PSI-membrane magnetization transfer in pH 2.0 buffer, B) PSI-membrane magnetization transfer in pH 2.0 buffer overlapped with 1-D spectra. Signal produced around 4 ppm of $^{1}$H was from acyl chains and the signal produced around 7.5 ppm $^{1}$H was from $H_2O$.**

With a mixture of charged phospholipid membrane, the StAP PSI was known to bind under acidic conditions and the interaction was induced by the hydrophobic regions on the PSI (Munoz et al., 2010; Bryksa et al., 2011; Munoz et al., 2011; Munoz et al., 2014). Munoz et al (2014) demonstrated through IR that upon the interaction of phospholipid membrane containing DMPG or DMPC with PSI, a secondary structural change was observed. However, these findings did not represent the topology and orientation of the PSI-membrane interaction. Previously studies on SAPLIP briefly looked into the critical parts responsible for saposin C-membrane interaction. Major conformational change took place from neutral to acidic pH in saposin C from the complete or partial burying of hydrophobic residues in the neutral condition to exposure of patches of hydrophobic surfaces in the acidic condition (de Alba et al., 2003). Vacarro suggested that the hydrophobic surfaces induced the insertion of saposin C (Vacarro et al., 1999) and that insertion took place at terminal helices by forming a "clip-on" mechanism (Vacarro et al., 1994). The phospholipid composition has a role in the topology and degree of protein insertion. It was found that phospholipid membrane destabilization increased with elevating the amount of PS (Vacarro et al., 1999). Further studies should be conducted to elucidate the degree of membrane insertion and the critical residues involved.

### 4.7 General Discussion

In general, the biological roles of the plant aspartic proteases containing a plant specific insert are less well defined in comparison to the aspartic proteases from other sources (Guevara et al., 2002; Guevara et al., 2004). The plant aspartic proteases found in *Solanum tuberosum* are known to be related to the innate plant defense response (Guevara et al., 2002). In both potato leaves and tubers, aspartic proteases exhibit antimicrobial activity by having specific peptide cleavage positions (Guevara et al., 2004). Upon the infection of *Phytophthora infestans*, the

resistant cultivar of potatoes express aspartic proteases at a higher and faster rate than the susceptible cultivars and are known to have direct inhibition effect on the germination of the microbial cysts (Guevara et al., 2002). Interestingly, it was also found that the aspartic proteases can directly interact with microbial surfaces followed by membrane permeabilization (Medieta et al., 2006). To elucidate the mechanistic of action of the *Solanum tuberosum* aspartic protease, understanding the functions of its plant specific insert is critical to the overall characterization.

The series of experiments undertaken in this study examined the monomer-dimer equilibrium, membrane interaction and protein topology. Specifically in the StAP PSI, previous research by Bryksa et al. (2011) had shown that it could function independently of the parent protein. The StAP PSI was toxic to selected plant and human pathogens by permeabilizing their plasma membranes (Bryksa et al., 2011). The size and composition of the phospholipid membrane can dramatically affect the binding of proteins (Vacarro et al., 1999). Although the StAP PSI is not a true saposin as the N- and C-terminus were swapped, its functions are similar to the proteins from the SAPLIP family (Egas et al., 2010; Munoz et al., 2010; Bryksa et al., 2011). The StAP PSI is cytotoxic to both gram-negative and gram-positive bacteria in a dose-dependent manner by directly interacting with the microbial cell wall or membrane (Munoz et al., 2010). The 3D structure of the protein resembles the saposin-like proteins (Egas et al., 2010); the cystine disulfide bridges are critical in stabilizing the overall structure and are important for its ability to induce leakage in a pH dependent and lipid composition dependent manner (Bryksa et al., 2011). The StAP PSI is known to be the most effective in reducing pathogen spores of *P.infestans* and *F.solani* in a dose dependent manner with an IC50 of approximately 1.25mM (Munoz et al., 2010). The PSI found in different parts of the potato plant can vary in the level of their activity and that they can function independently of the parent enzyme.

# Chapter 5: Conclusion

The present study provided significant insights into the mechanistic understanding of the plant aspartic protease plant specific insert which contributed to the natural plant host defense response against pathogen invasions. The combination of solution state and solid state NMR techniques characterized the pH dependent nature of the StAP PSI, its dynamics, and protein interaction topology. Findings reported in this thesis suggested that PSI is a monomer in the neutral pH and an active dimer in the acidic pH. The interaction between PSI and phospholipids is highly dependent upon the mixture of phospholipid composition. The PSI's active regions were located on its helical segments and they are embedded within the membrane during interaction, leaving the flexible loop on the outside. Lastly, the locations of which phospholipids interact with the StAP PSI were from its phosphate head group. The findings in this study contributed to the protein dynamics and mechanistic interaction for the StAP PSI and phospholipid membrane on a molecular level.

## Chapter 6: Future Research

Future studies using the NMR techniques are encouraged to elucidate a monomer structure of the PSI in the neutral pH to provide a better understanding of the monomer-dimer structural exchange. The monomeric structure of PSI will help to provide perspective information in characterizing the protein interaction mechanism at its critical residue and the protein dynamics of moving from the monomeric to the dimeric state.

Other experiments using solid-state NMR techniques can be used to explore the mechanism by which the StAP PSI interacts with phospholipids using $^{2}H$ and $^{31}P$ to examine the degree of lipid insertion. This will provide significant insights on the interaction activity from a phospholipid perspective.

Further, to reveal the StAP-phospholipid interaction from a residual level, site directed mutagenesis should be carried out to identify the critical amino acids for the StAP PSI interaction. In silico research can provide an overall visualization of the mechanism of interaction by 3-D modeling.

## References


Abu-Baker, S., Qi,X., Lorigan, G.A. (2007) Investigating the interaction of saposin C with POPS and POPC phospholipids: a solid-state NMR spectroscopic study, Biophysical Journal, 93, 3480-3490

Abu-Baker, S., Qi, X., Newstadt, J., Lorigan, G.A. (2005) Structural changes in a binary mixed phospholipid bilayer of DOPG and DOPS upon Sap C interaction at acidic pH utilizing $^{31}P$ and $^{2}H$ solid-state NMR spectroscopy, Biochimica et Biophysica Acta, 1717, 58–66.

Ahn, V.E., Faull, K.F., Whitelegge, J.P., Fluharty, A.L., Prive, G.G. (2003) Crystal structure of saposin B reveals a dimeric shell for lipid binding, Proceedings of the National Academy of Sciences, 100(1), 38-43

Ahn, V.E., Leyko, P., Alattia, J.E., Chen, L., Prive, G.G. (2006) Crystal structures of saposins A and C, Protein Science, 15, 1849-1857

Agrawal., A.A., Janssen, A., Bruin, J., Posthumus, M.A., Sabelis, M.W. (2002) An ecological cost of plant defence: attractiveness of bitter cucumber plants to natural enemies of herbivores, Ecology Letters, 5, 377-385

Alattia, J-R., Shaw, J.E., Yip, C.M., Prive, G.G. (2007) Molecular imaging of membrane interfaces reveals mode of beta-glucosidase activation by saposin C, Proceedings of the National Academy of Science, 104(44), 17394-17399

Alba, E., Weiler, S., Tjandra, N. (2003) Solution structure of human saposin C: pH-dependent interaction with phospholipid vesicles, Biochemistry, 42, 14729–14740

Aliev, A. (2014) Relaxation Lecture Notes, UCL Chemistry NMR Instruments, Retrieved on December 15th, 2016, Available Online: https://www.ucl.ac.uk/nmr/NMR_lecture_notes/

Anderson, D., Sawaya, M., Cascio, D., Ernst, W., Modlin, R., Krensky, A., Eisenberg, D. (2003) Granulysin crystal structure and a structure-derived lytic mechanism, Journal of Molecular Biology, 325, 355-365

Andreeva, N.S., Rumsh, L. D. (2001) Analysis of crystal structure of aspartic proteinases: On the role of amino acid residues adjacent to the catalytic site of pepsin-like enzymes, Protein Science, 10, 2439-2450

Asakura, T., Watanabe, H., Abe, K. and Arai, S. (1995) Rice aspartic proteinase, oryzasin, expressed during seed ripening and germination, has a gene organization distinct from those of animal and microbial aspartic proteinases. European Journal of Biochemistry. 232, 77–83.

Azuma, N., O'Brien, J.S., Moser, H.W., Kishimoto, Y. (1994) Stimulation of acid ceramidase activity by saposin D, Biochemistry and Biophysics, 311(2), 354-357

Baldus M, Petkova AT, Herzfeld J, Griffin RG (1998) Cross polarization in the tilted frame: assignment and spectral simplification in heteronuclear spin systems, Molecular Physics, 95,1197-1207

Beck, M.R., DeKoster, G.T., Cistola, D.P., Goldman, W.E. (2009) NMR structure of a fungal virulence factor reveals structural homology with mammalian saposin B, Molecular Microbiology, 72(2), 344-353

Berg, J.M., Tymoczko, J.L., Stryer, L. (2002) Section 4.5, Three-Dimensional Protein Structure Can Be Determined by NMR Spectroscopy and X-Ray Crystallography, Biochemistry, 5th edition, New York: W H Freeman, Available from: http://www.ncbi.nlm.nih.gov/books/NBK22393/

Brodelius, M., Hiraiwa, M., Marttila, S., Karadaghi, S.A., Picaud, S., Brodelius, P.E. (2005) Immunolocalization of the saposin-like insert of plant aspartic proteinase exhibiting saposin C activity. Expression in young flower tissues and in barley seeds, Physiologia Plantarum, 125, 405-418

Bruhn, F. (2005) A short guided tour through functional and structural features of saposin-like proteins, Biochemistry, 389, 249-257

Bryksa, B.C., Bhaumik, P., Magracheva, E., De Moura, D. C., Kurylowicz, M., Zdanov, A., Dutcher, J.R., Wlodawer, A., Yada, R.Y. (2011) Structure and mechanism of a saposin-like domain of a plant aspartic protease, Journal of Biological Chemistry, 286(32), 28265-28275

Bryksa, B. (2016) Structure-function insights into the biochemical properties and phospholipid bilayer interactions of the saposin-like domain of plant aspartic proteases, University of Guelph, Guelph, Canada

Byers, A.R., Ibrahim, S., Worku, M. (2014) Detection of prosaposin and mature saposins in goat milk, American Journal of Agricultural and Biological Sciences, 9(4), 1557-4989

Chen, F., Foolad, M.R., (1997) Molecular organization of a gene in barley which encodes a protein a similar to aspartic protease and its specific expression in nucellar cells during degeneration, Plant Molecular Biology, 35, 821–831.

Chou, P. Y., Fasman. G. D. (1978) Empirical predictions of protein conformation, Annual Review of Biochemistry, 47, 251-276

Chalmers, M., Busby, S., Pascal., B., He, Y., Hendrickson, C., Marshall, A., Griffin, P. (2006) Probing Protein Ligand Interaction by Automated Hydrogen/Deuterium Exchange Mass Spectrometry, Analytical Chemistry, 78 (4), 1005-1014

Ciaffoni, F., Salvioli, R., Tatti, M., Arancia, G., Crateri, P., Vaccaro, A.M. (2001) Saposin D solubilizes anionic phospholipid-containing membranes, Journal of Biological Chemistry, 276(34), 31583-31589

Clayberger, C., Krensky, A.M. (2003) Granulysin, Current Opinion in Immunology, 15, 560-565

Cordeiro, M.C., Xue, Z-T., Pietrzak, M., Pais, M.S., Brodelius, P.E. (1994) Isolation and characterization of a cDNA from flowers of Cynara cardunculus encoding cyprosin (an aspartic proteinase) and its use to study the organ-specific expression of cyprosin, Plant Molecular Biology, 24, 733-741

Curto, P. Lufrano, D., Pinto, C., Custodio, V., Gomes, A.C., Trejo, S.A., Bakas, L., Vairo-Cavalli, S., Faro, C., Simoes, I. (2014) Establishing the yeast *Kluyeromyces lactis* as an expression host for production of the saposin-like domain of the aspartic protease cirsin, Applied and Environmental Microbiology, 80(1), 86-96

Davies D (1990). The structure and function of the aspartic proteases, Annual Review of Biophysics and Biophysical Chem, 19, 189-215

de Alba, E., Weiler, S., and Tjandra, N. (2003) Solution structure of human saposin C: pH-dependent interaction with phospholipid vesicles, Biochemistry, 42, 14729-14740

Delaglio F, Grzesiek S, Vuister GW, Zhu G, Pfeifer J, Bax A (1995) Nmrpipe – a multidimensional spectral processing system based on unix pipes, Journal of Biomolecular NMR, 6, 277-293

De Moura, D.C., Bryksa, B., Yada, R.Y. (2014) *In silico* insights into protein-protein interactions and folding dynamics of the saposin-like domain of *Solanum tuberosum* aspartic protease, Public Library of Science, 9(9), e104315

Deverall, B.J. (2006) Plant protection using natural defence systems of plants, Advances in plant pathology, 211-212

Don. T.A., Bethony, J.M., Loukas, A. (2008) Saposin-like proteins are expressed in the gastrodermis of *Schistosoma mansoni* and are immunogenic in natural infections, International Journal of Infectious Disease, 12, 39-47

Dunn, B.M. (2002) Structure and mechanism of the pepsin-like family of aspartic peptidases, Chemistry Review, 102, 4431–4458

Egas, C., Lavoura, N., Resende, R., Bruito, R.M.M., Pires, E., Pedroso de Lima, M.C., Faro, C. (2000) The saposin-like domain of the plant aspartic proteinase precursor is a potent inducer of vesicle leakage, Journal of Biological Chemistry, 275 (49), 38190-38196

Espino, A.M., Hillyer, G.V. (2003) Molecular cloning of a member of the fasciola hepatica saposin-like protein family, Journal of Parasitology, 89(3), 545-552

Fabbro, D., Grabowski, G.A., (1991) Human acid glucosidase: use of inhibitory and activating monoclonal antibodies to investigate the enzyme's catalytic mechanism and saposin A and C binding sites, Journal Biological Chemistry, 266(23), 15021-15027

FAO (2015), Food Loss and Food Waste, Available at: http://www.fao.org/food-loss-and-food-waste/en/

Faro, C., Ramalho-Santos, M., Vieira, M. Mendes, A., Simoes, I., Andrade, R., Verissimo, P., Lin, X, Tang, J., Pires, E. (1999) Cloning and characterization of cDNA encoding cardosin A, an RGD-containing plant aspartic proteinase, Journal of Biological Chemistry, 274(40), 28724-28729

Farrow, N., Muhandiram, R., Singer, A., Pascal, S., Kay, C., Gish, G., Shoelson, S., Pawson, T., Forman-Kay, J., Kay, L. (1994) Backbone dynamics of a free and phosphopeptide-complexed Src homology 2 domain studied by $^{15}$N NMR relaxation, Biochemistry, 33, 5984-6003

Fiirst, W., Machleidt, W., Sandhoff, K. (1988) The precursor of sulfatide activator protein is processed to three different proteins, Journal Biological Chemistry, 369, 317-328

Frazao, C., Bento, I., Costa, J., Soares, C.M., Verissimo, P., Faro, C., Pires, E., Cooper, J., Carrondo, M.A. (1999) Crystal structure of cardosin A, a glycosylated and Arg-Gly-Asp-containing aspartic proteinase from the flowers of *Cynara cardunculus* L, Journal of Biological Chemistry, 274(39), 27694-27701

Fung BM, Khitrin AK, Ermolaev K (2000) An improved broadband decoupling sequence for liquid crystals and solids, Journal of Magnetic Resonance, 142, 97-101

Fushman, D., Cahill, S., Cowburn, D. (1997) The main-chain dynamics of the dynamin pleckstrin homology (PH) domain in solution: analysis of $^{15}$N relaxation with monomer/dimer equilibration, Journal of Molecular Biology, 266: 173-194

Grams, R., Adisakwattana, P., Ritthisunthorn, N., Eursitthichai, V., Vichasri-Gram, S., Viyanant, V. (2006) The saposin-like proteins 1, 2 and 3 of Fasciola gigantic, Molecular and Biochemical Parasitology, 148, 133-143

Guevara, M.G., Almeida, C., Mendieta, J.R., Faro, C.J., Verissimo, P., Pires, E.V., Daleo, G.R. (2005) Molecular cloning of a potato leaf cDNA encoding an aspartic protease (StAsp) and its expression after *P. infestans* infection, Plant Physiology and Biochemistry, 43, 882-889

Guevara, M.G., Oliva, C.R., Huarte, M., Daleo, G.R. (2002) An aspartic protease with antimicrobial activity is induced after infection and wounding in intercellular fluids of potato tubers, European Journal of Plant Pathology, 108, 131-137

Guevara, M.G., Ver ́ssimo, P., Pires, E., Faro, C., Daleo, G.R. (2004) Potato aspartic proteases: induction, antimicrobial activity and substrate specificity, Journal of Plant Pathology, 86(3), 233–238.

Hawkins, C. A., Alba, E., Tjandra, N. (2005) Solution structure of human saposin C in a detergent environment, Journal of Molecular Biology, 346, 1381– 1392.

He, H., Conrad, C., Nilsson, C., Ji, Y., Schaub, T., Marshall, A., Emmett, M. (2007) Method for lipidomic analysis: p53 expression modulation of sulfatide, ganglioside, and phospholipid composition of U87 MG glioblastoma cells, Journal of Analytical Chemistry, 79(22), 8423-8430

Higman, V. (2012) Protein NMR-Solution NMR, Retrieved on December 20th, 2016, Online Available: http://www.protein-nmr.org.uk/solution-nmr/

Hijman, B.J., Forbes, G.A., Walker, T.S. (2000) Estimating the global severity of potato late blight with GIS-linked disease forecast models, Plant Pathology, 49 (6), 697-705

Hiraiwa, M., O'Brien, J., Kishimoto, Y., Galdzicka, M., Fluharty, A.L., Ginns,E.I., Martin, B.M. (1993) Isolation, Characterization, and proteolysis of human prosaposin, the precursor of saposins (Sphingolipid Activator Proteins), Archives of Biochemistry and Biophysics, 304 (1), 110-116

Hitchens, G. (2006) Fundamentals of Protein NMR Spectroscopy, Focus on Structural Biology, Springer, Vol 5

Hong, Y.H., Lillehoj, H.S., Siragusa, G.R., Bannerman, D.D., Lillehoj, E.P. (2008) Antimicrobial activity of chicken NK-lysin against *Eimeria sporozoite*, Avian Disease, 52, 302-305

Hu, Y., Li, Y, Zhang, X., Guo, X., Xia, B, Jin, C. (2006) Solution structures and backbone dynamics of a flavodoxin MioC from *E.coli* in both Apo- and Holo-forms, The Journal of Biological Chemistry, 281(46), 35454-35466

Huster, D., Yao, X., Hong, M. (2002) Membrane protein topology probed by $^{1}$H spin diffusion from lipids using solid-state NMR spectroscopy, Journal of American Chemical Society, 124 (5), 874-883

John, M., Horsley, W., Klein, M. (1971) Spin- lattice relaxation measurements in slowly relaxing complex spectra, Journal of Chemical Physics, 55 (7), 3604-3605

John, M., Wendeler, M., Heller, M., Sandoff, K., Kessler, H. (2006) Characterization of human saposins by NMR spectroscopy, Biochemistry, 45, 5206-5216

Kadek, A., Tretyachenko, V., Mrazek, H., Ivanova, L., Halada, R., Rey, M., Schriemer, D.C, and Man, P. (2014) Expression and characterization of plant aspartic protease nepenthesin-1 from *Nepenthes gracilis*, Protein Expression and Purificaiton, 95, 121-128

Kaimal., V., Chu, Z., Mahller, Y.Y., Papahadjopoulos-Sternberg, B., Cripe, T.P., Holland, S.K., Qi, X. (2010) Saposin C coupled lipid nanovesicles enable cancer-selective optical and magnetic resonance imaging, Molecular Imaging Biology, 13, 886-897

Kazazic, S., Zhang, H., Schaub, T., Emmett, M., Hendrickson, C., Blakney, G., Marshall, A. (2010) Automated data reduction for hydrogen/deuterium exchange experiments, enabled by high-resolution Fourier transform ion cyclotron resonance mass spectrometry, Journal of the American Society for Mass Spectrometry, 21(4), 550-558

Kervinen, J., Tobin, G.J., Costa, J., Waugh, D.S., Wlodawer, A., Zdanov, A. (1999) Crystal structure of plant aspartic proteinase prophytepsin: inactivation and vacuolar targeting, European Molecular Biology Organization Journal, 18(14), 3947-3955

Kishimoto, Y., Hiraiwa, M., O'Brien, J.S. (1992) Saposins: structure, function, distribution and molecular genetics, Journal of Lipid Research, 33, 1255-1268

Koelsch, G.,Mares, M., Metcalf, P. and Fusek,M. (1994) Multiple functions of pro-parts of aspartic proteinase zymogens. Federation of European Biochemical Society, 343, 6–10.

Kondoh, K., Hineno, T., Sano, A., Kakimoto, Y. (1991) Isolation and characterization of prosaposin from human milk, Biochemical and Biophysical Research Communications, 181, 286-292

Laloi, M., McCarthy, J., Morandi, O., Gysler, C. and Bucheli, P.(2002)Molecular and biochemical characterisation of two aspartic proteinases TcAP1 and TcAP2 from *Theobroma* cacao seeds. Planta, 215, 754–762.

Liepinsh, E., Anderson, M., Ruysschaert, J.M., Otting, G. (1997) Saposin fold revealed by the NMR structure of NK-lysin, Nature Structural and Molecular Biology, 4, 793-795

Lipchock, J., Loria, P. (2009) Monitoring molecular interactions by NMR, Methods Molecular Biology, 490, 115-34

Locatelli-Hoops, S., Remmel, N., Klingenstein, R., Breiden, B., Rossocha, M., Schoeniger, M., Koenigs, C., Saenger, W., Sandhoff, K. (2006) Saposin A mobilizes lipids from low cholesterol and high bis (monoacylglycerol) phosphate-containing membranes, Journal of Biological Chemistry, 281(43), 32451-32460

Marion, D. (2013) An introduction to biological NMR spectroscopy, Molecular and Cellular Proteomics, 12(11), 3006-3024

Matsuda, J., Vanier, M.T., Saito, Y., Tohyama, J., Suzuki, K., Suzuki, K. (2001) A mutation in the saposin A domain of the sphingolipid activator protein (prosaposin) gene results in a late onset, chronic form of globoid cell leukodystrophy in the mouse, Human Molecular Genetics, 10 (11), 1191-1199

Mendieta, J., Pagano, M., Munoz, F., Daleo, G., Guevara, M. (2006) Antimicrobial activity of potato aspartic proteases (StAPs) involves membrane permeabilization, Microbiology, 152, 2039-2047

Michalek, M., Leippe, M. (2015) Mechanistic insights into the lipid interaction of an ancient saposin-like-protein, Journal of American Chemical Society, 54, 1778-1786

Morimoto, S., Kishimoto, Y., Tomich, J., Weiler, S., Ohashi, T., Barranger, J. A., Kretz, K. A., and O'Brien, J. S. (1990) Interaction of saposins, acidic lipids and glucosylceramidase, Journal of Biological Chemistry, 265, 1933-1937

Morimoto, S., Martin, B., Kishimoto, Y., O'Brien, J.S. (1988) Saposin D: a sphingomyelinase activator, Biochemical and Biophysics Research Communications, 156, 403-410

Munoz, F.F., Mendieta, J.R., Pagano, M.R., Paggi, R.A., Daleo, G.R., Guevara, M.G. (2010) The swaposin-like domain of potato aspartic protease (StAsp-PSI) exerts antimicrobial activity on plant and human pathogens, Peptides, 31, 777-785

Munoz, F., Palomares-Jerez, M., Daleo, G., Villanlain, J., Guevara, M.G. (2011) Cholestrol and membrane phospholipid compositions modulate the leakage capacity of the swaposin domain from a potato aspartic protease, Biochimica et Biophysica Acta, 1811, 1038-1044

Munoz, F., Palomares-Jerez, M., Daleo, G., Villalain, J., Guevara, M.G. (2014) Possible mechanism of structural transformations induced by StAsp-PSI in lipid membrane, Biochimica et Biophysica Acta, 1838, 339-347

O'Brien, J.S., Carson, G.S., Seo, H-C., Hiraiwa, M., Kishimoto, Y. (1994) Neurobiology indentification of prosaposin as a neurotrophic factor, Proceedings of the National Academy of Science, 91, 9593-9596

O'Brien, J. S., Carson, G. S., Seo, H-C., Hiraiwa, M., Weiler, S., Tomich, J. M., Barranger, J. A., Kahn, M., Azuma, N., Kishimoto, Y. (1995) Identification of the neurotrophic factor sequence of prosaposin, Official Journal of the Federation of American Societies for Experimental Biology, 9, 681-685

O'Brien, J.S., Kishimoto, Y. (1991) Saposin protein: structure, function, and role in human lysosomal storage disorder, Official Journal of the Federation of American Societies for Experimental Biology, 5, 301-308

O'Brien, M.J., Rich, A. E. (1976) Potato Diseases, Washington D.C, 25

Hijiman, R.J., Forbes, G.A., Walker, T.S (2000) Estimating global severity of potato late blight with GIS-linked disease forecast models, Plant Pathology, 49, 697:705

O'Connell, M.R., Gamsjaeger, R., Mackay, J.P. (2009) The structural analysis of protein-protein interactions by NMR spectroscopy, Proteomics, 9, 5224-5232

Pagano, M.R., Mendieta, J.R., Munoz, F.F, Daleo, G.R., Guevara, M.G. (2007) Roles of glycosylation on the antifungal activity and apoplast accumulation of StAPs *(Solanum tuberosum* aspartic proteases), International Journal of Biological Macromolecules, 41, 512-520

Pietzsch, J. (2003) Protein Folding Technology, Available at: http://www.nature.com/horizon/proteinfolding/background/technology.html

Pitt, J., Hocking, A. (2009) Fungi and food spoilage 3rd edition, New York, NY, Springer Potatoes

Popovic, K., Holyoake, J., Pomes, R., Prive, G.G. (2012) Structure of saposin A lipoprotein discs, Proceedings of the National Academy of Science, 109(8), 2908-2912

Popovic, K., Prive, G.G. (2008) Structures of the human ceramide activator protein saposin D, Acta Crystallographica, 64, 589-594

Qi, X., Grabowski, G.A. (2001) Differential membrane interactions of saposins A and C, Journal of Biological Chemistry, 276(29), 27010-27017

Rafalski, M., Ortiz, A., Rockwell, A., van Ginkel, L. C. (1991) Membrane fusion activity of the influenza virus hemagglutinin: Interaction of HA2 N-terminal peptides with phospholipid vesicles, Biochemistry, 30, 10211-10220

Rao MB, Tanksale AM, Ghatge MS, Deshpande VV (1998) Molecular and biotechnological aspects of microbial proteases, Microbiology Molecular Biology Reviews, 62:597–635

Ramalho-Santos, M., Verissimo, P., Cortes, L., Samyn, B., Beeumen, J.V., Pires, E., Faro, C. (1998) Identification and proteolytic processing of procardosin A, European Journal of Biochemistry, 255, 133-138

Rangus, M. (2007) NMR spectroscopy in solids: a comparison to NMR spectroscopy in liquids, Available from: http://www-f9.ijs.si/~krizan/sola/sempod/0607/rangus-seminar.pdf

Remmel, N., Locatelli-Hoops, S., Breiden, B., Schwarzmann, G., Sandhoff, K. (2007) Saposin B mobilizes lipids from cholesterol-poor and bis (monozcylglycero) phosphate-rich membranes at acidic pH, Federation of European Biochemical Societies, 274, 3406-3420

Rodrigo, I., Vera, P., Van Loo, L., Conejero, V. (1991) Degradation of tobacco pathogenesis-related protein, Plant Physiology, 95, 616-622

Runeberg-Roos, P., Tormakangas, K. and Ostman, A. (1991) Primary structure of a barley-grain aspartic proteinase. A plant aspartic proteinase resembling mammalian cathepsin D, European Journal of Biochemistry, 202, 1021–1027.

Sano, A., Hineno, T., Mizuno, T., Kondoh, K., Ueno, S., Kakimoto, Y., and Inui, K. (1989) Sphingolipid hydrolase activator proteins and their precursors. Biochemical and Biophysical Research Communications, 165, 1191-1197

Sano, A., Radin, N.S. (1988) The carbohydrate moiety of the activator protein for glucosylceramide /3-glucosidase, Biochemical and Biophysical Research Communications, 154, 1197-1203

Sattler, M. (2004) Introduction to bimolecular NMR spectroscopy, Lecture Slides at EMBL Heidelberg

Schaller, A., Ryan, C.A. (1996) Molecular cloning of a tomato leaf cDNA encoding an aspartic protease, a systemic wound response protein, Plant Molecular Biology, 31, 1073-1077

Schumann, G.L, D'Arcy, C.L (2005) Late Blight Disease of Potato and Tomato, Available at: http://www.apsnet.org/edcenter/intropp/lessons/fungi/oomycetes/Pages/LateBlight.aspx

Schurko (2003) An Introduction to Solid state NMR, Retrieved on December 12th, 2016, Available at: http://www.emory.edu/NMR/web_swu/SSNMR_redor/ssnmr_schurko

Shin, K.H, Maeda, H., Fujiwara, T., Akutsu, H. (1995) Molecular miscibility of phosphatidylcholine and phosphatidylethanolamine in binary mixed bilayers with acidic phospholipids studied by $^{2}H$ NMR and $^{31}P$ NMR, Biochemica et Biophysica Acta-Biomembrane, 1238, 11544-11554

Simoes, I., Faro, C. (2004) Structure and function of plant aspartic proteinases, European Journal of Biochemistry, 271, 2067-2075

Sun, Y., Zamzow, M., Ran, H., Zhang, W., Quinn, B., Barnes, S., Witte, D.P., Setchell, K.D.R., Williams, M.T., Vorhees, C.V., Grabowski, G.A. (2013) Tissue-specific effects of saposin A and saposin B on glycosphingolipid degradation in mutant mice, Human Molecular Genetics, 22 (12), 2435-2450

Szeci, P.B. (1992) The aspartic proteases, Scandinavian Journal of Clinical Laboratory Investigation, 52, 5-22

Tekely, P., Malcolm, H.L. (2002) Spin Dynamics: Basics of Nuclear Magnetic Resonance, Magnetic Resonance in Chemistry, John Wiley and Sons, pp 686

Teng, Q (2013) Structural Biology: Practical NMR Applications, Springer Science and Business Media, New York

Thurber, KR., Tycko, R. (2009) Measurement of sample temperatures under magic-angle Spinning from the chemical shift and spin-lattice relaxation rate of Br-79 in KBr powder, Journal of Magnetic Resonance,196, 84-87

Tormakangas, K., Hadlington, J.L., Pimpl, P., Hillmer, S., Brandizzi, F., Teeri, T.H., Denecke, J. (2001) A vacuolar sorting domain may also influence the way in which proteins leaves the endoplasmic reticulum, Plant Cell, 13, 2021-2032

Vaccaro, A., Ciaffoni, F., Tatti, M., Salvioli, R., Barca, A., Tognozzi, D., Scerch, C. (1995) Effect of saposin A and C on the enzymatic hydroplysis of liposomal glucosylceramide, The Journal of Biological Chemistry, 270(51), 30576-30580

Vaccaro, A., Salvioli, R., Tatti, M., Ciaffoni, F. (1999) Saposins and their interaction with lipids, Neurochemical Research, 24(2), 307-314

Vaccaro, A., Tatti, M., Ciaffoni, F., Salvioli, R., Serafino, A., Barca, A. (1994) Saposin C induces pH-dependent destabilization and fusion of phosphatidylserine-containing vesicles, Federation of European Biochemical Society Letters, 349, 181-186

Waring, A.J., Walther, F.J., Gordon, L.M., Hernandez-Juviel, J.M., Hong, T., Sherman, M.A., Alonso, C., Alig, T.,Braun, A., Bacon, D. and Zasadzinski, J.A. (2005) The role of charged amphipathic helices in the structure and function of surfactant protein B, Journal of Peptide Research, 66, 364–374.

White, P. C., Cordeiro, M.C., Arnold, D., Brodelius, P.E., Kay, J. (1999) Processing, activity and inhibition of recombinant cyprosin, an aspartic proteinase from cardoon, Journal of Biological Chemistry, 274(24), 16685-16693

Wider, G (2000) Structural determination of biological macromolecules in solution using NMR spectroscopy, Biological Techniques, 29, 1278-1294

Wishart, DS., Sykes, BD. (1994) The C-13 chemical-shift index- a simple method for the identification of protein secondary structure using C-13 chemical shift data, Journal of Biomolecular NMR, 4,171-180

Xia, Y., Suzuki, H., Borevitz, J., Blount, J., Guo, Z., Patel, K., Dixon, R.A., Lamb, C. (2004) An extracellular aspartic protease functions in Arabidopsis disease resistance signaling, European Molecular Biology Organization Journal., 23, 980-988

Yamashita, K., Inui, K., Totani, K., Kochibe, N., Furukawa, M., Okada, S. (1990) Characteristics of asparagine- linked sugar chains of sphingolipid activator protein purified from normal human liver and GM1 gangliosidosis (Type 1) liver, Biochemistry, 29, 3030-3039

Yang, F., Hu, W., Xu, H., Li, C., Xia, B., Jin, C (2007) Solution structure and backbone dynamics of an endopeptidase Hycl from *E.coli*, Journal of Biological Chemistry, 282(6), 3856-3863

You, H.X., Qi, X., Grabowski, G.A., Yu, L. (2003) Phospholipid membrane interactions of saposin C: in situ atomic force microscopic, Biophysical Journal., 84, 2043-2057

Yuan, W., Qi, X., Tsang, P., Kang, S-J, Illarionov, P.A., Besra, G.S., Gumperz, J., Cresswell, P. (2007) Saposin B is the dominant saposin that facilitates lipid binding to human CD1d molecules, Proceedings of the National Academy of Science, 104 (13), 5551-5556

Zhang, H., Kazazic, S., Schaub, T., Tipton, J., Emmett, M., Marshall, A. (2008) Enhanced digestion efficiency, peptide ionization efficiency, and sequence resolution for protein hydrogen/deuterium exchange monitored by Fourier transform ion cyclotron resonance mass spectrometry, Analytical Chemistry, 80(23), 9034-9041